Synthesis and Physicochemical Investigation of CuInS2 Quantum Dots based Photo Anode for Photovoltaic Devices

By

Hina Pervaiz

Reg#00000117886

Session 2015-17

Supervised by

Dr. Zuhair S. Khan

This thesis is submitted to the Centre for advanced studies in Energy in partial fulfillment of the requirements for the degree of

MASTERS of SCIENCE in

ENERGY SYSTEMS ENGINEERING

U.S Pakistan Center for Advanced Studies in Energy (USPCAS-E)

National University of Sciences and Technology (NUST)

H-12, Islamabad 44000, Pakistan

19th January, 2018

Synthesis and Physicochemical Investigation of CuInS2 Quantum Dots based Photo Anode for Photovoltaic Devices

By

Hina Pervaiz

Reg#00000117886

Session 2015-17

Supervised by

Dr. Zuhair S. Khan

This thesis is submitted to the Centre for advanced studies in Energy in partial fulfillment of the requirements for the degree of

MASTERS of SCIENCE in

ENERGY SYSTEMS ENGINEERING

U.S Pakistan Center for Advanced Studies in Energy (USPCAS-E)

National University of Sciences and Technology (NUST)

H-12, Islamabad 44000, Pakistan

19th January, 2018

Certificate

This is to certify that the work in this thesis has been carried out by **Ms. Hina Pervaiz** and completed under my supervision in Advanced Energy Materials & Systems Laboratory, U.S Pakistan Center for Advanced Studies in Energy (USPCAS-E), National University of Sciences & Technology (NUST), Islamabad, Pakistan.

Supervisor: _____

Dr. Zuhair S. Khan
USPCAS-E
NUST, Islamabad

GEC member # 1: _____

Dr. Muhammad. Bilal Khan
USPCAS-E
NUST, Islamabad

GEC member # 2: _____

Dr. Nadia Shahzad
USPCAS-E
NUST, Islamabad

GEC member # 3: _____

Dr. Uzma Habib
RCMS
NUST, Islamabad

HoD-USPCAS-E _____

Dr. Zuhair S. Khan
USPCAS-E
NUST, Islamabad

A/Principal/ Dean _____

Dr. Zuhair S. Khan
USPCAS-E
NUST, Islamabad

Abstract

The importance of energy is apparent in human life, especially in the modern time when almost every aspect in our daily life is related to energy consumption. However, with the explosion of the world's population and the depletion of fossil fuels, energy crisis is threatening the whole world now. Uninterrupted clean energy supply is a vital issue for all countries today. Solar energy is a promising solution to the problems of the energy crisis and environmental pollution, since solar energy is highly abundant, renewable and clean.

Quantum dot (QDs) based solar cells have gained substantial attention due to their prominent factors such as tunable band gap, quantum confinement effects that enhances their efficiency due to multiple excitons generation. Group I-III-IV are emerging material for solar cells due to their high absorption coefficient in visible light range, direct band gap, and low toxicity. Copper Indium Sulphide ($CuInS_2$) QDs are chosen in this work for use in solar cells as a photo anode material because of their relatively low toxicity compared to other QDs materials such as Cd, Pb etc.

This thesis is focused on the fabrication of $CuInS_2$ QDs based photo anode by simplest, safest and cheapest approach. The concerns about the synthesis of photo anode materials is also important. In this thesis, firstly nanostructured wide band gap oxide (TiO_2) material is synthesized by sol gel approach and then copper indium sulfide quantum dots (QDs) are synthesized by simple co-precipitation method. After synthesis procedure the CuInS2 QDs are annealed at different temperature to examine the effect on the crystalline structure and the sizes of the QDs. Electrophoretic deposition (EPD) is the simplest and low-cost approach used to deposit the nanostructured TiO_2 and $CuInS_2$ QDs. After the synthesis of photo anode materials the TiO_2 and $CuInS_2$ QDs films are fabricated on conducting FTO glass as an absorber layer for solar cells. As the quality and the thickness of the film play important role on the performance of the advanced nanostructured materials so different electrophoretic deposition parameters are investigated to achieve the required film because it is great challenge in EPD to create the stable and uniformly thick film. The effect of the EPD for $CuInS_2$ at different voltages over the smoothness and the thickness of the film was also studied in this thesis.

After the fabrication of photo anode the characterization (XRD, SEM/EDS, and UV-Vis spectroscopy) is performed to identify the crystallite size, phase, surface morphology, elemental composition and to figure out the size of the $CuInS_2$ QDs based on their band gap calculated by its optical properties. The XRD patterns indicates the chalcopyrite structure of $CuInS_2$ QDs. The SEM images shows that smooth film is obtained at low applied voltage (90V). The purity of the sample detected by EDS spectra. The calculated molar ratio for Cu:In:S are 1.03:1:1.65, which is closely matched with the nominal stoichiometry of $CuInS_2$ materials (1:1:2). Based on the UV-Vis spectral data the estimated band gap and particle size of the $CuInS_2$ are 2.33eV and 8.4nm respectively which confirmed the formation of QDs. Quantum mechanical simulation based on DFT methods using Gaussian 09 software is carried out to compare with the part of our experimental results.

Keywords: Quantum dots, $CuInS_2$, Photo anode, Electrophoresis deposition.

Acknowledgement

All praise to **Almighty Allah** who provided me with enough strength to accomplish this MS research work. All respects are for **His Holy Prophet (PBUH)** whose teachings are a true source of knowledge & guidance for whole mankind.

With deep regards and profound respect, I take this opportunity to express my deep sense of gratitude and indebtedness to my supervisor **Dr. Zuhair S. Khan** for his inspiring guidance, encouragement, and valuable suggestions throughout the research work. Without his continuous support and assistance it would not have been possible to complete this work. I am extremely grateful to him for his precious time. I owe all my success to my **beloved parents and family members** who proved to be a pillar of strength for me at every time.

I am also indebted to my GEC member **Dr. Uzma Habib** for her support, encouragement, and expert opinions. The realization of this thesis is the result of her constructive advice and valuable criticism.

I gratefully acknowledge the encouragement, guidance and cooperation of all faculty members of **USPCAS-E** NUST during the period of my study at this university.

I would like to pay my gratitude to Mr. Saeed Iqbal, Mr. Naveed, Mr. Qamar-ud din from **AEMS laboratory** and **Research Center for modelling and Simulation** (RCMS) NUST for their cooperation in my Research work.

Dedicated to My beloved parents and family

Table of Contents

Abstract iv
Acknowledgement vi
List of Figures xii
List of Tables xiv
List of Abbreviations xv
List of Journal/Conference Papers from this work xvii
Chapter No.1 17
Introduction 17
1.1 Need of Renewable Energy Resources 17
1.2 Development of Renewable Energy Resources 18
1.3 Solar Energy 19
1.3.1 Solar Photovoltaic Technology 19
1.3.2 Physics of Photovoltaic 20
1.4 Generations of Solar cell 21
1.4.1 First generation solar cell 21
1.4.2 Second Generation solar cell 21
1.4.3 Third Generation solar cell 21
1.5 Quantum dots sensitized solar cells (QDSSCs) 23
1.5.1 WHY Quantum Dots 23
1.5.2 Physics of Quantum Dots 23
1.5.3 Working of Quantum Dots 23
1.5.4 Bandgap Calculation 24
1.5.5 Quantum Dots Solar cells and their materials 25
1.5.5.1 Components of QDSSCs: 27
1.5.5.2 Role of Photoanode in QDSSCs 27
Summary 28
References 30
Chapter No.2 33
Why $CuInS_2$ QDs Based Photo Anode 33
for QDSSCs? 33
2.1 Photo Anode materials for QDSSCs 33
2.1.1 Metal Oxide materials 33
2.1.1.1 Titanium dioxide (TiO_2) 33

2.1.2 Quantum Dots Materials 34
2.1.2.1 III-V, II-VI groups based QDs 34
2.1.2.2 I-III-IV groups based QDs 36
2.2 $CuInS_2$ QDs based Photo Anode for QDSSCs 37
2.3 Efficiency Comparison of different QDSSCs 38
Summary 39
References 41
Chapter No.3 44
Overview of Synthesis Techniques and Characterization Tools 44
3.1 Synthesis and Deposition Techniques 44
3.1.1 Sol-gel Technique 45
3.1.2 Hydrothermal 46
3.1.3 Electro-deposition (ED) 46
3.1.4 Electrophoretic Deposition (EPD) 47
3.1.5 Spin Coating 49
3.2 Characterization Tools 50
3.2.1 UV-Vis Spectroscopy 50
3.2.2 X-ray Diffraction (XRD) 51
3.2.3 Scanning Electron Microscopy (SEM) 52
3.2.4 Energy Dispersive Spectroscopy (EDS) 53
3.2.5 Coating Thickness Tester 54
3.3 Computational Methods 54
3.3.1 Wave Function Theory Methods 54
3.3.1.1 Ab-initio Method 54
3.3.1.2 Semi-empirical Method 55
3.3.1.3 Electron Correlated Method 55
3.3.2 Density Function Theory Methods 55
Summary 56
References 57
Chapter No.4 59
Experimentation 59
4.1 Synthesis of Photo Anode materials 59
4.1.1 Synthesis of TiO_2 nanoparticles by sol gel technique 60
4.1.2 Synthesis of $CuInS_2$ Quantum dots 61

4.2 Film deposition/ electrode formation process 61
4.2.1 Electrophoretic deposition of TiO_2 nanoparticles 61
4.2.1.1 Optimization of different EPD process parameter 62
4.2.2 Electrophoretic deposition of $CuInS_2$ QDs 63
4.2.2.1 Applied voltage effect 64
4.3 Post heat treatment of Electrophoretically deposited film 64
4.3.1 TiO_2 deposited film heat treatment 64
4.3.2 Heat treatment of $CuInS_2$ QDs film deposited on TiO_2/FTO 64
4.4 Computational Analysis 65
4.4.1 Initial Geometries 65
4.4.2 Computational method detail 65
4.4.2.1 Optimization 65
4.4.2.2 Single Point Energy Calculations 66
4.4.3 Structure and Input File Set-Up 66
Summary 67
Chapter No.5 68
Results and Discussions 68
5.1 XRD Analysis 68
5.1.1 Effect of annealing temperature on CuInS2 crystallite phase 69
5.2 $CuInS_2$ Formation Mechanism 70
5.3 UV Vis Spectroscopy 71
5.3.1 Band gap and Particle size Calculations 71
5.4 SEM Results 73
5.4.1 Effect of Deposition Voltage 74
5.5 EDS Analysis 74
5.6 TiO_2 film thickness measurements 75
5.6.1 Applied Voltage 76
5.6.2 Distance between the Electrodes: 77
5.6.3 Deposition Time 78
5.6.4 Suspension aging time: 78
5.6.5 SEM Analysis of TiO_2 films 79
5.7 Computational Results 80
5.7.1 Band gap calculation from HOMO and LUMO of TiO_2 80
5.7.2 Theoretically calculated UV-Vis Spectra of TiO_2 81

5.8 Conclusions:..... 82
References..... 83
Annexure..... 84
Annexure I 97

List of Figures

Figure 1.1: Global Technical Potential of Different RES……...……...18
Figure 1.2: Different categories of Solar Cells…….…..21
Figure 1.3: Mechanism of excitation and emission…….……...24
Figure 1.4: Schematic of QDSSC and electron transfer mechanism…….……27
Figure 1.5: Schematic of electron transfer mechanism in QDSSC…….……28
Figure 3.1: Schematic diagram of electro deposition of film……..…47
Figure 3.2: Schematic diagram of Electrophoretic deposition (EPD)……..…..……48
Figure 3.3. Working of UV-Vis Spectroscopy…….……...…51
Figure 3.4: Working of X-Rays Diffraction (XRD)….……..…….52
Figure 3.5: Schematic diagram of Working of Scanning electron microscopy…..……..…53
Figure 4.1: Schematic diagram of Titanium dioxide (TiO_2) nanoparticles …….……..60
Figure 4.2: Schematic diagram of $CuInS_2$ quantum dots synthesis…….……61
Figure 4.3: TiO_2 NPs Suspension preparation for Electrophoretic deposition (EPD)…….62
Figure 4.4: $CuInS_2$ QDs suspension preparation for EPD……..…..……64
Figure 5.1: XRD pattern of (a) FTO coated glass. (b) As prepared TiO_2 (c) As prepared $CuInS_2$ and (d) $CuInS_2/TiO_2$ film……...…69
Figure 5.2:$CuInS_2$ QDs annealed at (A)300°C, (B)400°C and (c)500°C……....70
Figure 5.3: Image of synthesis process of $CuInS_2$ QDs…….……..71
Figure 5.4: UV- Vis absorption spectra of $CuInS_2$ QDs …….……...…72
Figure 5.5: OM and SEM images of $CuInS_2$ films deposited at FTO/TiO_2 substrate……73
Figure 5.6: Current density versus time curve at different voltages……..74
Figure 5.7: EDS spectra of $CuInS_2$ film deposited on TiO_2/FTO/glass substrate ….……75
Figure. 5.8: Effect of applied voltage on the thickness of TiO_2 Film …….……77
Figure 5.9: Effect of Distance on the thickness of TiO_2 film…….……...…77
Figure 5.1 0: Effect of deposition time on the thickness of the TiO2 film……78
Figure 5.11: Effect of suspension aging time on the thickness of the film…….……..…78
Figure 5.12 SEM images of TiO2 films…….…….79

Figure 5.13: Theoretically calculated UV-Vis spectra of TiO_2 Anatase phase……....81

List of Tables

Table 1.1: Comparison of different generations of Solar Cells……...……..…..….22

Table 1.2: Different types of Semiconductor Quantum Dots……..……..……..26

Table 2.1: Theoretical efficiencies of chalcopyrite solar cells…….…….…..36

Table 2.2: Comparison of deposition techniques for $CuInS_2$ QDs.……...……..37

Table 2.3: Particle sizes of $CuInS_2$ QDs.…….……...38

Table 2.4: Efficiencies comparison of Different Quantum Dots based solar cells……..…39

Table 3.1. Comparison of two electro-deposition techniques……...……..49

Table 4.1: Applied voltage, distance variation, deposition time and suspension aging at the same deposition time……...…...63

Table 4.2: voltage variation effect on the current density ……..64

Table 5.1: Applied voltage, distance variation and suspension aging effect…….…..75

List of Abbreviations

RES	Renewable Energy Sources
QDs	Quantum Dots
QDSSCs	Quantum Dots Sensitized Solar Cells
GHG	Green House Gas
GRS	Global Status Report
RE	Renewable Energy
TPES	Total Primary Energy Supply
EIA	Energy Information Administration
TWh	Terawatt-Hours
PV	Photovoltaic
TiO2	Titanium Dioxide
ZnO	Zinc Oxide
CdTe	Cadmium Telluride
CdS	Cadmium Sulfide
GaP	Gallium Phosphide
InP	Indium Phosphide
InAs	Indium Arsenide
$CuInS_2$	Copper Indium Sulfide
GaAs	Gallium Arsenide
GW	Giga Watt
Se	Selenium
Pb	Lead
CIGS	Copper Indium Gallium Diselenide

CTAB	Cetyltrimethylammonium Bromide
NREL	National Renewable Energy Laboratory
ED	Electro Deposition
EPD	Electrophoretic Deposition
XRD	X-rays Diffraction
SEM	Scanning Electron Microscopy
UV-Vis	Ultraviolet Visible
EDS	Energy Dispersive Spectroscopy
ARC	Anti-Reflection Coating
CB	Conduction Band
VB	Valance Band
HOMO	Highest Occupied Molecular Orbital
LUMO	Lowest Unoccupied Molecular Orbital
TCO	Transparent Conducting Oxide
FTO	Folurine Tin Oxide
IPCE	Internal Power Conversion Efficiency
CE	Counter Electrode

List of Journal/Conference Papers from this work

Journal Paper:

Hina Pervaiz, Zuhair S. Khan*

Synthesis andCharacterization of Electrophoretically deposited Chalcopyrite Copper Indium Sulfide ($CuInS_2$) Quantum dots (QDs) for Solar Cell Applications.

Thin Solid Films (Elsevier).

Conference Papers:

Hina Pervaiz, Maham Akhlaq, Zuhair S. Khan

The Influence of different Electrophoretic deposition (EPD) parameters on the thickness of the Titanium dioxide TiO_2 film.

3rd Conference on Emerging Materials and Processes **(CEMP 2017)** to be held on November 13th-14th, 2017 at School of Chemical and Materials Engineering (SCME), NUST, Islamabad.

Hina Pervaiz, Zuhair S. Khan

A Study on the Electrophoretic deposition parameters of TiO_2 nanoparticles, Synthesized by Sol gel Technique

International Conference on Solid State Physics 2017 to be held on December 10^{th}-14^{th}, 2017 at Center of Excellence in Solid State Physics, PU, Lahore

Chapter No.1
Introduction

1.1 Need of Renewable Energy Resources

In last decades, an increase in world population and industrialization is causing a drastic increase in the consumption of energy. As a result, rate of diminishing of fossil fuel reserves was increased to meet up this need. The significant improve in the consumption of fossil fuel opposing impact on the environment which leads to increase in risks of global climate change [1]. Due to climate change, it is becoming politically more acceptable in developing countries to seek environmental improvement. The need of the hour is to adopt the new policies about use of alternative energy resources for sustainable production, waste management and reduced emission of greenhouse gas. According to the survey it is observed that fossil fuel and cement hold increasing shares in global CO_2 emission [2, 3].

Studies show 31% increase in overall CO_2 levels in the past 200 years. Only deforestation added 20 Gt of Carbon into the environment since 1800. Methane gas concentration is also increased which is a major cause of ozone layer depletion. Raise in global surface temperature was observed about 0.4–0.8 °C in the last century [4]. Above on quarter (~ 37%) global GHG emissions is caused directly and indirectly by industry, of which over 80% is due to energy use. Promotion of unpolluted and clean energy is required readily because the extreme use of fossil fuel has created global warming by CO_2 [5].

Energy resources are divided into three main classes: fossil fuels, nuclear and renewable energy sources (RES). RES has a great potential and it plays a significant part in the global energy. Currently, renewable energy sources contribute around 24.3% of the overall world energy production from all the sources [6]. The percentage of renewable energy sources is predictable to increase very significantly up-to 30–80% in 2100 [7]. RES have the ability to produce clean energy free or nearly zero present emission of greenhouse gases [8]. Nowadays some of the energy technologies i.e. hydropower, wind energy, solar energy biomass energy etc. are contributing to the world energy. The energy attained from all these sources are reliable, affordable and environmentally sustainable.

1.2 Development of Renewable Energy Resources

The performance of renewable energy assets is more notable from the last few years. In 2012, renewable energy delivered expected 19% of the world-wide total energy consumption, and it increased to 23.7% in 2014. In 2015, around 103GW of renewable power capacity was built while in 2013 and 2011 it was 86GW and 80.5GW respectively [9]. It has been stated in the global status report (GSR) on renewables in 2016 that the most significant growth in sustainable energy arisen in the power area with the over-all aptitude exceeding 1560 GW from all the sources. The investment on the renewable energy resources has also enlarged meaningfully from the previous ten years. A total of 40 billion USD was invested by global investors in the area of renewable energies in 2004. The investment kept on increasing and reached 279 billion USD in 2011 but after 2011, it began decreasing. This decline is due to the drastic reduction in technology costs especially for solar PV, which saw a record of new installations in despite a reduction in dollar investment. The capital cost of the wind and solar PV has suddenly dropped in the last few years. In 2014, wind and solar PV were the main sources of renewable energy, producing 48GW and 46GW respectively.

The potential of different clean energy sectors is vast as compared to the non-renewable total primary energy supply (TPES) as shown below.

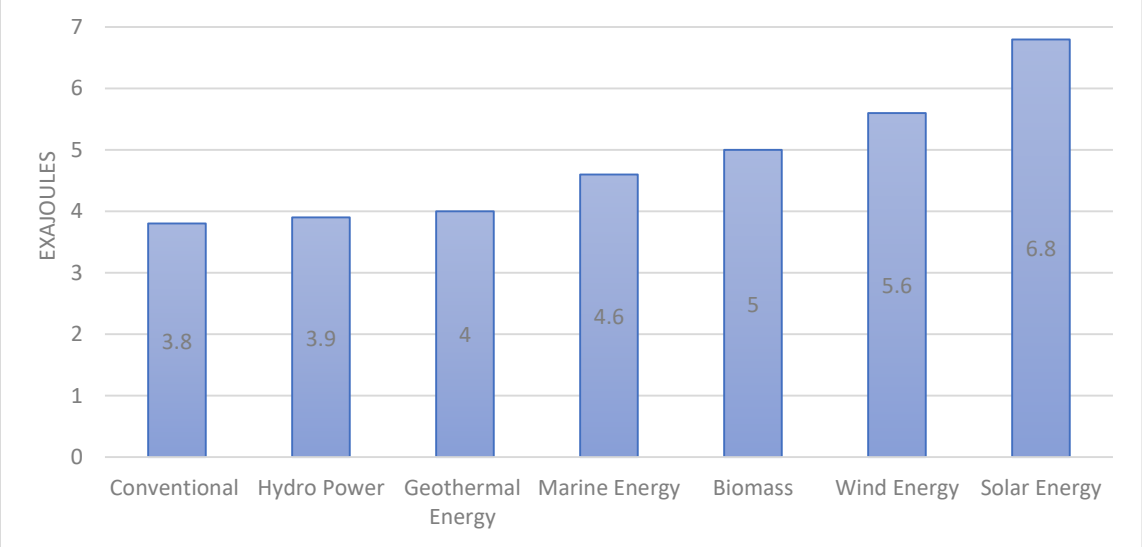

Figure 1. 1: Global Technical Potential Of Different Renewable Energy Sources Compared With Conventional Annual TPES [10].

The above figure shows that among the renewable energies solar energy has the highest potential, if we considering only the surface land. It can also be saw from the graph that world-wide non-renewable total primary energy supply (TPES) is lower than the nominal potential of all other clean energy resources [10].

1.3 Solar Energy

As far as clean renewable energy resources are considered solar is the best plentiful source. The sun emits 3.8×10^{23} kW energy, around 1.8×10^{11} kW received by earth [11]. According to national renewable energy laboratory (NREL), sunlight received on the surface of the earth within one hour (4.3×10^{24}J) is sufficient to encounter the yearly energy requirements of the people worldwide [12]. Compared to the present energy utilization on Earth (> 20 TW) the sun supplies sufficient energy to encounter our use. There is huge latitude to harness accessible solar energy, either by using solar PV devise, solar water heating systems or solar concentrators. The importance of solar energy is not neglected because of its benefits. There are several insulated regions in the world no other source of energy is available but solar irradiation is abundant. By utilizing this source production on energy (electricity) in these areas are quite possible. The other major advantage of the solar energy is it limit environmental reform as it yields no carbon emission. Solar energy is play vital role to meet the commitments made by U.S. to reduce the emission by 26-28% within 2005 to 2025.

Solar energy is capable for warming systems and power production using PV devices. These devices are usually fitted on the roof top of the individual buildings. According per U.S EIA this is valuable sources of power of household and viable industries.

1.3.1 Solar Photovoltaic Technology

Solar cells work by converting light photons directly into electricity (voltage) by photoelectric effect. PV effect depends on the interaction of the photons, with energy equal to, or greater than the energy of the band gap of the solar cell materials [13]. Due to this effect, solar cells also called photovoltaic (PV) cells. This Photovoltaic effect was defined in 1954, when scientists at Bell lab discovered that silicon created an electric charge when exposed to the sunlight. After that, silicon has become the most used material for the applications of solar cells.

1.3.2 Physics of Photovoltaic

Photovoltaic devices work on the phenomena of charge separation occurring at interface of two different materials. These materials have different conduction mechanism. Solar photovoltaic can be defined as the direct conversion of solar radiation into electric current. The materials that exhibit photoelectric effect absorb energy in form of photons of light and release free electrons. The separation or flow of these free electrons causes electric current to be generated. The working of a solar cell can be divided into three simple steps: 1) Absorption of light 2) Charge separation 3) Charge collection. The chemical and physical processes behind these basic steps are different in different types of cells and depend on the materials used. Efficiency of each of these steps affects the efficiency of the solar cell. Efficiency can be maximized by selecting compatible materials to the cell design. Generally, semiconductor wafer creates an electric field when treated to form a positive side and a negative side (p and n junctions). When solar cell is irradiated to light, electrons are knocked out from semiconductor atoms. If the circuit is completed by contacting electrical conductors attached to both sides (positive and negative), electric current is generated.

Photovoltaic has been ruled by p-n junction devices which are usually made up of silicon but development of third generation solar cells challenged this dominance of solid state junction devices. The current photovoltaic production includes many different technologies such as wafer based silicon and various thin film approaches. These two technologies are further categories, as shown in the Figure 2.

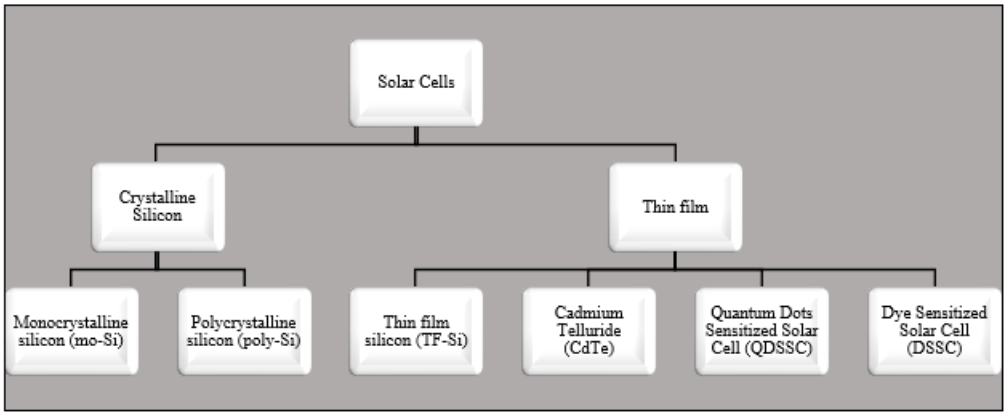

Figure 1.2: Different categories of Solar Cells.

1.4 Generations of Solar cell

The range of current and possible future solar based devices are distributed into three different generations.

1.4.1 First generation solar cell

1st generation solar cells are based on single or polycrystalline silicon wafers. These cells have achieved efficiency unto 24.7 % at lab scale while 22.7% on module based. A standard silicon solar cell consists of a metal substrate, a p-n junction formed by p-doped and n-doped silicon layers, an anti-reflection coating (ARC), and a collector for current. This generation of solar cell has many advantages such as good performance and high stability. Although the cost of production has decreased over the passage of time, but first generation solar cells are still very costly. The major drawback of these 1st generation technologies is the requirement of the high energy for their production. Need of the highly pure material for the manufacturing of the wafer is the other disadvantage of these technologies [14].

1.4.2 Second Generation solar cell

This technology is based on thin film solar cell such as Amorphous Silicon solar cells. Cadmium Telluride (CdTe), and Copper Indium Gallium diselenide (CIGS) based solar cells are also part of this technology. They are fabricated by depositing multiple layers to create a p-n junction. The efficiency of the 2nd generation solar cells is lower as compared to 1st generation solar cell but these are cost effective. Recently the calculated efficiency is up to 20% [15]. The major disadvantage of this kind of solar cells are it produce toxic material like cadmium or selenium in small amount which reduce the importance of these thin film based solar cells technology. While the amorphous silicon solar cells have very low 4-5% efficiency [16]. 2nd generation solar cells are low material consumption. The main reasons behind this kind of solar cells are simple fabrication technology and limit use of silicon wafers due to these reasons manufacture costs of these devices are low as compared to the first generation.

1.4.3 Third Generation solar cell

Third generation solar cells include. **A)** Quantum dots based solar cells, **B)** dye sensitized solar cells, **C)** organic or polymer based solar cells and **D)** concentrated solar cells. The efficiency of 3rd generation solar cells are quite low 12% as compared to 1st and 2nd

generation solar cells [17]. Different light-absorbing layers are used with different band gaps to collect as much of the solar spectrum. The price increase is due to the many steps required and the complexity of fabrication. Organic solar cells or polymer solar cells offer some advantages as they are simple and quick to fabricate, as well as inexpensive. While there are many benefits of organic solar cells the performance and stability are still very limited when compared with first and second generation solar cells.

Table 1.1: Comparison of different generations of Solar Cells.

	Advantages	Drawbacks
1st Generation	• High efficiency. • Developed technology.	• High manufacturing cost. • Requirement of highly purified material.
2nd Generation	• Low cost substrate. • High absorption coefficient. • Low cost synthesis techniques as compare to Si based.	• Low efficiency as compare to 1st generation. • Material are hard to find. • Fabrication processes contaminate the environment.
3rd Generation	• Minimal cost. • Raw material is easy to find. • Easier fabrication techniques rather than other two generations. • High theoretical efficiency.	• Liquid electrolyte. • Low efficiency.

DSSCs and QDSSCs are technical and economical alternatives for expensive p-n junction solar cells. These allow using less purified starting materials as they are not much sensitive to the impurities and defects while solid junction solar cells require high purity materials. This makes production of QDSSCs less costly and the energy payback period is shorter [18]. Most of the materials being used in DSSCs and QDSSCs are non-toxic. There is no health concern related to their production and there are minimal protective measures to be seen during their production. Table 1.1: shows the various advantages of 3rd generation over the 1st and 2nd generations of solar cells.

1.5 Quantum dots sensitized solar cells (QDSSCs)

1.5.1 WHY Quantum Dots

Semiconductor quantum dots (QDs) are of vital importance due to their distinctive dimension dependent properties and their possible applications as building blocks in nanoelectronics, nano-sensors, and in biology. From the last few years these semiconductor QDs has gain attention because of their narrow and intensive emission spectra. Nanoscale semiconductors have received attention as a visible candidate for use as electrode material in 3rd generation PV devices because of their advantages of tunable band gap, broad absorption spectrum, photo stability, size-dependent optical properties and low cost. [19]. While bulk semiconductor electrode materials (silicon, CdS, $CuInS_2$, GaAs) are used in 1st and 2nd generations of solar cells but these materials didn't show good stability when exposed to light. Ideal photovoltaic devices have broad absorption spectrum in visible region with efficient charge separation and charge transport [20].

1.5.2 Physics of Quantum Dots

The physics of quantum dots has been a very active and fruitful research topic because of their exceptional properties such as wide absorption spectrum. This kind of materials have also narrow photoluminescence spectra, and high quantum yield. Both optical as well as electrical properties of these QDs are dependent their sizes and shape. Generally, as the size of the particle decreases, the difference in energy between the HOMO and the LUMO increases. Greater amount of energy is required to stimulate the electron, and greater energy is emitted when the electron come back to its stable state, resulting in a colour change from red to blue. Hence, quantum dots made from the same material can emit over a wide range of energy spectrum simply due to the change in the dot size. The band gap can be further tuned by carefully controlling the nature of the materials forming up the quantum dot.

1.5.3 Working of Quantum Dots

When light photon is supplied to an atom, electrons present in the atom are excited and move to higher state. When these excited electron returns to its stable state, an amount of energy proportional to the energy difference of the two levels is emitted as light corresponding to its frequency. These dots work in the similar manner, when excited, the wavelength of light emitted is controlled by the relationship between the size of the nano-

crystal and the level of confinement (quantized energy levels) of the electrons within the particle.

Thus, Quantum Dots have the distinctive capability to radiate light showing the complete spectral of colours from the similar basic material based specially on the size of the particles of that material being excited.

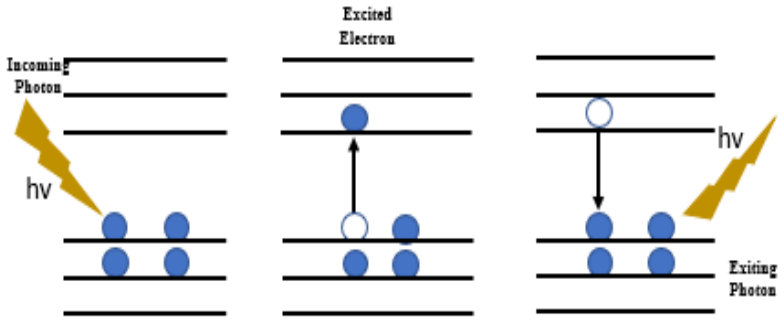

Figure 1.3: Mechanism of excitation and emission due to radiative recombination of an electron and hole.

The largest quantum dots yield the highest wavelengths, while the smallest dots yield reduced wavelengths [21]. A small dot has a higher band gap, so it takes more energy to stimulate it; because there is a direct relation between the frequency of emitted light is and the energy. Smaller quantum dots produce higher frequencies (and lower wavelengths). Larger dots have more spaced energy levels, so they give out lower frequencies (and higher wavelengths).

1.5.4 Bandgap Calculation

As quantum dots are electromagnetic absorbers or emitters with tunable band gap. Therefore, the distance between the HOMO and LUMO level increases in energy as the size of a quantum dot decreases and vice versa. A small size dot has a large gap and absorbs high energy photons (shorter wavelengths or bluer light), while a larger quantum dot has a narrow band gap. Hence the wavelength absorption or emission properties of a quantum dot depend on the size of the dot.

The band gap of a quantum dot can be calculated approximately using Brus Equation. Brus provided the first theoretical calculation for semiconductor QDs stand on “effective

mass approximation" (EMA). This approximation contains the exciton confinement to a spherical volume of the crystallite and the mass of electron and hole is substituted by their effective masses.

$$E_g^{nano} = E_g^{bulk} + \frac{\hbar^2\pi^2}{2r^2}\left(\frac{1}{m_e^*} + \frac{1}{m_h^*}\right) - \frac{1.8e^2}{4\pi\varepsilon\varepsilon_0 r}$$

$E_g{}^{nano}$is the band gap energy of nanoparticles (QDs), $E_g{}^{bulk}$is the band gap energy of bulk semiconductor, m^*_e and m^*_h are the effective mass of electron and hole, respectively, ε is the relative permittivity of the solid, ε_0 is the permittivity, *e* is the charge and r is the quantum dot radius.

1.5.5 Quantum Dots Solar cells and their materials

The study of semiconductor quantum dots began in the late '80s and early '90s and have since become an active research topic both experimentally and theoretically [22]. Quantum dot solar cells have gained substantial attention due to their prominent factors such as low production costs, tunable band gap, quantum confinement effects and the main property that enhances their efficiency due to multiple excitons generation [23]. Several configurations of quantum dots solar cells have been proposed and demonstrated such as Schottky cell, Depleted heterojunction cell and hybrid polymer cell. But focus will be on depleted heterojunction cell. This device is consists of three major parts,1st is oxide layer (TiO_2 or ZnO) fabricated on conducting glass, on top of oxide layer a multilayer of QDs is deposited and the other contact of the device is a metal (Au) layer [24]. This device has greater efficiency than others due to the nanostructure thin film that act as electron conducting phase and helps in extracting the electron from the quantum dots.

The capability to alter optical and electronic properties of semiconductor materials by changing the crystallite size and using the multi-components has become a hallmark of quantum dots. Many types of compound semiconductor (II-VI, I-III-IV, IV-VI) QDs have been developed with tunable properties since late 18s, shown in Table 1.2 [25]:

Table 1.2: Different types of Semiconductor Quantum Dots.

Groups	Quantum Dots
II-VI	CdS, CdSe, CdTe, ZnSe
III-V	InP, InAs
IV-VI	PbS, PbSe
I-III-V	CuInS2, CuInSe

1.5.5.1 Components of QDSSCs:

A QDs solar cell consists of two electrodes (anode and counter electrode) sandwiching an electron extraction layer (usually nanoparticles) and QD film [20]. Nanoparticles provide a path for photo-excited electrons towards the electrodes. QD films are photoelectron generators by absorbing incident light. Electrons are guided towards anode and holes are collected at gold contact also called cathode. This system generates photocurrent [20]. These types of heterojunction solar cells are called quantum dot sensitized solar cells. The schematic of electron transfer and heterojunction or QDSSC is shown in the Figure 1.4.

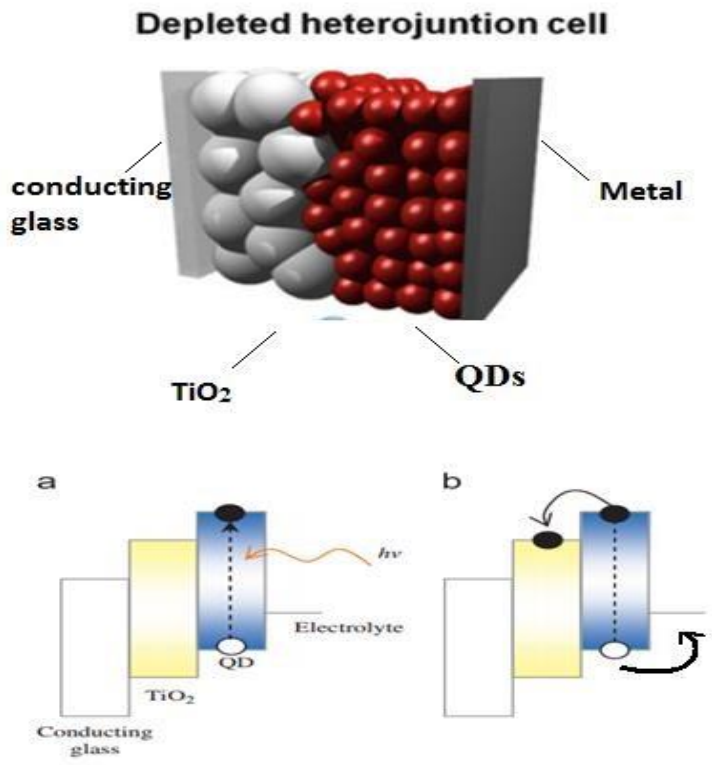

Figure 1.4: Schematic of QDSSC and electron transfer mechanism.

1.5.5.2 Role of Photoanode in QDSSCs

Photoanode of QDSSC consists of a conducting oxide (TCO) substrate on the top of which is deposited a semiconducting oxide layer (generally TiO_2) and the QDs sensitizer. In quantum dots sensitised solar cell photoanode plays three important roles:

1. It provides the medium for the QDs adsorption or other nanomaterials.
2. It accepts the QDs into conduction band.

3. It transports electron towards the transparent conducting oxide (TCO) for the injection in external circuit and then into counter electrode as shown in Figure 1.5.

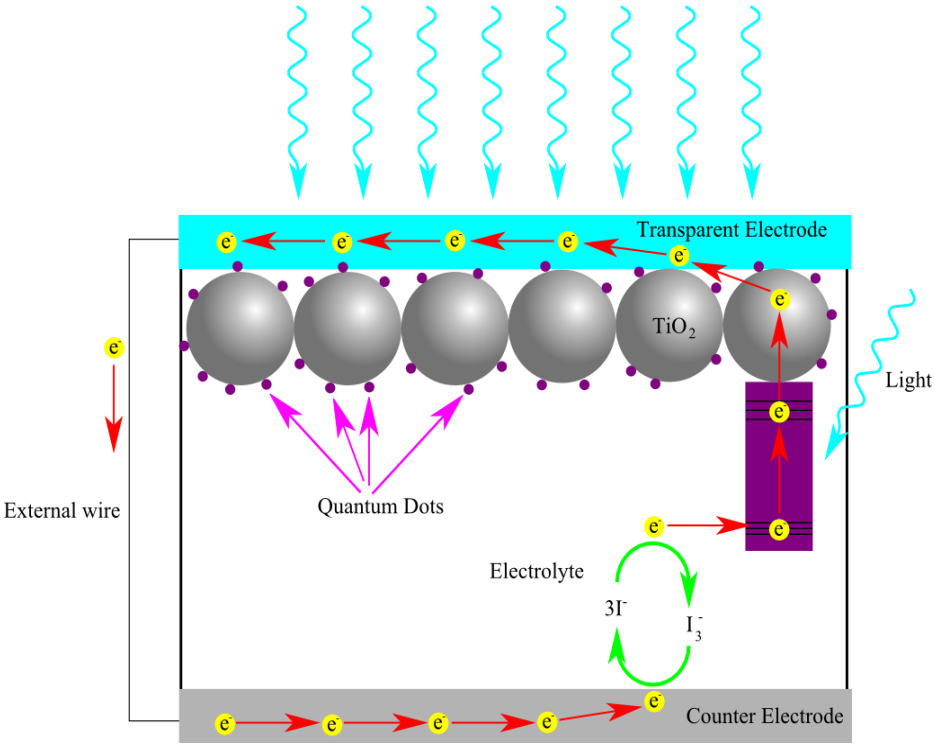

Figure 1.5: Schematic of electron transfer mechanism in QDSSC.

The metal oxide semiconductor nanoparticles have gained great attention due to their wide potential applications in solar cells, and optoelectronic devices [26, 29]. Thus, wide band gap materials such as TiO2 are used as electrode material which act as an electron transporting media [27].

Summary

In this chapter an introduction to the total energy resources and the world-wide energy consumption is discussed. The need to move on green energy resources due to increase in risks of global climate change is also described here. The global surface temperature has raised by 0.4–0.8 °C in the last century due to consumption of fossil fuel and emission of CO_2 and other hazardous gases. Nowadays some of the renewable energy technologies are contributing to the world energy. The energy attained from all these sources are reliable, affordable and environmentally sustainable. Solar energy is one of the most reliable technology because the total solar radiation that received on the surface of the earth within

one hour is enough to meet the annual energy needs of the people worldwide. The current photovoltaic production includes many different technologies such as wafer based silicon and various thin film approaches such as thin film silicon solar cells, cadmium telluride thin film solar cells, and include 3rd generation solar cells (DSSCs, QDSSCs). The experimental efficiency of 3rd generation solar cells are quite low 12% as compared to 1st and 2nd generation solar cells but theoretical efficiency is larger. Quantum dot solar cells (QDSSCs) have gained considerable attention over the other solar cells due to their prominent factors such as low production costs, tunable band gap, quantum confinement effects and the main property that enhances their efficiency due to multiple excitons generation. Several configurations of quantum dots solar cells have been proposed and demonstrated such as Schottky cell, Depleted heterojunction cell and hybrid polymer cell. But focus will be on depleted heterojunction cell. This device is consists of three major parts,1st is oxide layer (TiO_2 or ZnO) fabricated on conducting glass, on top of oxide layer a multilayer of QDs is deposited and the other contact of the device is a metal (Au) layer [24].This device has greater efficiency than others due to the nanostructure thin film that act as electron conducting phase and helps in extracting the electron from the quantum dots.

References

[1] S. Farhad, M. Saffar-Avval, M. Younessi-Sinaki, Efficient design of feedwater heaters network in steam power plants using pinch technology and exergy analysis, International journal of energy research, 32 (2008) 1-11.

[2] Y. Pan, R.A. Birdsey, J. Fang, R. Houghton, P.E. Kauppi, W.A. Kurz, O.L. Phillips, A. Shvidenko, S.L. Lewis, J.G. Canadell, A large and persistent carbon sink in the world's forests, Science, 333 (2011) 988-993.

[3] G.A. Meehl, T.F. Stocker, W.D. Collins, A. Friedlingstein, A.T. Gaye, J.M. Gregory, A. Kitoh, R. Knutti, J.M. Murphy, A. Noda, Global climate projections, (2007).

[4] H. Le Treut, U. Cubasch, M. Allen, Historical overview of climate change science, 2007.

[5] D. Hall, Cooling the greenhouse with bioenergy, Nature, 353 (1991) 11-12.

[6] M. Pacesila, S.G. Burcea, S.E. Colesca, Analysis of renewable energies in European Union, Renewable and Sustainable Energy Reviews, 56 (2016) 156-170.

[7] I.B. Fridleifsson, Geothermal energy for the benefit of the people, Renewable and Sustainable Energy Reviews, 5 (2001) 299-312.

[8] N. Panwar, S. Kaushik, S. Kothari, Role of renewable energy sources in environmental protection: a review, Renewable and Sustainable Energy Reviews, 15 (2011) 1513-1524.

[9] A. Hussain, S.M. Arif, M. Aslam, Emerging renewable and sustainable energy technologies: State of the art, Renewable and Sustainable Energy Reviews, 71 (2017) 12-28.

[10] R. Guerrero-Lemus, J.M. Martínez-Duart, Renewable Energies and CO2: Cost Analysis, Environmental Impacts and Technological Trends-2012 Edition, Springer Science & Business Media2012.

[11] B. Parida, S. Iniyan, R. Goic, A review of solar photovoltaic technologies, Renewable and Sustainable Energy Reviews, 15 (2011) 1625-1636.

[12] J. Tsao, N. Lewis, G. Crabtree, Solar FAQs, US department of Energy, (2006).

[13] D.Y. Goswami, S. Vijayaraghavan, S. Lu, G. Tamm, New and emerging developments in solar energy, Solar energy, 76 (2004) 33-43.

[14] J. Zhao, A. Wang, M.A. Green, F. Ferrazza, 19.8% efficient “honeycomb” textured multicrystalline and 24.4% monocrystalline silicon solar cells, Applied Physics Letters, 73 (1998) 1991-1993.

[15] P. Jackson, D. Hariskos, E. Lotter, S. Paetel, R. Wuerz, R. Menner, W. Wischmann, M. Powalla, New world record efficiency for Cu (In, Ga) Se2 thin-film solar cells beyond 20%, Progress in Photovoltaics: Research and Applications, 19 (2011) 894-897.

[16] B. Li, L. Wang, B. Kang, P. Wang, Y. Qiu, Review of recent progress in solid-state dye-sensitized solar cells, Solar Energy Materials and Solar Cells, 90 (2006) 549-573.

[17] A. Hagfeldt, Brief overview of dye-sensitized solar cells, Ambio, 41 (2012) 151-155.

[18] C.-L. Lee, W.-H. Lee, W.-T. Li, C.-H. Yang, P.-C. Kao, StSt/TiO 2 compact layer/TiO 2 triple-layered conducting substrates for large active area dye-sensitized solar cells, Materials Research Bulletin, 48 (2013) 2625-2629.

[19] A.M. Smith, S. Nie, Semiconductor nanocrystals: structure, properties, and band gap engineering, Acc. Chem. Res, 43 (2010) 190-200.

[20] C.J. Murphy, J.L. Coffer, Quantum dots: a primer, Applied Spectroscopy, 56 (2002) 16A-27A.

[21] E. Arthur, A. Lucky, Synthesis and characterization of Cds and Cdse quantum dots by UV-VIS spectroscopy, Journal of Emerging Trends in Engineering and Applied Sciences (JETEAS), 4 (2013) 273-280.

[22] D.K. Pandurangan, K. Mounika, Quantum dot aptamers-an emerging technology with wide scope in pharmacy, Int J Pharm Pharm Sci, 4 (2012) 24-31.

[23] K. Park, H.J. Yu, W.K. Chung, B.-J. Kim, S.H. Kim, Effect of heat-treatment on CdS and CdS/ZnS nanoparticles, Journal of materials science, 44 (2009) 4315-4320.

[24] S. Park, B. Kim, O. Yavuzcetin, M.T. Tuominen, T.P. Russell, Ordering of PS-b-P4VP on patterned silicon surfaces, ACS nano, 2 (2008) 1363-1370.

[25] C. Yuan, The Study of II-VI Semiconductor Nanocrystals Sensitized Solar Cells, KTH Royal Institute of Technology, 2012.

[26] C.S. Lim, J.H. Ryu, D.-H. Kim, S.-Y. Cho, W.-C. Oh, Reaction morphology and the effect of pH on the preparation of TiO 2 nanoparticles by a sol-gel method, Journal of Ceramic Processing Research, 11 (2010) 736-741.

[27] N. Venkatachalam, M. Palanichamy, V. Murugesan, Sol–gel preparation and characterization of nanosize TiO 2: its photocatalytic performance, Materials Chemistry and Physics, 104 (2007) 454-459.

[28] A.R. Boccaccini, I. Zhitomirsky, Application of electrophoretic and electrolytic deposition techniques in ceramics processing, Current Opinion in Solid State and Materials Science, 6 (2002) 251-260.

[29] S. Nadzirah, K. Foo, U. Hashim, Morphological reaction on the different stabilizers of titanium dioxide nanoparticles, Int J Electrochem Sci, 10 (2015) 5498-5512.

[30] R.S. Sabry, Y.K. Al-Haidarie, M.A. Kudhier, Synthesis and photocatalytic activity of TiO2 nanoparticles prepared by sol–gel method, Journal of Sol-Gel Science and Technology, 78 (2016) 299-30

Chapter No.2

Why $CuInS_2$ QDs Based Photo Anode for QDSSCs?

2.1 Photo Anode materials for QDSSCs

As mention in the previous chapter, photo anode of QDSSC consists of a transparent conducting oxide (TCO) substrate, a semiconducting oxide layer (generally TiO_2) and the layer of QDs material. So, the selection of metal oxide layer and QDs material is important because to implement as in case photo anode, the metal oxide based materials are utilized for QDs adsorption which must have certain properties like larger surface area, high porosity for enough mass transport through diffusion phenomenon and suitable QDs associated band gap for electron injection and rapid transport.

2.1.1 Metal Oxide materials

Nano scale materials have received attention as a visible candidate for use as electrode material in 3rd generation PV devices [1]. A verity of metal oxide is used as an anode material for solar cells.

2.1.1.1 Titanium dioxide (TiO_2)

Nano scale TiO_2 is a multifunctional material that has its applications as anode material in QDSSCs and many other fields. Titanium dioxide is the most important candidate in thin film technology due to its unique properties, e.g. non-toxicity, easy availability, and long-term chemical stability under several conditions [2, 3]. Titanium dioxide is an n-type semiconductor and has different polymorphs like brookite, anatase, and rutile at an ambient pressure [4]. Anatase is thermodynamically bearing the highest band gap energy of 3.2eV and exhibits higher photo catalytic activity than the other TiO_2 forms [5]. The optical and the photo catalytic properties of TiO_2 nanoparticles have further dependence to the size, morphology and the crystalline phase of the prepared material [6]. By tuning the size and the crystallographic phase, performance of the nanostructured material can be improved [7].

The electron transfer mechanism in TiO_2 starts with the absorption of photon. The excitation occurs when the photons with energy equal to or greater than the band gap of TiO_2 is absorbed [8]. This allows the formation of an electron-hole pair on the surface of TiO_2 molecule. A hole (positive) is created in Valence band (VB) and an excited electron is promoted to the Conduction Band (CB). The electrons in Excited-state can get trapped in metastable states on surface, dissipate the input energy as heat due to recombination or react with electron acceptors/donors on semiconductor surface [9]. These electrons regenerate sin nanosecond timescale range. The purity of the semiconducting material is not as crucial as in other generation of solar cells. Anatase possesses the energy band 3.2 eV, which corresponds to 400 nm in electromagnetic spectra. About 40 % solar photons belongs to visible region.

2.1.2 Quantum Dots Materials

Currently, binary and ternary semiconductors materials such as group III-V, II-VI and I-III-IV are used for the quantum dots solar cell. But the excessive use of some materials is not feasible for environment due to the presence of toxic elements so the selection on QDs materials is crucial for the green energy devices.

2.1.2.1 III-V, II-VI groups based QDs

The binary semiconductors materials include Gallium Phosphide (GaP), Gallium Arsenide (GaAs), Indium Phosphide (InP), and Indium Arsenide (InAs) from group III-V. While II-IV semiconductors include Cadmium Sulphide (CdS), Cadmium Selenide (CdSe), and Cadmium Telluride (CdTe) [9]. Synthesis of III-V materials at nano-scale level is difficult due to achieving crystallinity. Relatively, the II-IV semiconductor nanoparticles are easy to synthesize. The facile synthesis of the latter is one of the reasons, why a lot of scientific work has been done on these materials.

Cadmium Sulphide (CdS) is a vastly studied semiconductor material which has found diverse applications [10, 11]. The precursors for CdS are easily available and are readily crystallized due to the strong ionic bonding between cadmium and sulfide ions [11]. This material offers a characteristic wide and direct band gap varying from 2.40 eV to 2.5 eV [12]. At room temperature the band gap of bulk CdS is reported to be 2.4 eV. This

corresponds to the wavelength of 520 nm which lies in the visible range. The band gaps of quantum dots (QDs) of CdS are expected to range from visible region to ultraviolet.

A variety of colloidal semiconductor QDs are easily grown in solution phase [13]. Colloidal synthesis of CdS nanoparticles commonly involves two methods [14]:

- Organometallic synthesis using ligands
- Reverse micelles

Organometallic synthesis of CdS nanoparticles was first reported in 1983 [15]. This method involves the injection of organometallic precursors into the growth solution [13]. The precursors are then decomposed at high temperatures with the solvent and a stabilizing agent [14]. This method produces very narrow size distribution (5%) of QDs, which shows good control of the size of the particles and produces high quality, mono dispersed particles with highly reproducible and efficient luminescence qualities [13]. Nano crystals produced thus can be merged into polymer and sol-gel hosts for their application [15].

Reverse micelles method is the second common method used for the colloidal synthesis of QDs. It is less complicated and is more reproducible as compared to the organometallic synthesis because it does not involve the ligand exchange [13]. This is a wet synthesis technique and achieves good mono-dispersity and size distribution. The process is very simple and does not need special instruments or extreme conditions. However, this technique requires the presence of surfactant during synthesis [11]. Surfactants are substances which produce spheroidal aggregates in organic solvents having a polar core that solubilizes water. These aqueous aggregates in organic solvents are called reverse micelles [11, 16]. For the synthesis of CdS QDs, Cetyltrimethylammonium bromide (CTAB) has been studied as surfactants.

But there are some drawbacks, the excessive use of these binary materials is not feasible for biosphere due to the presence of toxic elements such as cadmium (Cd), Selenium (Se) and lead (Pb) [17]. Among these group, the scarcity of gallium (Ga), tellurium (Te) is another hurdle that prohibited their commercial use.[18].

2.1.2.2 I-III-IV groups based QDs

Group I-III-IV are emerging material for solar cells due to their high absorption coefficient in visible light range, direct band gap, and low toxicity. In the last 5 years, a large number of publications have been reported in the literature with emphasis on $CuInS_2$ and $CuInSe_2$ based nanoparticles [18-20]. In principle, solar cell based on sulfur chalcopyrite have the same potential for high efficiencies as those based on selenium.

The achieved efficiency of the $CuInS_2$-based solar cells is low. Based on the fundamental considerations the greatest theoretical efficiency of $CuInS_2$ is superior to other ternary such as $Cu(In, Ga)Se_2$, $CuInSe_2$, and $CuGaSe_2$ solar cells. (Table 2.1)

Table 2.1: Theoretical efficiencies of chalcopyrite solar cells [21].

Material	Band gap	Theoretical efficiency
$CuInSe_2$	1.04	25%
Cu (In, Ga) Se_2	1.21	27.5%
$CuInS_2$	1.53	28.5%
$CuGaSe_2$	1.68	26%

There are many methods employed to synthesize the I-III-IV nano crystallite. In solar cell applications, solution based synthetic techniques have gained consideration due to low cost and large scale fabrication of thin films [22]. Generally, two types of solution synthesis approaches are used 1) precursor solution based, 2) nanoparticle based [23]. In precursor solution based synthesis approach metal chloride, nitrates, acetates are dissolved in an organic solvent with the addition of the polymer binder, further prepared solution is coated onto the conducting substrate, and then annealed in the inert environment. While in second approach, nanoparticles are first synthesized and then re-dispersed in volatile organic material to prepare the colloidal suspension/ ink and the ink is printed on the substrate. After being coated on the substrate the film is heat treated.

2.2 $CuInS_2$ QDs based Photo Anode for QDSSCs

Copper indium sulfide has been highlighted as an active next-generation solar cell material due to its nontoxicity and cost effectiveness over the past few years. The major shift on ternary $CuInS_2$ is due to wide range of electronic and optical properties, it has a direct band gap of around 1.54eV, and high absorption coefficient ($\sim 10^5$ cm^{-1}). Furthermore, the constituent elements of $CuInS_2$ are non-toxic and exhibit stability under solar spectrum also as compared to binary compounds. All these properties make $CuInS_2$ a potential substitute to replace all the costly and toxic photovoltaic materials. So, Copper indium sulfide ($CuInS_2$) is a promising alternative to the II−VI systems (CdS, CdSe, CdTe).

There are many methods employed for the production and deposition of the copper indium sulfide nano crystallite such as molecular source decomposition and the solution synthesis [24]. A comparison of above discussed techniques is given in the table 2. 2.

Table 2. 2: Comparison of different production and deposition techniques for $CuInS_2$ QDs [25].

Molecular Source Decomposition	**Solution Synthesis**
❖ Use to produce QDs ❖ Expensive starting materials. ❖ Different Methods: ➢ Thermolysis ➢ photolysis ➢ Single source evaporation	❖ Widely adopted for preparing the nanostructured. ❖ Low cost process without involving any expensive machine. ❖ Synthesized precursor solution can be used for film deposition.

To control the size of the QDs much work has been done recently [16]. A variety of methods have been employed such as thermolysis, photolysis, single source evaporation and many solutions based techniques. The below Table 2.3 .shows the comparison of synthesis techniques verses particles sizes.

Table 2. 3: Particle sizes of $CuInS_2$ QDs and nano crystallite synthesized with different chemical routs [26-29].

Methods	Particle Sizes	References
Molecular Source Decomposition:	3-30 nm 2 nm 1.8-2.8 nm	Castro et al. (2004) Nairne et al. (2006) Kino et al. (2008)
Solution Synthesis:	20–25 nm 27 nm 3.5–7.5 nm	Lu et al. (2000) Wei and Mu. (2005) Nakamura et al. (2006)

In this thesis, major research targets are cost reduction and smallest size of the $CuInS_2$ particles while smallest sizes are attained by molecular source decomposition techniques, but these are not cost effective due to high cost of equipment and precursors used. Cost reduction is mainly related to the use of efficient and simple processing techniques Cost reduction is mainly related to the use of efficient and simple processing techniques so, to attain the minimum sizes of the CuInS2 we will use solution synthesis route which is a great challenge.

2.3 Efficiency Comparison of different QDSSCs

Currently, PV market is dominated by the first generation of solar cells, but the cost of these cells is extremely high. These cells have achieved efficiency unto 24.7 % at lab scale while 22.7% on module based Alternative technologies to produce PV devises have been widely researched already foe many years [30]. Second generation PV technologies have achieved efficiency up to 20% while the efficiency of the third generation is quite low, but

this technology is highly cost effective. Efficiencies comparison of QDs based solar cells are shown in the Table. 2.4.

Table 2.4: Efficiencies comparison of Different Quantum Dots based solar cells [31-35].

Materials	Efficiencies	References
PbS, PbSe	Up-to 9.2%	Labelle, A. J et al. (2015)
CdS	3.2%	Li, Ling, et al. (2011)
CdSe	5.4%	Zhang, H., et al. (2012)
InP	2.57%	Yang, Suolong, et al. (2015)
$CuInS_2$	2.52%	Pan, Zhenxiao, et al. (2014)

However, there is still a gap between the performance of copper based QD solar cells and that of conventional cadmium- and lead-QD based devices, which might be due to the lack of understandings on the control of the carriers in these I-III-VI materials based quantum dots solar cells.

Summary

In this chapter the importance of I-III-IV group materials and other photo anode materials for QDSSCs have been discussed. A verity of metal oxide is used as an anode material for solar cells. Titanium dioxide is the most important candidate in thin film technology due to its unique properties such as stability and good performance. Currently, binary and ternary semiconductors materials such as group III-V, II-VI and I-III-IV are used for the quantum dots solar cell. Copper indium sulfide has been highlighted as an active next-generation solar cell material due to its nontoxicity and cost effectiveness. The major shift on ternary $CuInS_2$ is due to wide range of electronic and optical properties, it has a direct band gap of around 1.54eV, and high absorption coefficient ($\sim 10^5$ cm^{-1}). Furthermore, the constituent elements of $CuInS_2$ are non-toxic and exhibit stability under solar spectrum

also as compared to binary compounds. All these properties make $CuInS_2$ a potential substitute to replace all the costly and toxic photovoltaic materials. So, Copper indium sulfide (CIS) is a promising alternative to the II−VI systems (CdS, CdSe, CdTe). A variety of methods have been employed such as thermolysis, photolysis, single source evaporation and many solutions based techniques are used for the production and development of $CuInS_2$ QDs based photo anode.

References

[1] A.M. Smith, S. Nie, Semiconductor nanocrystals: structure, properties, and band gap engineering, Acc. Chem. Res, 43 (2010) 190-200.

[2] C.S. Lim, J.H. Ryu, D.-H. Kim, S.-Y. Cho, W.-C. Oh, Reaction morphology and the effect of pH on the preparation of TiO 2 nanoparticles by a sol-gel method, Journal of Ceramic Processing Research, 11 (2010) 736-741.

[3] A.R. Boccaccini, I. Zhitomirsky, Application of electrophoretic and electrolytic deposition techniques in ceramics processing, Current Opinion in Solid State and Materials Science, 6 (2002) 251-260.

[4] S. Nadzirah, K. Foo, U. Hashim, Morphological reaction on the different stabilizers of titanium dioxide nanoparticles, Int J Electrochem Sci, 10 (2015) 5498-5512.

[5] R.S. Sabry, Y.K. Al-Haidarie, M.A. Kudhier, Synthesis and photocatalytic activity of TiO2 nanoparticles prepared by sol–gel method, Journal of Sol-Gel Science and Technology, 78 (2016) 299-306.

[6] S. Mahshid, M. Askari, M.S. Ghamsari, Synthesis of TiO 2 nanoparticles by hydrolysis and peptization of titanium isopropoxide solution, Journal of Materials Processing Technology, 189 (2007) 296-300.

[7] P. Chaudhari, V. Chaudhari, S. Mishra, Low Temperature Synthesis of Mixed Phase Titania Nanoparticles with High Yield, its Mechanism and Enhanced Photoactivity, Materials Research, 19 (2016) 446-450.

[8] M.R. Hoffmann, S.T. Martin, W. Choi, D.W. Bahnemann, Environmental applications of semiconductor photocatalysis, Chemical reviews, 95 (1995) 69-96.

[9] C.J. Murphy, J.L. Coffer, Quantum dots: a primer, Applied Spectroscopy, 56 (2002) 16A-27A.

[10] K. Manickathai, S.K. Viswanathan, M. Alagar, Synthesis and characterization of CdO and CdS nanoparticles, (2008).

[11] S.S. Prasad, J. Madhavan, Synthesis and characterization of CdS quantum dots by reverse micelles method, Der Pharma Chemica, 5 (2013) 1-4.

[12] S. Baskoutas, A.F. Terzis, Size-dependent band gap of colloidal quantum dots, Journal of applied physics, 99 (2006) 013708.

[13] B. Ji, Synthesis and optical properties of plasmonic fluorescent quantum dots, Université Pierre et Marie Curie-Paris VI, 2014.

[14] L.F. Gonçalves, C.J. Silva, F.K. Kanodarwala, J.A. Stride, M.J. Gomes, Synthesis and characterization of organic–inorganic hybrid materials prepared by sol–gel and containing

CdS nanoparticles prepared by a colloidal method using poly (N-vinyl-2-pyrrolidone), Journal of sol-gel science and technology, 71 (2014) 69-78.

[15] E. Klem, Infrared Sensitive Solution-processed Quantum Dot Photovoltaics in a Nanoporous Architecture, 2008.

[16] L. Motte, C. Petit, L. Boulanger, P. Lixon, M. Pileni, Synthesis of cadmium sulfide in situ in cadmium bis (2-ethylhexyl) sulfosuccinate reverse micelle: polydispersity and photochemical reaction, Langmuir, 8 (1992) 1049-1053.

[17] Y. Zhang, W. Chen, J. Zhang, J. Liu, G. Chen, C. Pope, In vitro and in vivo toxicity of CdTe nanoparticles, Journal of nanoscience and nanotechnology, 7 (2007) 497-503.

[18] M. Redlinger, R. Eggert, M. Woodhouse, Evaluating the availability of gallium, indium, and tellurium from recycled photovoltaic modules, Solar Energy Materials and Solar Cells, 138 (2015) 58-71.

[19] S.K. Batabyal, L. Tian, N. Venkatram, W. Ji, J.J. Vittal, Phase-selective synthesis of CuInS2 nanocrystals, The Journal of Physical Chemistry C, 113 (2009) 15037-15042.

[20] S. Liu, H. Zhang, Y. Qiao, X. Su, One-pot synthesis of ternary CuInS 2 quantum dots with near-infrared fluorescence in aqueous solution, Rsc Advances, 2 (2012) 819-825.

[21] S. Siebentritt, Wide gap chalcopyrites: material properties and solar cells, Thin Solid Films, 403 (2002) 1-8.

[22] S.E. Habas, H.A. Platt, M.F. Van Hest, D.S. Ginley, Low-cost inorganic solar cells: from ink to printed device, Chemical reviews, 110 (2010) 6571-6594.

[23] J.W. Cho, S.J. Park, W. Kim, B.K. Min, Fabrication of nanocrystal ink based superstrate-type CuInS2 thin film solar cells, Nanotechnology, 23 (2012) 265401.

[24] H. Zhong, Y. Zhou, M. Ye, Y. He, J. Ye, C. He, C. Yang, Y. Li, Controlled synthesis and optical properties of colloidal ternary chalcogenide CuInS2 nanocrystals, Chemistry of Materials, 20 (2008) 6434-6443.

[25] J. Kolny-Olesiak, H. Weller, Synthesis and application of colloidal CuInS2 semiconductor nanocrystals, ACS applied materials & interfaces, 5 (2013) 12221-12237.

[26] J.J. Nairn, P.J. Shapiro, B. Twamley, T. Pounds, R. Von Wandruszka, T.R. Fletcher, M. Williams, C. Wang, M.G. Norton, Preparation of ultrafine chalcopyrite nanoparticles via the photochemical decomposition of molecular single-source precursors, Nano letters, 6 (2006) 1218-1223.

[27] T.-L. Li, H. Teng, Solution synthesis of high-quality CuInS 2 quantum dots as sensitizers for TiO 2 photoelectrodes, Journal of Materials Chemistry, 20 (2010) 3656-3664.

[28] Q. Lu, J. Hu, K. Tang, Y. Qian, G. Zhou, X. Liu, Synthesis of nanocrystalline CuMS2 (M= In or Ga) through a solvothermal process, Inorganic chemistry, 39 (2000) 1606-1607.

[29] F. Bensebaa, C. Durand, A. Aouadou, L. Scoles, X. Du, D. Wang, Y. Le Page, A new green synthesis method of CuInS2 and CuInSe2 nanoparticles and their integration into thin films, Journal of Nanoparticle Research, 12 (2010) 1897-1903.

[30] J. Zhao, A. Wang, M.A. Green, F. Ferrazza, 19.8% efficient “honeycomb” textured multicrystalline and 24.4% monocrystalline silicon solar cells, Applied Physics Letters, 73 (1998) 1991-1993.

[31] Z. Pan, I.n. Mora-Seró, Q. Shen, H. Zhang, Y. Li, K. Zhao, J. Wang, X. Zhong, J. Bisquert, High-efficiency “green” quantum dot solar cells, Journal of the American Chemical Society, 136 (2014) 9203-9210.

[32] S. Yang, P. Zhao, X. Zhao, L. Qu, X. Lai, InP and Sn: InP based quantum dot sensitized solar cells, Journal of Materials Chemistry A, 3 (2015) 21922-21929.

[33] L.L. Li, K.P. Liu, G.H. Yang, C.M. Wang, J.R. Zhang, J.J. Zhu, Fabrication of graphene–quantum dots composites for sensitive electrogenerated chemiluminescence immunosensing, Advanced Functional Materials, 21 (2011) 869-878.

[34] A.J. Labelle, S.M. Thon, S. Masala, M.M. Adachi, H. Dong, M. Farahani, A.H. Ip, A. Fratalocchi, E.H. Sargent, Colloidal quantum dot solar cells exploiting hierarchical structuring, Nano letters, 15 (2015) 1101-1108.

[35] X. Huang, X. Qi, F. Boey, H. Zhang, Graphene-based composites, Chemical Society Reviews, 41 (2012) 666-686.

Chapter No.3

Overview of Synthesis Techniques and Characterization Tools

3.1 Synthesis and Deposition Techniques

Various physical and chemical top down and bottom up approaches have been used to synthesize the $CuInS_2$ nanoparticles and to develop the $CuInS_2$ thin film. Physical methods involving the use of vacuum conditions which are highly energy intensive. On the other hand, chemical methods are less energy intensive.

There are many methods employed to synthesize the copper indium sulfide nano-crystallite. Solution based synthetic techniques have gained consideration due to low cost and large scale fabrication of thin films [1]. Generally, two types of solution synthesis approaches are used 1) precursor solution based, 2) nanoparticle based [2]. In precursor solution based synthesis approach metal chloride, nitrates, acetates are dissolved in an organic solvent in the addition of the polymer binder, further prepared solution is coated onto the conducting substrate, and then annealed in the inert environment. While in second approach nanoparticles are first synthesized and then re-dispersed in volatile organic material to prepare the colloidal suspension/ ink and the ink is printed on the substrate. After being coated on the substrate the film is heat treated.

Top down approach is more of a traditional process. The nanoparticles made through these techniques are referred to as submicron particles because the nanostructures synthesized by this process are limited to the size of 1 – 10 nm. Quantum dots have sizes smaller than Bohr exciton radius which is not achieved in this process. To control the size of the nanoparticles, bottom-up approach is more favourable. It involves the growth of colloid quantum dots through the reaction of its atomic constituents or molecular or ionic precursors [3]. One of the commonly used bottom-up approaches is epitaxial growth technique or assembly technique which can either be dry or wet. It involves the growth of

quantum dot layer onto a matrix. The appropriate methods for stable $CuInS_2$ films are two stage process, molecular beam epitaxy, electrophoresis deposition, etc [4, 5].

A verity of solution based techniques such as sol gel, hydrothermal, spin coating, electrophoretic deposition, electrodeposition, molecular beam epitaxy etc. are used for the synthesis and deposition of copper indium sulphide nanoparticles and QDs are discussed below [6].

3.1.1 Sol-gel Technique

Sol gel is the one of the most common and simple approach to synthesize the nanoparticles [7]. This is mostly used for the fabrication of ceramic and glassy materials. Sol is the colloidal suspension of solid particles in the liquid. The sol is converted gradually towards gel form have both liquid and solid phase. Two types of approaches are involved in Sol gel synthesis,

- A metal-organic approach in which metal alkoxides are dissolved in organic solvents
- A metal-inorganic approach in which metal salts like nitrates, chlorides, oxychlorides etc. are used as precursors in water.

Second synthesis approach is much cheaper than the first approach but the reactions are rapid and difficult to control [8]. In metal organic approach the reaction take place in three stages. The first step is the hydrolysis of the metal alkoxide. The second stage is poly condensation and it occurs in two steps. Firstly, the formation of oxalation and secondly the formation of olation. Therefore, these processes generate the metal-oxo or metal hydroxo polymers in the solution.

After that a gel is formed which contained the structures, are formed due to recombination of metal oxo polymers. Drying process is conducted to remove the liquid phase from the gel. After the drying procedure, the obtained material is heat treated at desire temperature to get the nanoparticles.

3.1.2 Hydrothermal

The hydrothermal approach for nanostructures synthesis gained attention due to its practical applications and can be used on large area production. It is also the low cost, environmentally friendly technique. It works at slightly high temperature and pressure than the room conditions [9]. The other important factor in this technique is the water solubility. The used precursors must be highly soluble in water because synthesis process and conditions depend on the solubility. To provide the appropriate conditions, crystal growth and synthesis is done in an autoclave. Autoclave is a pressure vessel made up of steel and usually lined with Teflon. The precursor is dissolved in hot water and the mixture is placed in autoclave at high temperature. Different temperature is maintained at two ends of autoclave. Cooler end is the site for the crystal growth and at hotter end solute gets dissolved.

In hydrothermal process the size and shape of the crystallite are controlled by optimizing the operating conditions. It is because the size and shape of synthesized particles depends on the operating conditions like reaction path, pressure and temperature [10]. Hydrothermal process works at high temperature therefore, high vapor pressure materials can easily be synthesized. In this technique, it is very difficult to observe the phenomenon during growth of the crystal. Now-a-days hydrothermal reactors are available making it even easier to control the conditions. The reactor is turned on after setting desired conditions of temperature and pressure. When the desired conditions are achieved in the reactor, the raw material is pumped into it [9].

3.1.3 Electro-deposition (ED)

ED is a long-established way to deposit metal layers on a conducting substrate. Homogenous ionic solution is used for the deposition on the metallic cathode surface. ED is a fast process and permits deposition on the complex cathode shapes. The thickness of the deposited films depend on the current density and also the rate for which current flows. The deposit can be detached if the substrate is chosen to be soluble by dissolving it away.

Electro-deposition is relatively cheap process with respect to other deposition techniques. This process is performed at low temperature which can decrease the deposition cost and

also minimize inter diffusion of materials. It can be used for the deposition of small scale thickness to large dimension.

The film thickness easily controlled in this process because it depends on the amount of charged delivered. Whereas the deposition rate on of the current flow rate and deposition time. Magnitude of applied potential also play important role in the deposition behaviour. Defect rate can be controlled by monitoring the applied potential. Pulsing and cycling the applied current or the potential in a solution containing a mixture of precursors allows the production of a multi-layered material.

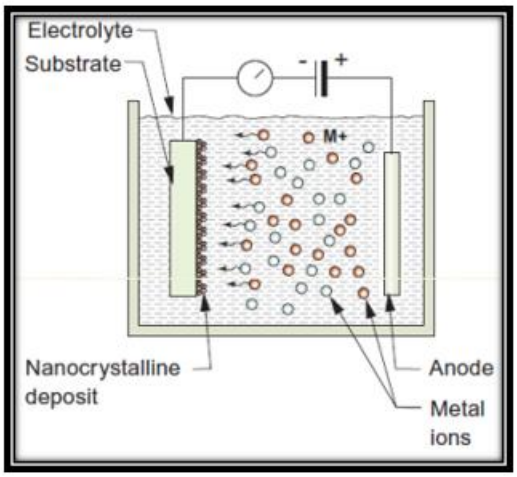

Figure 3.1: Schematic diagram of electro-deposition of film.

The potential during the pulse will figure out the species deposited. Whereas, the thickness of the single layers is determined by the charge passed. Alternatively, the substrate can be transferred periodically from one electrolytic cell to another. The obtained thickness of films are in the range of few nm to tens of microns. ED can be used to for the preparation of large area specimens and this deposition technique is appropriate for commercial and industrial applications.

3.1.4 Electrophoretic Deposition (EPD)

EPD is the most emerging technology due to its usefulness, ease and low cost [11]. This technique has known since 1808, observed first time in clay particle in water by the Russian scientist. But in 1933 it is first time practically applied on thoria particles deposition in the USA [12]. This technique has extensive range of unique applications in the processing of

ceramic materials and metallic coatings. It acquired great interest in both industry and academia. The major advantage of it is cost effectiveness requiring simplest apparatus.

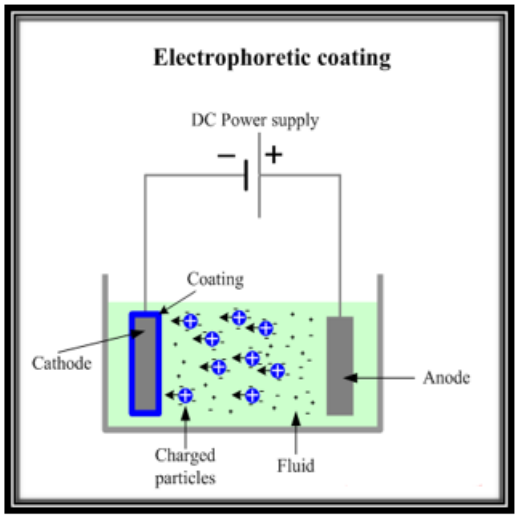

Figure 3.2: Schematic diagram of Electrophoretic deposition (EPD).

The phenomena involved in this process is depend on the movement of charged particles. These charged particles are suspended in the homogenous suspension and move due to the applied electric field towards an oppositely charged electrode to form a homogenous coating and controlled assembly of nanoparticles [11]. It is one of the colloidal process and has many benefits such as less deposition time, no need of binder, and little restriction of the shape of the substrate.

Related to other metallic coating procedures, the EPD is very flexible because in can be easily modified for specific application. For example, film fabricatio can be made in any kind of substrate such as flat, cylindrical or any other shape. It is offers easy control of the film thickness and its morphology by simple adjusting the deposition time and applied voltage [12].

EPD is quite different from the Electroplating or electrodeposition. The main differences in these two techniques are shown the table 3.1.

Table 3.1. Comparison of two electro-deposition techniques.

Property	EPD	Electroplating
Moving species	Solid particles	Ions
Charged transfer on deposition	None	Ion reduction
Conductance of the liquid media	Low	High
Preferred liquid	Organic	Water

Therefore, it is important to use similarly charged particles and similar solvent–binder–dispersant systems for gaining better control of layer thickness. The principal driving force for electrophoretic deposition (EPD) is the charge on the particle and the electrophoretic mobility of the particles in the solvent under the influence of an applied electric field.

3.1.5 Spin Coating

Spin coating is the simplest approach in the thin film applications. In the fabrication of semiconductor devices, a spin coating process is applied to coat the conducting layer on the substrate [15]. A layer of few nanometres is obtained through this process by using the desire solution.

A coating procedure consists of following steps:

- In the first step hold the substrate by using the spin chunk and creating the vacuum using vacuum pump.
- Set the rpm and the time for homogenous coating. Rotate the substrate by rotating spin chunk, and apply the coating liquid onto the substrate [16]. The airflow then dry most the solvent leaving a plasticized film.

Spin coating technique normally used to coat the small substrates. This technique is used for the deposition of nano materials, synthetic metals, transparent conducting oxide layers

etc. And these fabricated films are use in different application such as in thin film solar cells applications, and many kind of semiconductor devices.

3.2 Characterization Tools

Characterization techniques can be employed for optical analysis, structural analysis, surface analysis, composition analysis etc. Few of the techniques are explained below.

3.2.1 UV-Vis Spectroscopy

UV-Vis spectroscopy is used to obtain the absorbance spectra of the samples. It is a simple, versatile, fast, accurate and cost-effective technique for the measurement of the absorption of light by a material in ultraviolet (UV) to visible light range. To provide the radiation from UV region to the visible range more than one source is required by the spectroscope. Hydrogen or deuterium lamp is used for UV radiation and tungsten/halogen lamp is used for the visible light [17].

Working Principle

The absorption of light occurs due to the electronic transitions in the material when radiation falls on it. The radiation source is fixed. Selective radiation is made to fall on the target solution by using a diffraction grating or diffractometer. After the diffraction grating there is a very narrow slit to allow the light of very narrow waveband (monochromatic) to pass through. The samples are poured into cuvette which is then placed in sample cell in spectroscope. A reference sample containing solvent is also placed. The light is passed through sample and reference simultaneously. The radiation that passes through the sample solution is detected by a photomultiplier or a photodiode. The detector converts the radiation photons into electrical signals which give the absorption. Spectrometer compares the radiation intensity passing through the reference and the sample to calculate absorption [18, 19].

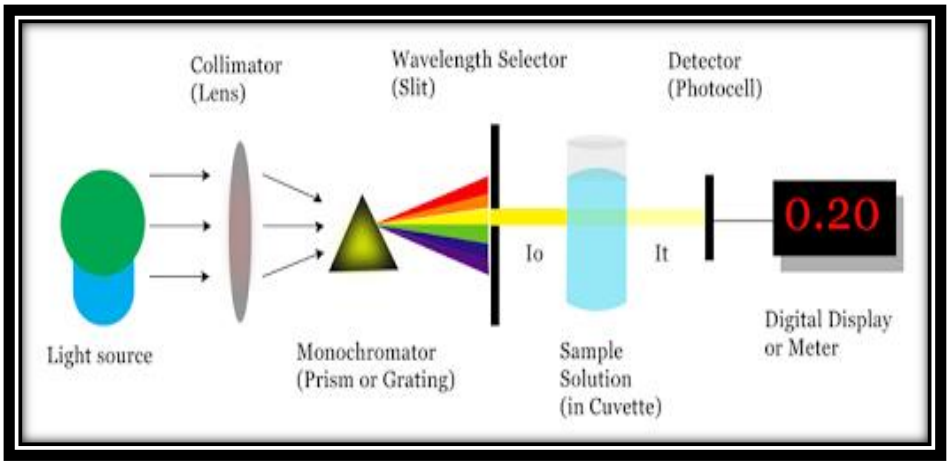

Figure 3. 3. Working of UV-Vis Spectroscopy.

3.2.2 X-ray Diffraction (XRD)

XRD is a powerful analytical tool for identification of crystalline phases, degree of crystallinity, and orientations in crystalline compounds. It is a technique that give quantitative and qualitative analysis of the crystalline specimen. XRD is a non-destructive technique that gives the information related to structure of the specimen. It is useful in determining structural properties like crystal size, lattice parameters etc. [20]. XRD is used to characterize the verity of materials such as ceramics and composites, metals, semiconductors, polymers, building materials, soils and clays. This technique is also use for the characterization of thin films.

Working Principle

X-rays are the electromagnetic radiations having a wavelength that is shorter than UV but longer than γ-rays in the electromagnetic spectrum. Production of X-rays involve the acceleration of high energy charged electron beam through a high voltage field and is bombarded on a solid target, normally copper or molybdenum. When X-rays hit the atoms, the electrons in atoms start vibrating with frequency same as the frequency of striking X-rays. Bragg's law is used to describe the working of XRD.

$$\boldsymbol{n \times \lambda = 2d \times Sin\theta}$$

Where, λ is the wavelength of the X-rays, θ is the incident angle, and d is the spacing between the planes.

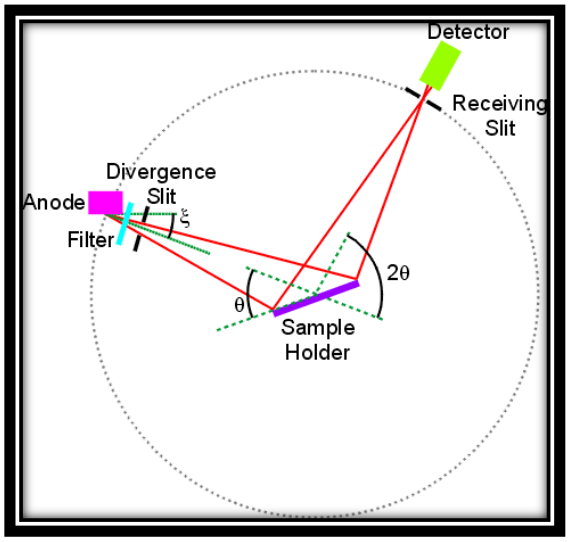

Figure 3. 4: Working of X-Rays Diffraction (XRD).

Inner shell electron in atoms are ejected through the process of ionization as a result of collision of incident electrons having relatively much high energy. The vacancy that is created by this process is filled by a free electron in an outer orbital and because of this transition, energy will be released in the form of X-ray photon.

3.2.3 Scanning Electron Microscopy (SEM)

The scanning electron microscope is a microscope that works by scanning a focused beam of electrons on the sample. The electron has wavelength about 1000 times shorter than that of the visible light, so electron microscopes have the tendency to yield much higher resolution than that can be obtained from light powered optical microscopy [21]. A Scanning Electron Microscope (SEM) yields images using focused electron beam that scans a rectangular area of the sample. The main components of the SEM include: Source of electrons, condenser lenses, electron detector, sample chamber, and display screen.

Working Principle

Electron are produced at the top of the column by using the tungsten metal due to its high melting point and low vapor pressure, and these electrons are passed through the column of condenser lenses. The focusing of electron beams is achieved by using numerous condenser lenses to a spot with ~4–50 Å diameters and, before they finally strike the specimen, their adjustment and control is obtained using deflection coils. When the electrons beam strikes the sample, the electrons lose energy and this loss appears in other

forms such as emission of secondary electrons, heat and emission of X-rays or light that can be detected by specific detectors [22]. SEM is design to operate in low vacuum so both the lenses column and chamber are evacuated by using the pumps. And this level of the vacuum depends upon the design microscope [21].

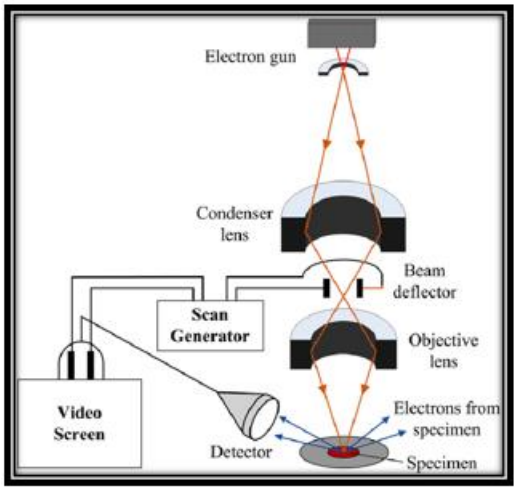

Figure 3.5: Schematic diagram of Working of Scanning electron microscopy [23].

3.2.4 Energy Dispersive Spectroscopy (EDS)

EDS is a compositional elemental analysis technique for chemical characterization of the sample. The electrons have an effective probing depth of 1µm.

Working principle

When focused beam of high energy electrons is bombarded on to a solid sample, X- rays are emitted. The detector in make use of these x-rays to obtain localized chemical analysis. When electrons strike the sample, the electrons contained in specimen are excited creating vacant places in the atomic shells. Electrons in the higher shells fill these vacancies. The energy is released in this process in form of X-rays. All elements emit X-rays with characteristic energy values. Each element in periodic table has its specific energy value which makes elemental analysis through EDS possible. Kα -rays are emitted when an electron from L shell fills the vacancy in K shell of the atom. Letters K, L, M is the shell from where electrons are emitted. Sample preparation is same as for SEM.

3.2.5 Coating Thickness Tester

CG204 Coating thickness tester is a portable device. It is using to measure the thickness of no invasive coatings. It is automatically recognized the dual type of the substrate (ferrous and non-ferrous).

The EXTECH thickness tester has the following features.

- Two measuring modes: single and continuous
- high memory storage up-to 400 readings
- Two working modes: direct and group
- Easy to use, etc.

3.3 Computational Methods

Computational chemistry is one of the emerging fields in natural sciences based on computer simulation to study the properties of atoms, molecules, and chemicals reactions. It can assist the experimental chemist in solving the problems or it can challenge the experimental chemist to find entirely new chemical objects. The various kinds of quantum mechanical and empirical approaches are used to in computational chemistry.

3.3.1 Wave Function Theory Methods

Wave function theory has three methods.

3.3.1.1 Ab-initio Method

This is a computation method based on computational chemistry. Ab initio is a group of methods used for the calculation of moleculer structures. Schrödinger equation, the values of the fundamental constants and the atomic numbers are used for the calculation of structures. Explicit treatment of electrons in atoms and molecules requires quantum mechanics which invokes a wave function, to describe the system of electrons and nuclei. It is appropriate for wide range of structures, capable of calculating transition states and excited states and it not depend on empirical data.

The important methods used in ab initio are Hartee fock (HF) and post Hartee Fock. Hartree-Fock (HF) method is a simple method because in this method electron-electron repulsion is not specifically treated. In this method, only average effect of electron repulsion is included.

3.3.1.2 Semi-empirical Method

Semiempirical methods are based on HF formalism, but make many approximations and obtain some parameters from empirical data.This method is useful for treating large molecules. It has been formulated specifically for the organic and inorganic chemistry. It is faster than Ab initio method. It is also capable for the calculation of transition states and excited states. Semi-empirical methods require experimental as well as ab initio data.

3.3.1.3 Electron Correlated Method

Electron Correlation method describe the interaction between electrons in the electronic structure of a quantum system. It is critical for accurate and quantitative evaluation of molecular energies (difference between the nonrelativistic energy of the system and the HF energy). In this method treatment of electron correlation is based on perturbation theory.

3.3.2 Density Function Theory Methods

Density functional theory (DFT) is a quantum mechanical method used in physics and chemistry to study the electronic structure (principally the ground state) of many-body structures, atoms, molecules, and the condensed phases. In DFT, the properties of a many-electron system can be determined by using functional based on electron density. In this theory total energy is expressed in terms of total one-electron density rather than the wave function. Correct energy can be derived from the correct charge density, where all the ground state properties of a system are functionals of charge density.

The Thomas-Fermi model was the first DFT model proposed in 1927. The model based on uniform electron density. The total energy of the atom obtained by using classical expression for the electron-electron potential and nuclear-nuclear potential

Common methods used for DFT are following:

- LDA- Local Density Approximation
- P86, PW91, B91-Correlation functionals
- B3- Hybrid methods
- BLYP, BP86, B3LYP- Combined exchange and correlation functionals (Hybrid Functions).

Summary

In this chapter, various physical and chemical techniques have been discussed for the synthesis and deposition of the copper indium sulfide quantum dots films. The different characterization tools (XRD, SEM, EDS, UV-Vis Spectroscopy, and Coating thickness tester) and their working principles also explained in this chapter. Solution based techniques are used for the preparation of particles and deposition. Because these techniques are non-vacuum and cost effective, ease to use. Electrophoretic deposition is the simplest technique for the deposition of the film and no equipment is required for the deposition. Vacuum based techniques are expensive and purity of the precursors also considered in these approaches.

After the synthesis procedure the next step is to characterize the prepared samples by using characterizing tools such as XRD, SEM, EDS, UV Vis spectroscopy. XRD is used to analyze the crystallographic structure, and phases. The surface morphology of the films is studied with SEM while elemental composition of the prepared samples is investigated by EDS. The absorbance and other optical properties are identified by using UV-Vis spectroscopy and coating thickness tester is used to find the thickness of the film. Gaussian 09 software is use here for DFT studies to predicting many properties of atoms, molecules and reactive systems, for examples molecular energies, structures, vibrational frequencies, and electron densities.

References

[1] S.E. Habas, H.A. Platt, M.F. Van Hest, D.S. Ginley, Low-cost inorganic solar cells: from ink to printed device, Chemical reviews, 110 (2010) 6571-6594.

[2] J.W. Cho, S.J. Park, W. Kim, B.K. Min, Fabrication of nanocrystal ink based superstrate-type CuInS2 thin film solar cells, Nanotechnology, 23 (2012) 265401.

[3] E.B. Stokes, A.D. Stiff-Roberts, C.T. Dameron, Quantum dots in semiconductor optoelectronic devices, Interface-Electrochemical Society, 15 (2006) 23-27.

[4] Y. Cui, M.T. Björk, J.A. Liddle, C. Sönnichsen, B. Boussert, A.P. Alivisatos, Integration of colloidal nanocrystals into lithographically patterned devices, Nano letters, 4 (2004) 1093-1098.

[5] T.-L. Li, Y.-L. Lee, H. Teng, High-performance quantum dot-sensitized solar cells based on sensitization with CuInS2 quantum dots/CdS heterostructure, Energy & Environmental Science, 5 (2012) 5315-5324.

[6] O. Amiri, M. Salavati-Niasari, M. Sabet, D. Ghanbari, Sonochemical method for preparation of copper indium sulfide nanoparticles and their application for solar cell, Combinatorial chemistry & high throughput screening, 17 (2014) 183-189.

[7] L. Klein, G. Garvey, Kinetics of the sol/gel transition, Journal of Non-Crystalline Solids, 38 (1980) 45-50.

[8] M.A. Aegerter, M. Mennig, Sol-gel technologies for glass producers and users, Springer Science & Business Media2013.

[9] A.B. Djurisic, Y.Y. Xi, Y.F. Hsu, W.K. Chan, Hydrothermal synthesis of nanostructures, Recent patents on nanotechnology, 1 (2007) 121-128.

[10] K. Byrappa, M. Yoshimura, Handbook of hydrothermal technology, William Andrew2012.

[11] S. Cabanas-Polo, A.R. Boccaccini, Electrophoretic deposition of nanoscale TiO 2: technology and applications, Journal of the European Ceramic Society, 36 (2016) 265-283.

[12] L. Besra, M. Liu, A review on fundamentals and applications of electrophoretic deposition (EPD), Progress in materials science, 52 (2007) 1-61.

[13] R.M. Brydson, C. Hammond, Generic methodologies for nanotechnology: classification and fabrication, Nanoscale science and technology, (2005) 1-55.

[14] R. Kelsall, I.W. Hamley, M. Geoghegan, Nanoscale science and technology, John Wiley & Sons2005.

[15] S. Sakawaki, Spin coating process, Google Patents, 1981.

[16] M. Sakai, H. Takamori, M. Nomura, Spin coating process, Google Patents, 2000.

[17] H.-H. Perkampus, H.-C. Grinter, T. Threlfall, UV-VIS Spectroscopy and its Applications, Springer1992.

[18] A.M. Beale, A.M. van der Eerden, K. Kervinen, M.A. Newton, B.M. Weckhuysen, Adding a third dimension to operando spectroscopy: a combined UV-Vis, Raman and XAFS setup to study heterogeneous catalysts under working conditions, Chemical Communications, (2005) 3015-3017.

[19] L.C. Pump, UV-VIS Spectrophotometer, Analytical Chemistry, 50 (1978).

[20] B. Cullity, S. Stock, S. Stock, Elements of X-ray Diffraction, 3rd editionPrentice Hall, New Jersey, (2001).

[21] D.C. Joy, Scanning electron microscopy, Wiley Online Library2006.

[22] H. Todokoro, M. Ezumi, Scanning electron microscope, Google Patents, 1999.

[23] F.-Y. Zhu, Q.-Q. Wang, X.-S. Zhang, W. Hu, X. Zhao, H.-X. Zhang, 3D nanostructure reconstruction based on the SEM imaging principle, and applications, Nanotechnology, 25 (2014) 185705.

Chapter No.4
Experimentation

This chapter describes the series of experiments which were performed for the synthesis and deposition of the $CuInS_2$ based photo anode. A list of detailed experiments is categories into two parts which is given below.

Synthesis of Photo Anode materials

- Synthesis of TiO_2 nanoparticles by sol gel technique.
- Synthesis of $CuInS_2$ quantum dots by co-precipitation method and characterization of $CuInS_2$ at different annealing temperature.

Film deposition/ electrode formation process:

- Electrophoretic deposition of TiO_2 nanoparticles on FTO electrode surface.
- Optimization of the TiO_2 film thickness by varying different electrophoresis process parameters.
  - Applied Voltage
  - Deposition Time
  - Distance between the electrodes
  - Suspension aging times
- Electrophoretic deposition of $CuInS_2$ QDs on TiO_2/FTO electrode at different applied voltage.
- Post heat treatment and characterization of Electrophoretically deposited film.

After the experimental study theoretical calculations of buffer layer is also performed.

4.1 Synthesis of Photo Anode materials

Materials

Copper chloride dehydrate ($CuCl_2.2H_2O$), Indium chloride tetrahydrate ($InCl_3.4H_2O$), Thiourea (CH_4N_2S), Ethylene Glycol ($C_2H_6O_2$), Ethanol (C_2H_5OH), Methanol (CH_3OH), Titanium tetra Isopropoxide ($C_{12}H_{28}O_4Ti$), Acetylacetone ($C_5H_8O_2$), Hydrochloric acid

(HCl), FTO coated glass, and distilled water are used for the synthesis of TiO_2 nanoparticles nad $CuInS_2$ QDs.

Equipment

Beakers, Magnetic Stirrer, Hot Plate, Fume hood, centrifuge, Vaccum oven, Box furnace, Wealtec Elite 300 plus electrophoretic deposition setup and CG204 coating thickness tester.

4.1.1 Synthesis of TiO_2 nanoparticles by sol gel technique

Titanium tetra Isopropoxide (TIP) was used as a Titanium precursor and ethanol used as solvent. 5ml of TIP was added to 10ml ethanol and stirred gently for 1 h. Another 8ml solution was prepared combining a mixture of 3ml water and 5ml ethanol. This solution then added into TIP and Ethanol solution and stirred until homogenous sol of TiO_2 was prepared. Few drops of HCl was added into the mixture for rapid hydrolysis and maintained the pH 3. Then, this mixture was placed at room temperature for 24 h. The resultant suspension was dried at 80°C in an oven for 5 h, and white particles were obtained.

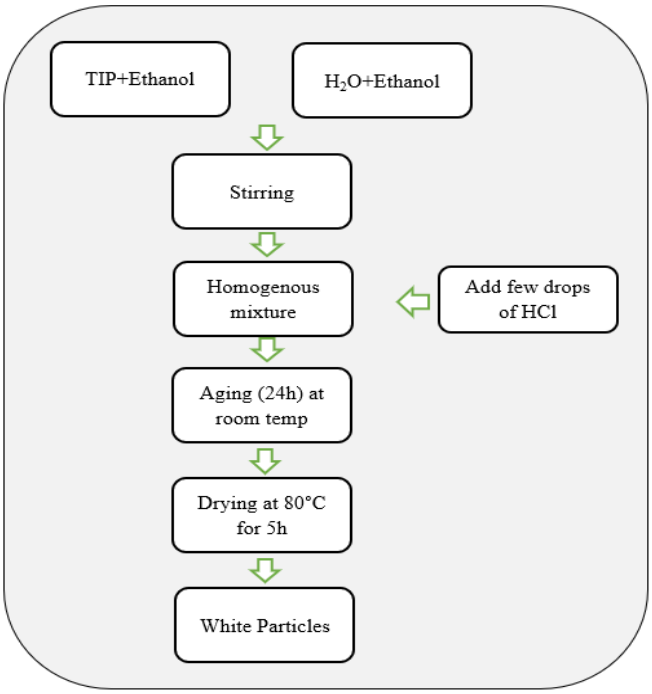

Figure. 4.1: Schematic diagram of Titanium dioxide (TiO_2) nanoparticles synthesis via sol gel technique.

4.1.2 Synthesis of $CuInS_2$ Quantum dots

To synthesize the $CuInS_2$ QDs, 1.7g indium chloride and 1.2g copper chloride were dissolved into 40ml ethylene glycol under constant stirring of 1 h. At the same time solution of sulfur was separately prepared by adding 2.48g thiourea into 40ml ethylene glycol and stirred the solution until it dissolved. After preparing two solutions, thiourea solution was slowly added into the first solution. After that, the combined solution was heated at 180°C for 2 h. The colour of the solution was changed from colourless to dark brown and finally to black which shows the formation of $CuInS_2$ QDs. Left the final solution for some time to cool down at room temperature. The obtained colloidal solution was then centrifuged at 3500rpm for 10 min. The isolated precipitates were washed with methanol, then vacuum dried at 90°C for 5-6 h.

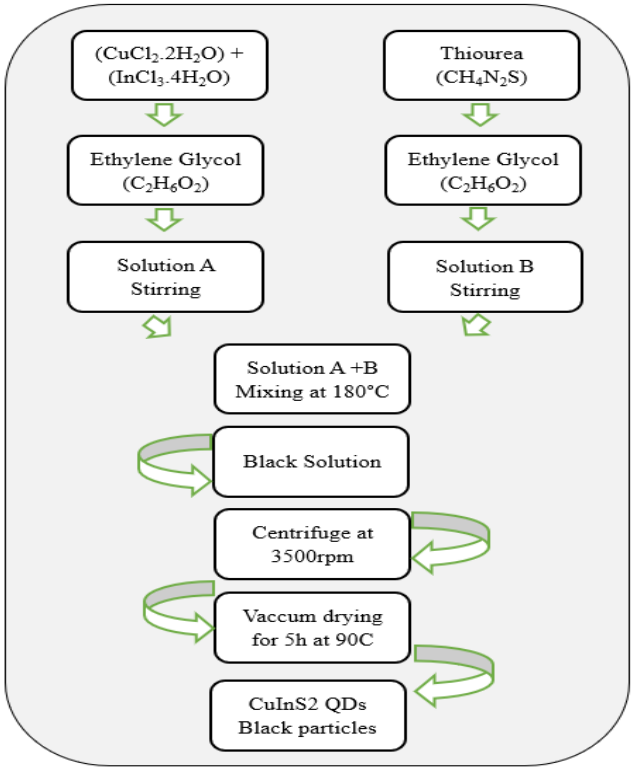

Figure. 4.2: Schematic diagram of Copper indium sulfide (CuInS2) quantum dots synthesis.

4.2 Film deposition/ electrode formation process

4.2.1 Electrophoretic deposition of TiO_2 nanoparticles

As synthesized TiO_2 nanoparticles powder (0.2g) was dispersed in ethanol (50ml) and magnetic stir/ sonicated for 30min. Few drops of acetyl acetone was added in to the

colloidal solution which act as a surfactant. Deposition of TiO_2 nanoparticles via EPD was performed at constant voltage mode. Thickness of titanium dioxide was optimized by various process parameters such as varied voltage between 30 to 130V and similarly by distance from 3mm to 1cm between the electrodes. The desired thickness of the TiO_2 was obtained at 70V and 5mm distance.

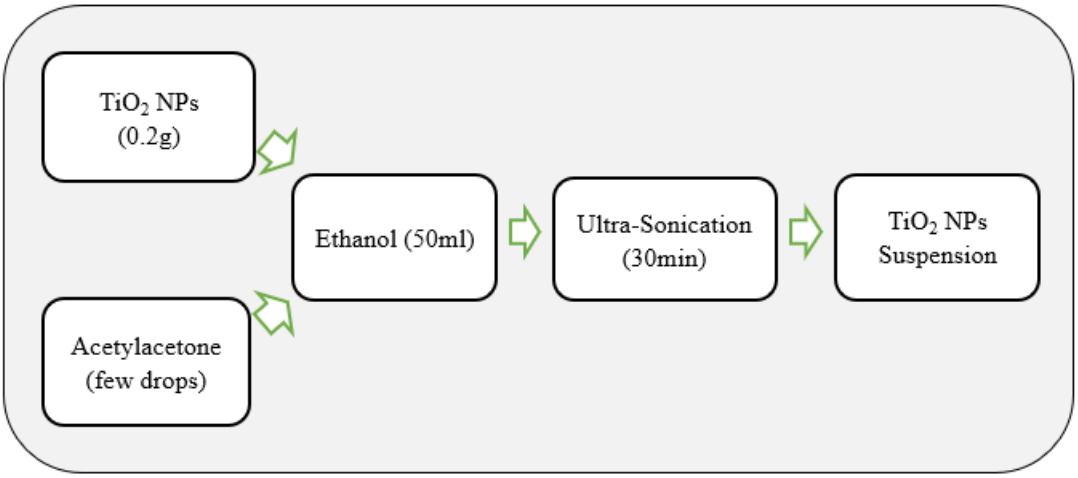

Figure. 4.3: TiO_2 NPs Suspension preparation for Electrophoretic deposition (EPD).

After the suspension preparation, the main steps for the preparation of the electrodes and EPD is given below:

- Clean the FTO coated glass by using ethanol and acetone in ultra-sonicator.
- Dry the Substrate at room temperature.
- Set the parameters for EPD.
- Electrophoretic deposition of the TiO2 on FTO coated glass.
- After EPD remove the substrate from the set-up and wash with ethanol.

4.2.1.1 Optimization of different EPD process parameter

The aim of this work was to study the main process parameters such as properties of the suspension, applied voltage and distance between the electrodes and current effect on the thickness of the film. The following table shows the variation in the applied voltage, distance between the electrodes and suspension aging time.

Table. 4.1: Applied voltage, distance variation, deposition time and suspension aging at the same deposition time.

Group	Applied Voltage (V)	Distance b/w the electrodes (cm)	Deposition time (min)	Suspension aging time
1	**30** **50** **70** **100** **130**	0.7	5	As prepared
2	70	**0.3** **0.5** **0.7** **1.0**	5	As prepared
3	70	0.7	**3** **5** **8** **10**	As prepared
4	30 50 70 100 130	0.7	5	**After 5 days**

4.2.2 Electrophoretic deposition of $CuInS_2$ QDs

As synthesized $CuInS_2$ QDs was dispersed in ethanol (50ml) and magnetic stir/ sonicated for 30min. Few drops of ethylene glycol was added in to the colloidal solution which act as a surfactant. Deposition of $CuInS_2$ QDs via EPD was performed at constant voltage mode. FTO/TiO2 was used as anode while FTO coated glass is used as a cathode. Ethanol was used as a suspension media for the deposition of the film. After the deposition, the film was washed with ethanol and dried at room temperature.

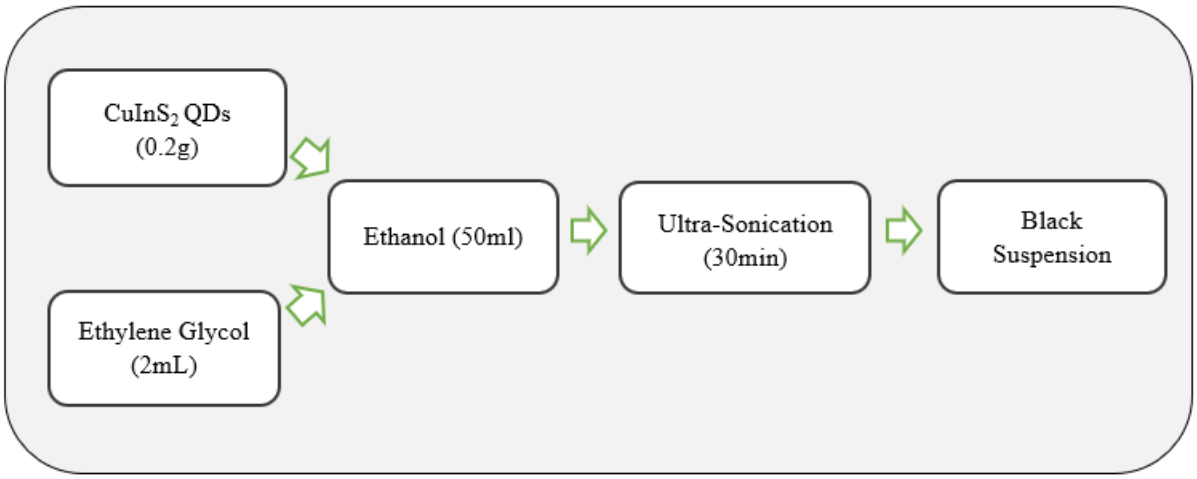

Figure. 4.4: $CuInS_2$ QDs suspension preparation for EPD.

4.2.2.1 Applied voltage effect

$CuInS_2$ film was deposited at FTO/TiO_2 electrode at 90, 100 and 110V for 20 mins in air. Ethanol was used as a suspension media for the deposition of the film. After the deposition, the film was washed with ethanol and dried at room temperature.

Table. 4.2: voltage variation effect on the current density at same deposition time in EPD.

Sample Name	Voltage (V)	Deposition time (min)
A	90	20
B	100	20
C	110	20

4.3 Post heat treatment of Electrophoretically deposited film

4.3.1 TiO_2 deposited film heat treatment

After the deposition of the films at different electrophoretic parameters the films are dried at room temperature. After the drying these films are heat treated at 450C for 1 h in a resistance box furnace to get the desired phase of the TiO_2 nanoparticles.

4.3.2 Heat treatment of $CuInS_2$ QDs film deposited on TiO_2/FTO

Similarly, as mention earlier the deposited CuInS2 films on TiO_2/FTO are dried and then heat treated at different temperature without inert environment in the box furnace to attain the chalcopyrite phase of the $CuInS_2$ Quantum dots.

4.4 Computational Analysis

In this study Density Functional Theory (DFT) calculations were carried using Gaussian 09 software. The major steps involved in the study are given below:

(a) Initial geometries generation

(b) Geometry optimization

(c) Single point Energy calculations

(d) Data Compilation & Interpretation

4.4.1 Initial Geometries

Initial geometries of TiO_2 anatase was obtained from crystallographic data. Gauss View was used to model initial geometries of Titanium dioxide anatase. Gaussian 09 software and Molden program, installed on Super computer established in 2012 at RCMS, was used for the computational analysis of the model and to visualize the output geometries respectively. Super computer installed with 8KVA 38 backup UPS and 12-ton cooling system. It consists of 2 head nodes and 32 computing nodes. The total storage area network is 22 TB for user data. The overall system consists of 272 processing cores along with 30720 GPU cores.

4.4.2 Computational method detail

The energy, optimization and other calculation of TiO_2 anatase is performed by using Gaussian 09. Gauss view is graphical interface use to sketch the structure of TiO_2 molecule and make calculation preparation. Following steps are used for the calculation of TiO_2 molecule.

4.4.2.1 Optimization

Computational analysis of TiO_2 anatase was performed with the help of B3LYP hybrid DFT methods and 6-31G basis sets (a basis set is used to express the unknown MOs in terms of a set of known functions which are combined in linear combinations to create molecular orbitals). B3LYP, a hybrid DFT method is found useful for geometry optimizations of transition metal complexes. For the comparison of geometry and spectroscopic parameters with crystal data, IR spectroscopy and TD-DFT has been performed on the optimized geometries.

4.4.2.2 Single Point Energy Calculations

Single point energy calculations are performed in gas phase using Stuttgart Dresdon Method (SSD) as well as Self-consistence reaction field (SCRF) calculations using conductor like polarizable continuum method (CPCM) model in the ethanol (solvent). All bond lengths and bond angles are compared with experimental work done. Computational results obtained by this hybrid functional and basis set is then compared with the reported data.

4.4.3 Structure and Input File Set-Up

The below figure shows the 3D sketch of TiO_2 anatase phase.

- Sketch in molecules using its advanced 3D Structure Builder, or load in molecules from standard files.
- Set up and submit Gaussian jobs right from the interface, and monitor their progress as they run.
- Examine calculation results graphically via state-of-the-art visualization features: display molecular orbitals and other surfaces, view spectra, and geometry optimizations.

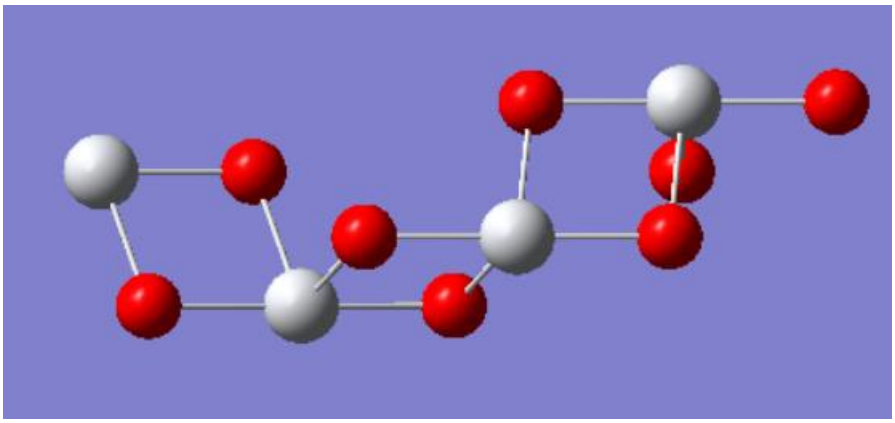

Figure 4.5: 3D sketch of TiO2 Anatase phase.

Summary

In this chapter, the synthesis procedures of TiO2 nanoparticles and CuInS2 QDs are discussed. And the fabrication of photo anode via electrophoretic deposition is also described here. Firstly, TiO2 nanoparticles are prepared with sol gel technique. Then these particles are deposited on FTO coated glass via cheapest approach. The electrophoretic parameters such as applied voltage, deposition time, distance between the electrode and suspension aging time are also studied. The thickness of the films is measure with coating thickness tester to study the behavior of these different parameters.

In the next stage $CuInS_2$ QDs are synthesized successfully via co-precipitation method at 180C. For the fabrication of photo anode these QDs are deposited at FTO/TiO_2 with electrophoretic deposition technique. After the fabrication the film is heat treated at the desired temperature. The structure properties of these synthesis particles are investigated through DFT studies performed on Gaussian 09 software. Gauss view is a graphical interface designed to be use with Gaussian to make calculation preparation (sketch molecules, setup Gaussian input file).

Chapter No.5

Results and Discussions

The crystallinity of the samples was characterized by D8 Advance X-ray Diffractometer with monochromatic Cu Kα. The surface morphology of the film was studied by Advanced Metallurgical Microscope EQ-MM500T, ScopeTek and VEGA3 scanning electron microscopy. And elemental composition of the samples was analysed using Energy Dispersive X-ray spectroscopy. UV-Vis spectroscopy was performed to study the optical properties of the sample. And the thickness of the film was measured with the help of EXTECH CG204 coating thickness tester.

5.1 XRD Analysis

The XRD analysis of the as prepared TiO_2 and $CuInS_2$ powders and films was performed to collect the information of the crystallographic structure and phase composition. Figure. 5.1(a) shows the XRD pattern of FTO coated glass taken before the deposition of the TiO_2 and $CuInS_2$ films. The XRD pattern of as prepared TiO_2 nanoparticles via sol-gel technique and annealed at 450°C is shown in Figure. 5.1(b). This pattern shows the crystalline structure and all diffraction peaks purely matched with the standard anatase pattern of TiO_2 (JCPDS 73-1764).

Figure. 5.1(c) shows the XRD pattern of as synthesized $CuInS_2$ powder via co-precipitation method. The peaks at 2θ values of 27.89°, 32.45°, 46.29°& 55.08° can be assigned to (112), (200), (204) & (312) planes of tetragonal phase of $CuInS_2$ respectively. While the most prominent reflections of $CuInS_2$ is observed along the plane (112) at $2\theta = 27.89^{\circ}$. No binary compounds appeared at 300°C temperature. This pattern is well matched with the standard chalcopyrite structure of $CuInS_2$ (JCPDS 85-1575). The lattice constants of tetragonal (I-42d (122)) phase of $CuInS_2$ are calculated to be a = 5.52279 Å, b = 5.52279 Å, c = 11.13295 Å.

Figure. 5.1(d) shows the XRD of $CuInS_2/TiO_2$ films deposited on FTO coated glass. This pattern is consistence with the previously reported standard patterns of $CuInS_2$ and TiO_2.

The crystallite size of $CuInS_2$ was obtained from peak broadening of highest intensity peak using Scherrer equation [1] .

$$t = k\lambda / \beta cos\theta \quad (1)$$

Where t is the crystallite size in nm, k is a crystallite shape factor λ is the wavelength of X-ray which is 0.154 nm for Cu Kα, β is the full width at half maximum (FWHM) in radian and θ is the Bragg's diffraction angle also in radian. The calculated crystallite size of $CuInS_2$ powder sample was to be 14.6 nm.

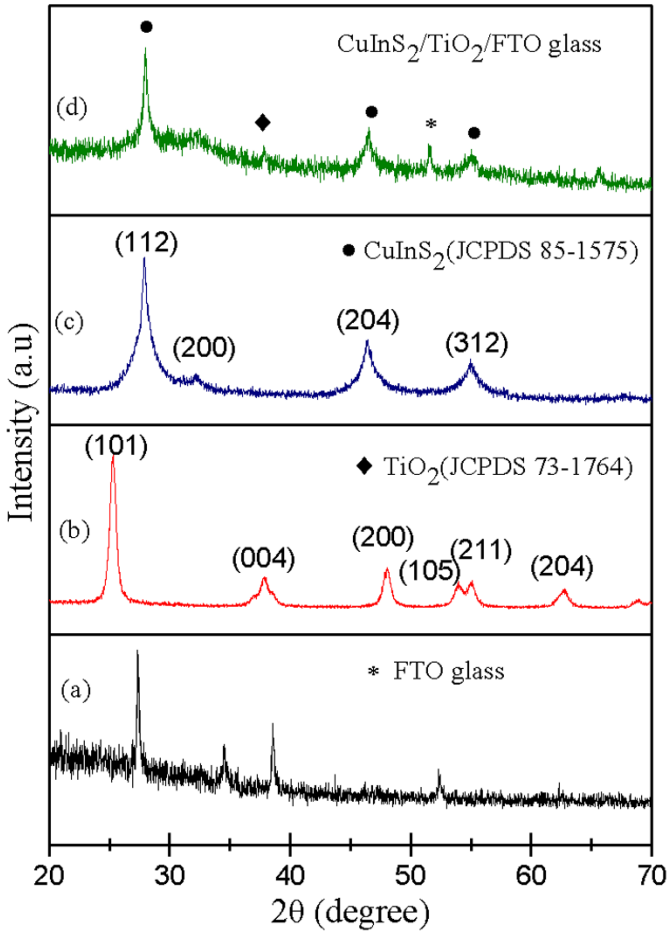

Figure. 5.1: XRD pattern of (a) FTO coated glass. (b) As prepared TiO2 powder sample annealed at 450°C for 1h. (c) As prepared $CuInS_2$ powder sample annealed at 300°C for 1h and (d) $CuInS_2/TiO_2$ film deposited on FTO coated glass via electrophoretic deposition.

5.1.1 Effect of annealing temperature on CuInS2 crystallite phase

Figure 5.2 shows the XRD pattern of $CuInS_2$ powder annealed at three different temperatures range from 300°C to 500°C. It is observed that with the increase in the temperature $CuInS_2$ decompose into In_2O_3 and $CuSO_4$. Usually $CuInS_2$ is synthesized in the inert environment because it immediately react with oxygen and formed their oxides.

The formed oxides are match with the standard pattern of In_2O_3 (JSPDS 76-0152) and $CuSO_4$ (JSPDS 80-2209).

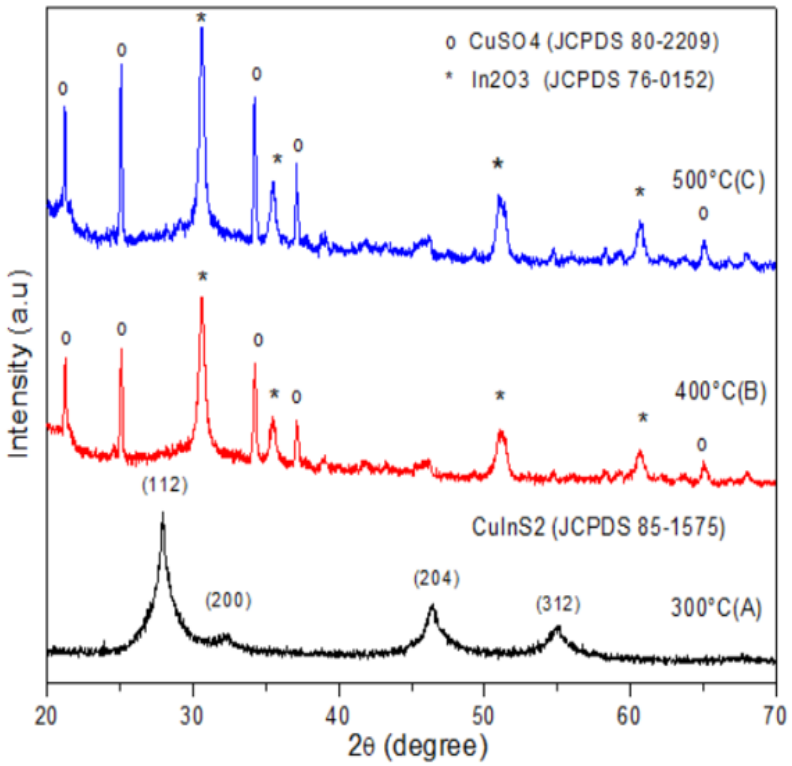

Figure 5.2:$CuInS_2$ QDs annealed at temperature, (A) 300°C, (B) 400°C and (c) 500°C

5.2 $CuInS_2$ Formation Mechanism

The expected formation of $CuInS_2$ nano crystallite depends on the experimental mechanism. In this work metal chlorides and sulfur source were used as precursors, dissolved in ethylene glycol which is used as solvent. In this processing mechanism, the formation of $Cu(EG)^{+1}$ and $In(EG)^{+1}$ complexes can be detected by colour variation. When the precursor solution was heated above 100°C to dissolve the metal salts, the formation of metal complexes occurs as shown in the equations 2 and 3. First, the solution color changed to sky blue due to the formation of Copper complex with the increase in the temperature the color changed from light green to dark green due to the formation of indium complex. As temperature rises to 170°C the dark green solution converted into transparent solution which indicates the formation of metal ions due to the decomposition of metal complexes. In the other side the transparent solution of sulfur source was prepared by dissolving thiourea in ethylene glycol.

$$CuCl2.2H2O + C2H6O2 \rightarrow [Cu(EG)]^{1+} \quad (2)$$

$$InCl3.4H2O + C2H6O2 \rightarrow [In(EG)]^{1+} \quad (3)$$

After that the sulfur solution is injected into metal ions solution and increase the temperature up-to 180°C. At about 180°C, the smoke began to evolve, and the colour of mixed solution turned from transparent to brown and finally to black as shown in Figure.

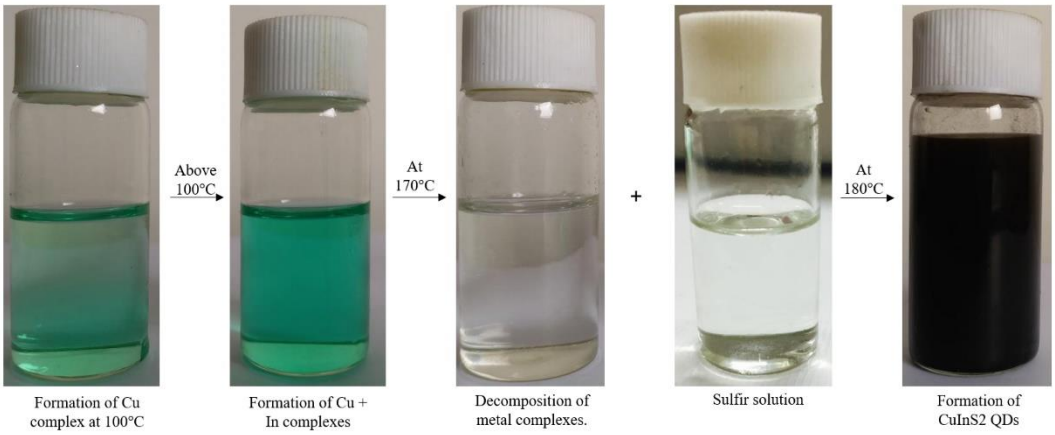

Figure. 5.3: Image of synthesis process of copper indium sulfide quantum dots in ethylene glycol via co-precipitation method.

$$Cu^{+} + In^{3+} + S^{2-} \rightarrow CuInS2 \quad (4)$$

In this experiment, ethylene glycol acted as a solvent as well as reductant, and in this reaction mechanism it reduced Cu(II) into Cu(I).

5.3 UV Vis Spectroscopy

UV-Vis spectroscopy technique is used to find the maximum absorbance and the average particle size of the nanoparticles based on the "absorbance onset" at specific wavelength of the spectrum. Figure. 5.4 shows the UV Vis absorption spectra of as prepared $CuInS_2$ QDs. The spectra consist of three portions. First part is a slope indicating an absorption edge. Second part is a plateau region where absorption seems constant or show gradual change with increasing wavelength. Third part is the second absorption edge. The wavelengths of each nanoparticle that were obtained by the tangential fitting of the linear portion of the spectrum, called cut off wavelength, which gives the onset wavelength of light that is absorbed.

5.3.1 Band gap and Particle size Calculations

The band gap of the $CuInS_2$ was calculated from the formula given in equation 5.

$$Eg = \frac{1240}{\lambda\ (nm)} \quad (5)$$

Where λ is the absorption edge and value of absorption edge was 530nm. So, the calculated Eg was 2.33 eV which was blue shifted in comparison with bulk $CuInS_2$ (Eg = 1.5eV). As reported in the literature, the nanoparticles smaller than excitation bohr diameter can be calculated from the absorption edge by using effective approximation method [2, 3]. The band gap can be calculated by Brus relation as shown in equation 6.

$$E_g^{nano} = E_g^{bulk} + \frac{\hbar^2\pi^2}{2r^2}\left(\frac{1}{m_e^*} + \frac{1}{m_h^*}\right) - \frac{1.786e^2}{\varepsilon r} \quad (6)$$

Where E_g^{nano} and E_g^{bulk} are the band gap energy of the $CuInS_2$ nanoparticles and the bulk materials respectively, r is the radius of QDs, ε is the dielectric constant which is 11 for $CuInS_2$, m_e^* and m_h^* are the effective mass of electron and holes [3]. In case of $CuInS_2$ nanoparticles the value of m_e^* and m_h^* are $0.16m_e$ and $1.3m_e$ respectively. Based on the above formula, the calculated radius of the $CuInS_2$ QDs was 4.2nm, so the estimated QDs size could be 8.4nm. The increase in crystallite size calculated through Scherrer equation might be due to increased agglomeration and fusion of particles as also evident through SEM images.

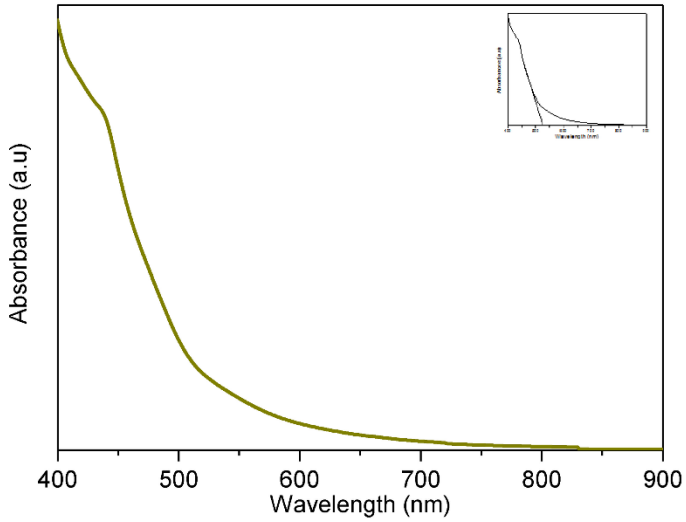

Figure. 5. 4: UV- Vis absorption spectra of as prepared Copper indium sulfide quantum dots.

5.4 SEM Results

The surface morphologies of the annealed Copper indium sulphide ($CuInS_2$) films were characterized by optical microscopy. Figure. 5.5(a-c) shows the OM images of the $CuInS_2$ films deposited on FTO/TiO_2 at 90, 100 and 110V via electrophoretic deposition (EPD). The film deposited at 90V applied voltage shows the even and smooth surface. However, when the applied voltage increased up to 100V, micro cracks appear on the surface of the film as shown in Figure. 5.5(b). It is observed that the width of micro cracks increased by further rise in the voltage. Moreover, the large level of agglomeration and surface roughness also observed at higher applied voltages.

Figure. 5.5(d-f) shows the SEM images of Copper indium sulphide ($CuInS_2$) films. The top view of the samples shows that the surface morphology of the film is changed with increasing deposition voltages.

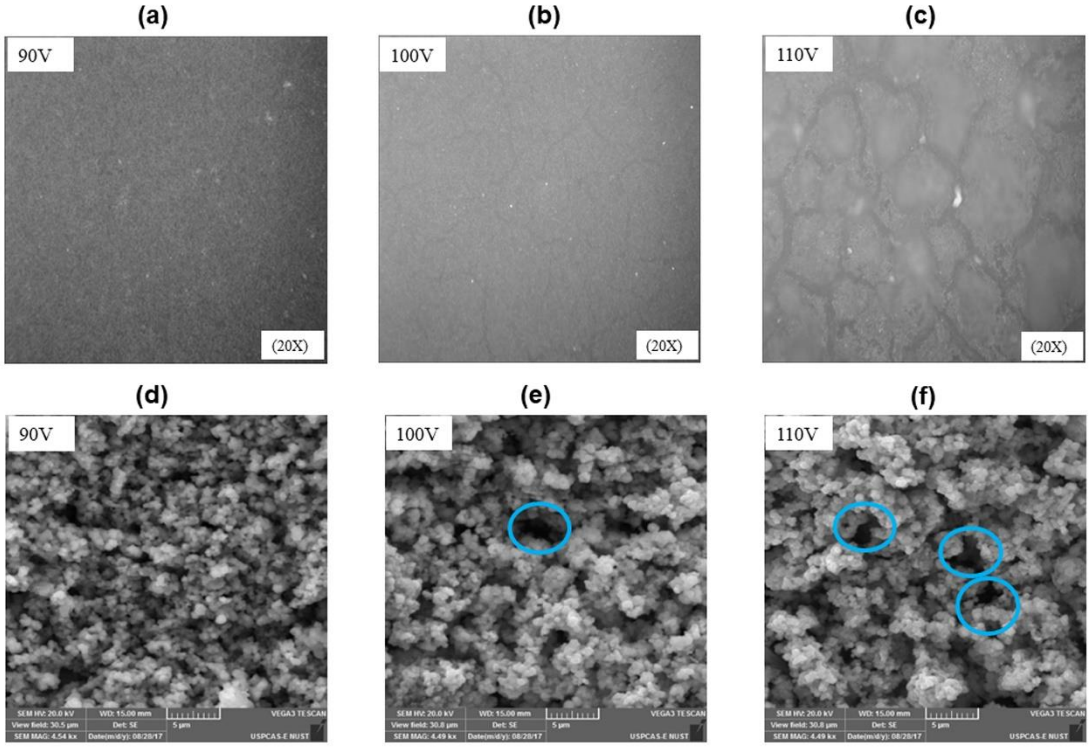

Figure. 5.5: OM and SEM images of CuInS2 films deposited at FTO/TiO2 substrate synthesized via Electrophoretic deposition at 90V (a and d), 100V (b and e), and 110V (c and f respectively).

At low applied voltage 90V deposited film is more uniform and non-porous. While by applying higher deposition voltages (100V) the film shows the interconnected and high agglomerated nanoparticles. Bluish circle in Figure. 5.5(e, f) shows the pores in the film,

which may be caused due to instability of current densities. It can also see that the porosity of the film increased at higher deposition voltages. The rate of bubble bursting at higher applied voltage lead to abrupt change in the current densities, which may increase the porosity of the film. It is essential to control the agglomeration and bubble bursting rate. The performance of deposited film can be drastically affected by these factors so voltage below the 100V is more effective. More uniform, non-porous and smooth film is achieved using 90V applied voltage.

5.4.1 Effect of Deposition Voltage

The effect of increasing applied voltage is shown in Figure. 5.5. The increase in deposition rate at higher voltage leads to non-uniformity of film. At higher voltage, the effect on current density also observed. Figure. 5.6 shows that at 90V the value of current density is constant (4 mA/cm^2) while by raised the value of voltage from 90 to 100V and then 110V current density varied from (6.5-4) mA/cm^2 and (9-7) mA/cm^2 respectively. At high current densities, the deposition rate is also high because the nanoparticles take less time to find a position on the substrate to deposit properly. This kind of deposition potentially gives the non-uniform and thick film.

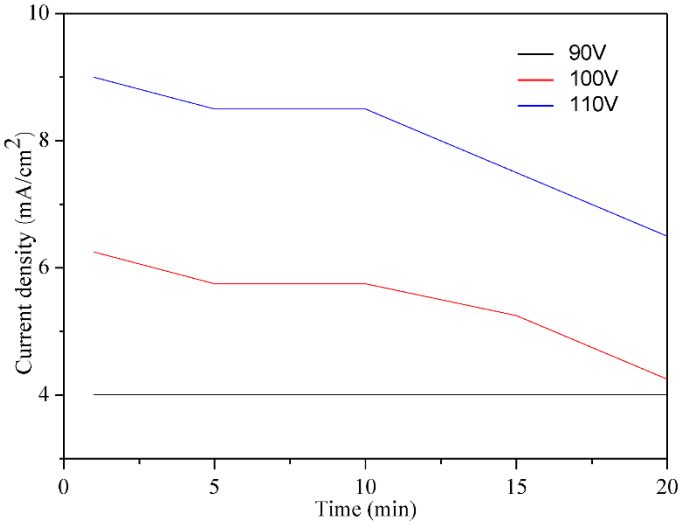

Figure. 5.6: Current density versus time curve at three different voltages (90, 100 and 110V).

5.5 EDS Analysis

The energy dispersive spectrometry analysis of the $CuInS_2$ film synthesized at 90V was performed to analyse the chemical composition. In EDS spectra of $CuInS_2$ obtained from

the samples prepared from electrophoretic deposition shown in Figure. 5.6. Cu, In, S elements are detected from the film as shown in Figure. 5.7.

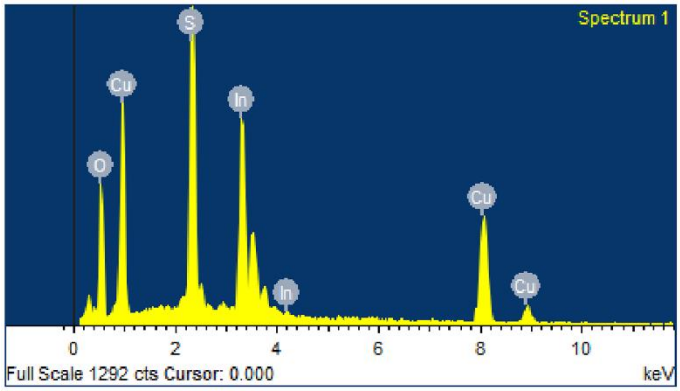

Figure 5.7: EDS spectra of CuInS2 film deposited on TiO2/FTO/glass substrate via electrophoretic deposition.

The calculated molar ratio for Cu:In:S are 1.03:1:1.65, which is closely matched with the nominal stoichiometry of $CuInS_2$ materials (1:1:2). The purity of the sample detected by EDS spectra because the extra peak for oxygen (O) belongs to the FTO glass substrate.

5.6 TiO_2 film thickness measurements

As the quality and thickness of the film can play important role on the performance of the advanced nano materials so to create stable and uniformly thick film is a great challenge in EPD. A series of experiments were conducted under the same environmental condition and the effect of film thickness was observed. The four different sets of experiments were performed at constant voltage mode and data of the film thickness was recorded as shown in table .5.1.

Table 5.1: Applied voltage, distance variation and suspension aging effect on the thickness of the film at the same deposition time

Group	Applied Voltage (V)	Distance b/w the electrodes (cm)	Deposition time (min)	Suspension aging time	Thickness (µm)
1	**30**	0.7	5	As prepared	3.25
	50				4.10
	70				4.98
	100				10.48
	130				14.11

2	70	**0.3** **0.5** **0.7** **1.0**	5	As prepared	7.81 4.86 4.98 3.58
3	70	0.7	**3** **5** **8** **10**	As prepared	2.90 4.98 7.32 9.63
4	30 50 70 100 130	0.7	5	**After 5 days**	0.65 0.88 2.01 2.43 3.48

5.6.1 Applied Voltage

Figure 5.8 shows the effects of applied voltage on the coating thickness. The films were fabricated at different voltages. The potential varied in the range of 30-130V and the time was fixed 5min per deposition. The present data reveals the direct relationship between the applied voltage and coating thickness. The thickness of the films was measured with EXTECH CG204 coating thickness tester. The highest coating thickness (14.11 µm) was obtained at 130V because the increased applied voltage provides the greater dragging force therefore, this effect increases the deposition rate.

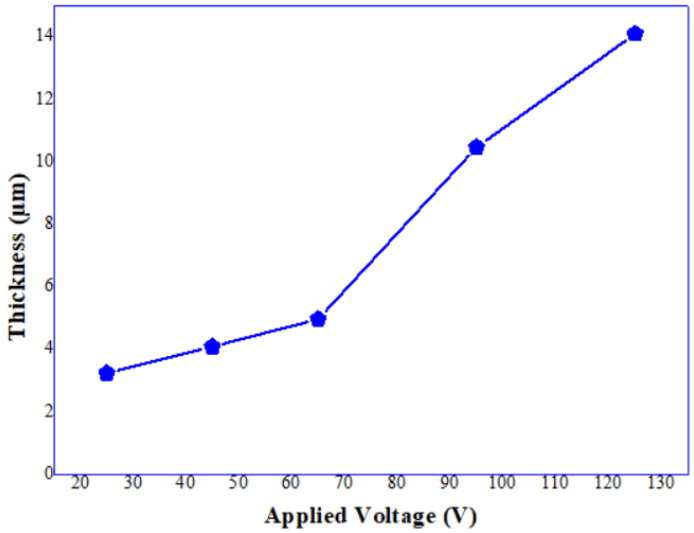

Figure. 5. 8: Effect of applied voltage on the thickness of TiO_2 Film deposited by Electrophoretic deposition.

5.6.2 Distance between the Electrodes:

Figure. 5.9 shows that the thickness of the film decreases with the increasing distance between the electrodes. The decrease in the thickness was due to increase the collision between the nanoparticles at higher distance (between the electrodes) which reduce the deposition rate due to deceleration of nanoparticles.

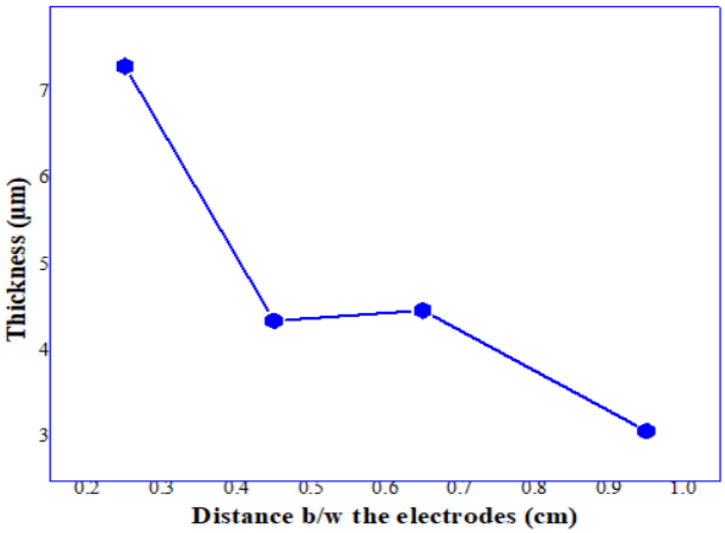

Figure 5. 9: Effect of Distance (between cathode and anode) on the thickness of TiO2 film.

5.6.3 Deposition Time

Investigation towards the effect of deposition time to the deposition behaviour of TiO_2 nanoparticles using electrophoretic deposition (EPD) technique shows that coating thickness increases as increasing the deposition time.

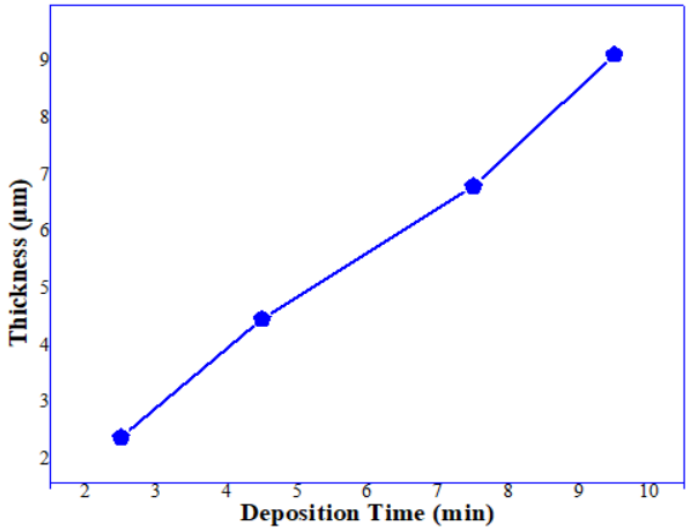

Figure 5. 10: Effect of deposition time on the thickness of the TiO2 film.

5.6.4 Suspension aging time:

The film thickness as a function of suspension aging time are represented in figure 5.11. After 5 days the huge change was observed.

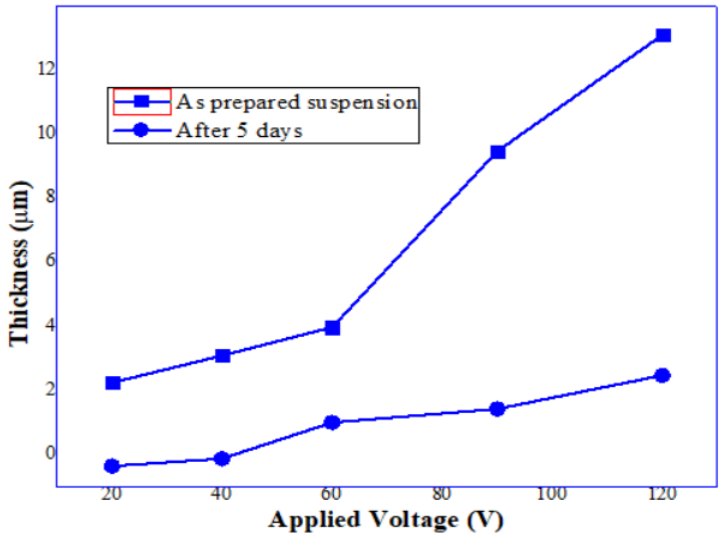

Figure 5.11: Effect of suspension aging time on the thickness of the film.

At higher voltage (130V) only 3.48µm thick film was obtained. This is 4 time less than the film deposited at 130V from as prepared suspension. So, suspension aging is the major factor that effect the film thickness because after five days the rate of current that pass between the electrodes decrease which effect the deposition rate.

5.6.5 SEM Analysis of TiO_2 films

SEM images of TiO2 films are shown in a figure 5.12. It is observed that increasing applied voltage significantly increase the thickness of the film.

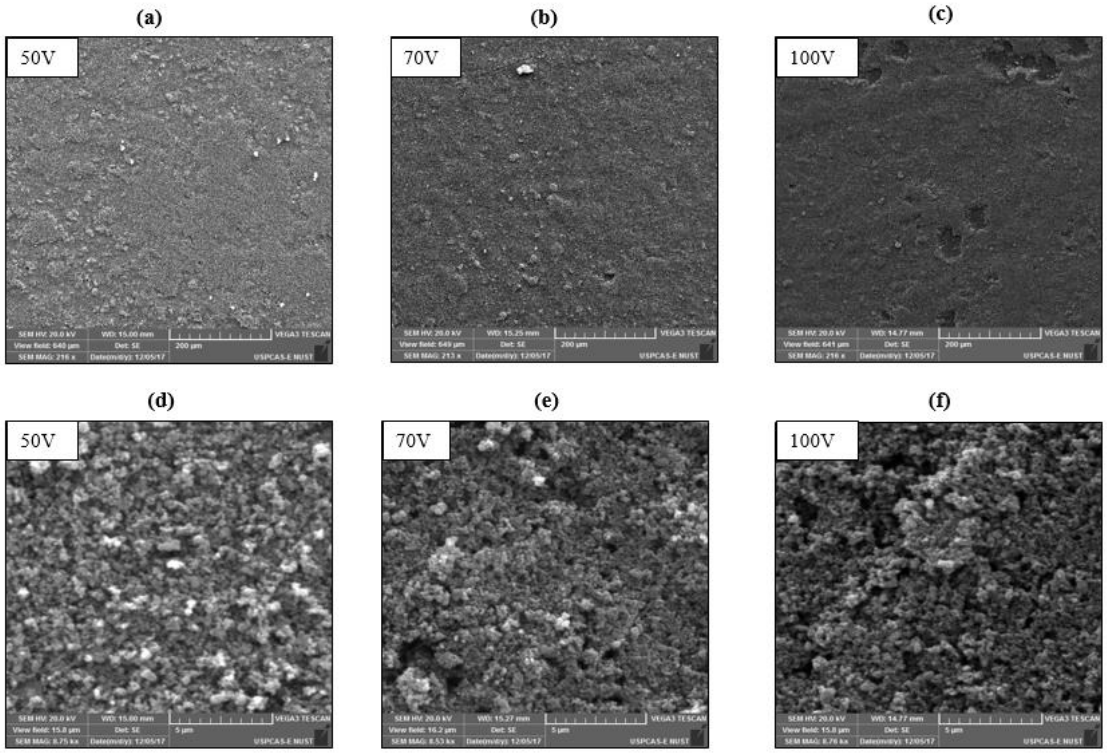

Figure 5. 12 SEM images of TiO2 films synthesized via Electrophoretic deposition at 50V (a and d), 70V (b and e), and 100V (c and f respectively).

The top view of SEM images shown in figure 5.12(a-c) reveal that the different deposition condition change the surface of the film. At low applied voltage 50V deposited film is more uniform and non-porous. While by applying higher deposition voltages (100V) the film shows the interconnected and high agglomerated nanoparticles.

At high voltage the thickness of the film increases due to faster deposition rate which reduce the uniformity of the film because the particles have less time to properly attach on

the surface of the film. So, depending on the applied voltage and deposition time, smooth thin films of a few μm can be directly deposited on an electrically conductive substrate.

5.7 Computational Results

5.7.1 Band gap calculation from HOMO and LUMO of TiO_2

The theoretically calculated band gap from HOMO and LUMO of TiO_2 anatase is match with the standard given value of band gap.

The below figures show the calculated HOMO and LUMO level of TiO2 anatase phase.

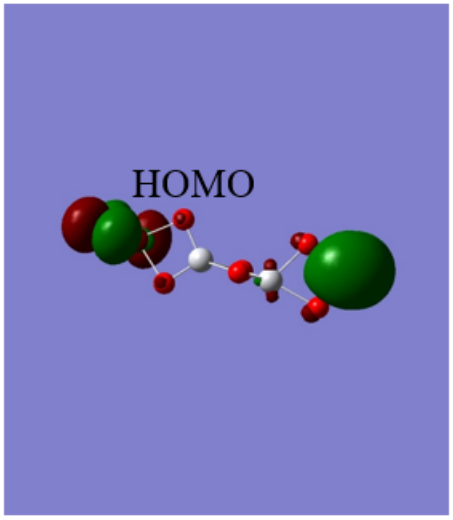

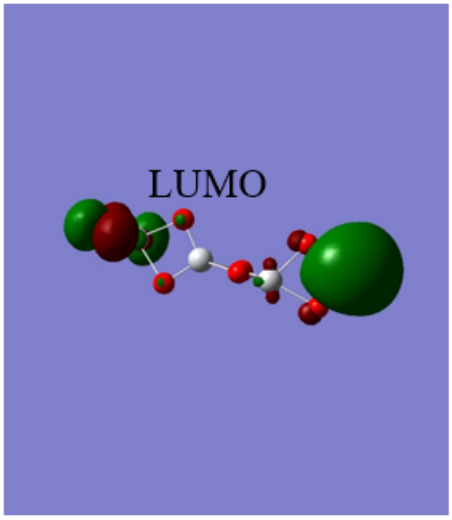

Value of highest occupied molecular orbital (HOMO) = 0.20711HF

Value of lowest unoccupied molecular orbital (LUMO) = 0.21887HF

LUMO-HOMO= 0.01176HF

Difference between HOMO and LUMO= 0.01176HF

Hartee energy, HF is the unit of energy used in molecular orbital calculations.

1HF=27.2114eV

Band gap in eV= (0.01176*27.2114)

Eg= 3.2eV

5.7.2 Theoretically calculated UV-Vis Spectra of TiO_2

The below figure shows the theoretically calculated band gap of TiO_2 anatase phase. It is observed that the band gap is lie in visible range which is match with band gap calculated from HOMO and LUMO levels.

The spectra consist of three portions. First part is a slope indicating an absorption edge. Second part is a plateau region where absorption seems constant or show gradual change with increasing wavelength. Third part is the second absorption edge. The wavelengths of each nanoparticle that were obtained by the tangential fitting of the linear portion of the spectrum, called cut off wavelength, which gives the onset wavelength of light that is absorbed.

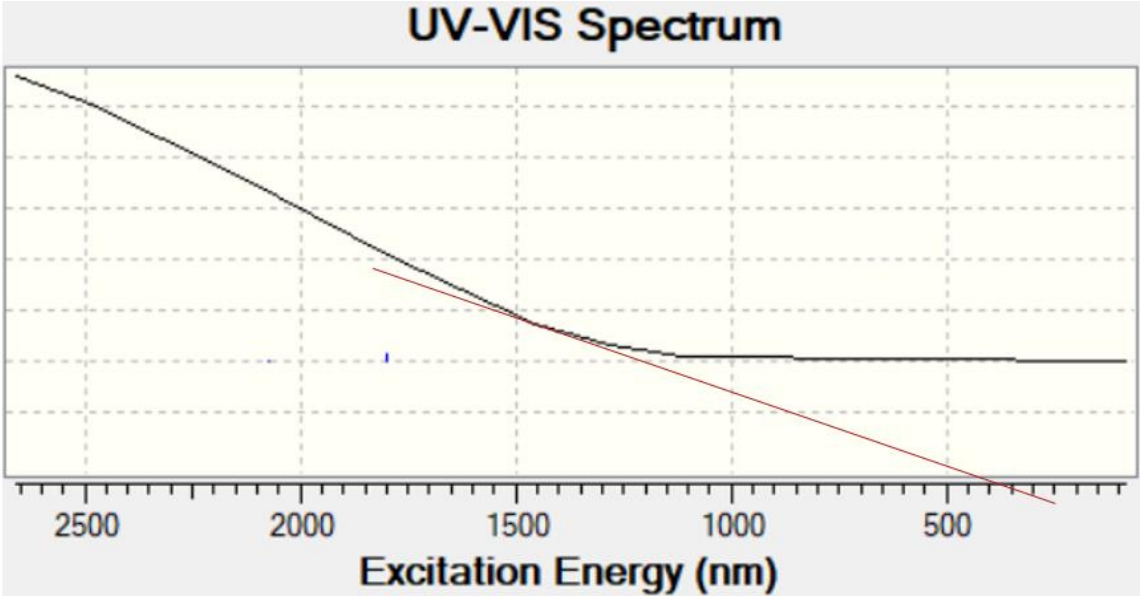

Figure 5.13: Theoretically calculated UV-Vis spectra of TiO_2 Anatase phase.

For the conformation the band gap of the TiO_2 is calculated by using cut off wavelength from the below given formula

$$Eg = \frac{1240}{\lambda\ (nm)}$$

Where λ is the absorption edge and value of absorption edge was 400nm. So, the calculated Eg is 3.2 eV.

5.8 Conclusions:

In summary the TiO_2 nanoparticles and ternary $CuInS_2$ QDs have been synthesized by sol gel and modified co-precipitation method respectively. The XRD patterns indicates the formation of chalcopyrite structure of $CuInS_2$ QDs at 300C annealing temperature. But at high temperature $CuInS_2$ transform into $CuSO_4$ and In_2O_3. UV-Vis spectral data confirm the formation of QDs because the estimated band gap and particle size of the $CuInS_2$ are 2.33eV and 8.4nm respectively. The EDS reveals that the films of the TiO_2 and $CuInS_2$ are highly pure. And the calculated molar ratio for Cu:In:S are closely matched with the nominal stoichiometry of $CuInS_2$ materials. The SEM shows the effect of applied voltage over the smoothness of the film which reveals that high agglomeration of the particles at increased applied voltages. The smooth film is obtained at low applied voltage (90V).

Theoretically calculated UV-Vis spectra and band gap of TiO_2 anatase phase reveals that this is suitable for solar cell applications due to higher absorption range. So, the adopted synthesis and deposition technique is cost effective and safer to produce photovoltaic materials and films.

References

[1] A. Singh, R. Manivannan, S.N. Victoria, Simple one-pot sonochemical synthesis of copper sulphide nanoparticles for solar cell applications, Arabian Journal of Chemistry, (2015).

[2] T. Trindade, P. O'Brien, N.L. Pickett, Nanocrystalline semiconductors: synthesis, properties, and perspectives, Chemistry of materials, 13 (2001) 3843-3858.

[3] S. Peng, Y. Liang, F. Cheng, J. Liang, Size-controlled chalcopyrite CuInS 2 nanocrystals: One-pot synthesis and optical characterization, Science China Chemistry, 55 (2012) 1236-1241.

[4] M. Montazeri-Pour, N. Riahi-Noori, A. Mehdikhani, Synthesis of single-phase anatase TiO2 nanoparticles by hydrothermal treatment with application potential for photoanode electrodes of dye sensitized solar cells, J. Ceram. Process. Res, 14 (2013) 595-600.

[5] T. Theivasanthi, M. Alagar, Titanium dioxide (TiO2) Nanoparticles XRD Analyses: An Insight, arXiv preprint arXiv:1307.1091, (2013).

Annexure

Synthesis and Characterization of Electrophoretically deposited Chalcopyrite Copper Indium Sulfide ($CuInS_2$) Quantum dots (QDs) for Solar Cell applications.

*Hina Pervaiz, Zuhair S Khan**

Advanced Energy Materials and Systems Lab, US-Pakistan Center for Advanced Studies in Energy (USPCAS-E), National University of Science and Technology (NUST), H-12 Islamabad, Pakistan.

Thin Solid Films (Elsevier)

Abstract

Copper indium sulfide has been highlighted as an active next-generation solar cell material due to its nontoxicity and cost effectiveness over the past few years. There are several methods employed to synthesize and create Copper Indium sulfide quantum dots and films. In the present work, copper indium sulfide quantum dots (QDs) were synthesized at 180°C by simple co-precipitation method, using ethylene glycol as a solvent. The $CuInS_2$ films were prepared on chemically stable TiO_2/FTO as an absorber layer for solar cells. Electrophoretic deposition (EPD) is the simplest and low-cost approach used to deposit the $CuInS_2$ QDs. The effect of the EPD at different voltages over the smoothness of the film was studied in this paper. The synthesized $CuInS_2$ chalcopyrite phase and crystallite sizes were identified by X-rays diffraction (XRD). Furthermore, calcinated films were characterized by scanning electron microscope (SEM) to study the surface morphology of films. UV-Vis Spectroscopy was used to figure out the size of the $CuInS_2$ QDs based on their band gap calculated by its optical properties (Absorption).

Keywords: Copper indium sulfide, chalcopyrite, electrophoresis deposition, solar cell.

Introduction

Over the past few years, quantum dots (QDs) have been the focus of great scientific and technological efforts in optoelectronic applications because of their advantages of tuneable band gap, broad absorption spectrum, photo stability, size-dependent optical properties and low cost. Currently, binary semiconductors such as group IV-VI, III-V and II-VI are the most common material for the solar cell but their excessive use is not feasible for biosphere [1]. Among these groups, the scarcity of gallium (Ga), tellurium (Te) is another hurdle that

prohibited their commercial use [2]. Ternary (I-III-IV) semiconductor compounds are attractive candidates and have a great potential for next generation photovoltaic devices [3]. Within I-III-IV semiconductor material $CuInS_2$ is a promising choice as an absorber layer in thin film technology. The major shift on ternary $CuInS_2$ is due to its wide range of electronic and optical properties, it has a direct band gap of around 1.53eV, and high absorption coefficient (~10^5 cm^{-1}) [4-6]. Furthermore, the constituent elements of $CuInS_2$ are non-toxic and exhibit stability under solar spectrum also as compared to binary compounds [7, 8]. All these properties make $CuInS_2$ a potential substitute to replace all the costly and toxic photovoltaic materials.

There are many methods employed to synthesize the copper indium sulfide nanocrystallite. In solar cell applications, solution based synthetic techniques have gained consideration due to low cost and large scale fabrication of thin films [9]. Generally, two types of solution synthesis approaches are used 1) precursor solution based, 2) nanoparticle based [10]. In precursor solution based synthesis approach metal chloride, nitrates, acetates are dissolved in an organic solvent with the addition of the polymer binder, further prepared solution is coated onto the conducting substrate, and then annealed in the inert environment. While in second approach, nanoparticles are first synthesized and then re-dispersed in volatile organic material to prepare the colloidal suspension/ ink and the ink is printed on the substrate. After being coated on the substrate the film is heat treated.

To synthesize the thin films of $CuInS_2$ QDs for photo-anode of the solar cell there are numerous coating techniques such as chemical vapor deposition (CVD) [11], spray pyrolysis [12], sputtering [13], vacuum evaporation [14], chemical bath deposition [15], molecular beam deposition [16], ion plating [17], and electro-deposition (ED) [18] are applied. EPD is the one of the most emerging technology due to its versatility, ease and low cost [19, 20]. This technique has known since 1808, but in 1933 for the first time practically applied on thoria particles deposition [20]. The phenomena involved in the EPD is based on the movement of charged particle in a suspension under the influence of the electric field towards an oppositely charged electrode to form a homogenous coating and controlled assembly of nanoparticles [19].

$CuInS_2$ in nanophase is mostly synthesized in a harsh environment and special conditions, which make the reaction more difficult to control. In this work, successful synthesis of

chalcopyrite $CuInS_2$ QDs at 180°C was conducted by simply modified co-precipitation method and size of crystallite is 14.6nm was attained at 300°C annealing temperature. $CuInS_2$ QDs films were prepared on chemically stable TiO_2/FTO coated glass by EPD at different voltages to get the smooth and uniform absorber layer for solar cells with nanoparticles based solution method.

Experimental Section

Materials and Methods:

For the synthesis of CuInS2 QDs, Copper chloride dehydrate ($CuCl_2.2H_2O$, Honeywell), Indium chloride tetrahydrate ($InCl_3.4H_2O$, Sigma-Aldrich), Thiourea (CH_4N_2S, RDH) were used as a copper, indium and sulfur source respectively, and Ethylene Glycol ($C_2H_6O_2$, Merck) as a solvent. While Ethanol (C_2H_5OH, BDH-UK), Titanium tetra Isopropoxide ($C_{12}H_{28}O_4Ti$, Sigma-Aldrich), Acetylacetone ($C_5H_8O_2$, Merck), Hydrochloric acid (HCl, Sigma-Aldrich), and distilled water were used as starting materials for the synthesis and deposition of TiO_2 nanoparticles buffer layer. Fluorine tin oxide (FTO, Sigma-Aldrich) glass was used as film deposition substrate. *Synthesis of CuInS2 Quantum Dots:*

To synthesize the $CuInS_2$ QDs, indium chloride tetrahydrate (1.70g) and copper chloride dehydrate (1.20g) were dissolved into 40ml ethylene glycol under constant stirring of 1 h. Meanwhile, solution of sulfur was separately prepared by adding thiourea (2.48g) into 40ml ethylene glycol and stirred the solution until it dissolved. After preparing two solutions, thiourea solution was slowly added into the first solution. After that, the combined solution was heated at 180°C for 2 h. The colour of the solution was changed from colourless to dark brown and finally to black which indicates the formation of $CuInS_2$ QDs. Left the final solution for some time to cool down at room temperature. The obtained solution was then centrifuged at 3500rpm for 10 min. The isolated precipitates were washed with methanol, and then vacuum dried at 90°C for 5-6 h.

Film fabrication:

As synthesized 0.2g CuInS2 QDs were dispersed in 50ml ethanol and 1ml acetylacetone to prepare the suspension. To prepare the homogenous suspension the mixture was sonicated at room temperature for 1h using ultra-sonicator bath. The deposition $CuInS_2$ QDs was carried out by Wealtec Elite 300 plus electrophoretic deposition setup. FTO

coated glasses were used as an electrodes material due to flat and conducting surface. After the suspension preparation, the electrodes were immersed vertically in the suspension at a fixed distance.

Before the deposition $CuInS_2$ QDs the thin buffer layer of TiO_2 NPs was deposited on FTO coated glass. After the deposition, the TiO_2 film was annealed at 450°C for 1h. $CuInS_2$ films were deposited at FTO/TiO_2 electrodes at 90V-110V for 20 minutes in air with sample name a, b and c respectively. The experimental conditions for EPD are given in table 1. After the deposition, the film was washed with ethanol and dried at room temperature. After that the film was heat treated at 300°C for 1h.

Characterization:

The crystal structures and phase analysis of the $CuInS_2$ and TiO_2 powder and films were carried out by D8 Advance X-ray Diffractometer using CuKα radiations (40KV, 30mA). The surface morphologies of the films were characterized by Advanced metallurgical microscopy (EQ MM 500T) and VEGA3 scanning electron microscopy. And chemical composition of the film was investigated using Energy Dispersive X-ray spectroscopy. UV-3600 plus UV-Vis NIR Spectrophotometer was used to figure out the size of the $CuInS_2$ QDs based on their band gap calculated by its optical properties.

Results and Discussions:

The XRD analysis of the as prepared TiO_2 and $CuInS_2$ powders and films was performed to collect the information of the crystallographic structure and phase composition. Fig. 1(a) shows the XRD pattern of FTO coated glass taken before the deposition of the TiO_2 and $CuInS_2$ films. The XRD pattern of as prepared TiO_2 nanoparticles via sol-gel technique and annealed at 450°C is shown in Fig. 1(b). This pattern shows the crystalline structure and all diffraction peaks purely matched with the standard anatase pattern of TiO_2 (JCPDS 73-1764).

Fig 1(c) shows the XRD pattern of as synthesized $CuInS_2$ powder via co-precipitation method. The peaks at 2θ values of 27.89°, 32.45°, 46.29°& 55.08° can be assigned to (112), (200), (204) & (312) planes of tetragonal phase of $CuInS_2$ respectively. While the most prominent reflections of $CuInS_2$ is observed along the plane (112) at $2\theta = 27.89^{o}$. No binary compounds appeared at 300°C temperature. This pattern is well matched with the standard chalcopyrite structure of $CuInS_2$ (JCPDS 85-1575). The lattice constants of tetragonal (I-

42d (122)) phase of $CuInS_2$ are calculated to be a = 5.52279 Å, b = 5.52279 Å, c = 11.13295 Å.

Fig. 1(d) shows the XRD of $CuInS_2/TiO_2$ films deposited on FTO coated glass. This pattern is consistence with the previously reported standard patterns of $CuInS_2$ and TiO_2.

The crystallite size of $CuInS_2$ was obtained from peak broadening of highest intensity peak using Scherrer equation [21] .

$$t = k\lambda / \beta cos\theta \quad (5)$$

Where t is the crystallite size in nm, k is a crystallite shape factor λ is the wavelength of X-ray which is 0.154 nm for Cu Kα, β is the full width at half maximum (FWHM) in radian and θ is the Bragg's diffraction angle also in radian. The calculated crystallite size of $CuInS_2$ powder sample was to be 14.6 nm.

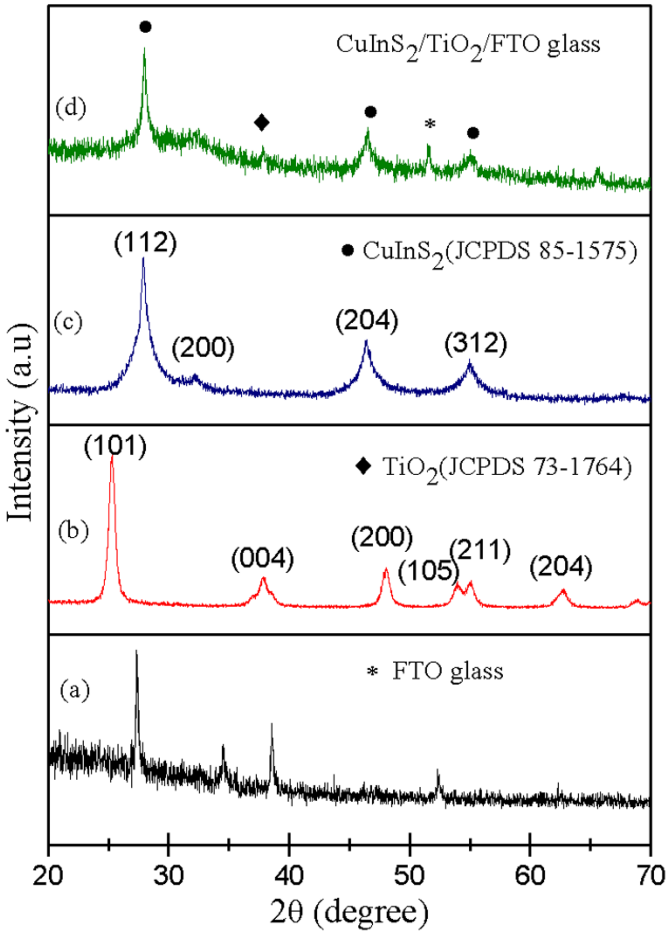

Fig. 1. XRD pattern of (a) FTO coated glass. (b) as prepared TiO_2 powder sample annealed at 450°C for 1h. (c) as prepared $CuInS_2$ powder sample annealed at 300°C for 1h and (d) $CuInS_2/TiO_2$ film deposited on FTO coated glass via electrophoretic deposition at room temperature and annealed at 450°C and 300°Cfor TiO_2 and $CuInS_2$ respectively.

The expected formation of $CuInS_2$ nanocrystallite depends on the experimental mechanism. In this work metal chlorides and sulfur source were used as precursors, dissolved in ethylene glycol which is used as solvent. In this processing mechanism, the formation of $Cu(EG)^{+1}$ and $In(EG^{)+1}$ complexes can be detected by colour variation. When the precursor solution was heated above 100°C to dissolve the metal salts, the formation of metal complexes occurs as shown in the equations 2 and 3. First, the solution color changed to sky blue due to the formation of Copper complex with the increase in the temperature the color changed from light green to dark green due to the formation of indium complex. As temperature rises to 170°C the dark green solution converted into transparent solution which indicates the formation of metal ions due to the decomposition of metal complexes. In the other side the transparent solution of sulfur source was prepared by dissolving thiourea in ethylene glycol.

$$CuCl2.2H2O + C2H6O2 \rightarrow [Cu(EG)]^{1+} \quad (6)$$

$$InCl3.4H2O + C2H6O2 \rightarrow [In(EG)]^{1+} \quad (7)$$

After that the sulfur solution is injected into metal ions solution and increase the temperature up-to 180°C. At about 180°C, the smoke began to evolve, and the colour of mixed solution turned from transparent to brown and finally to black as shown in Fig. 2.

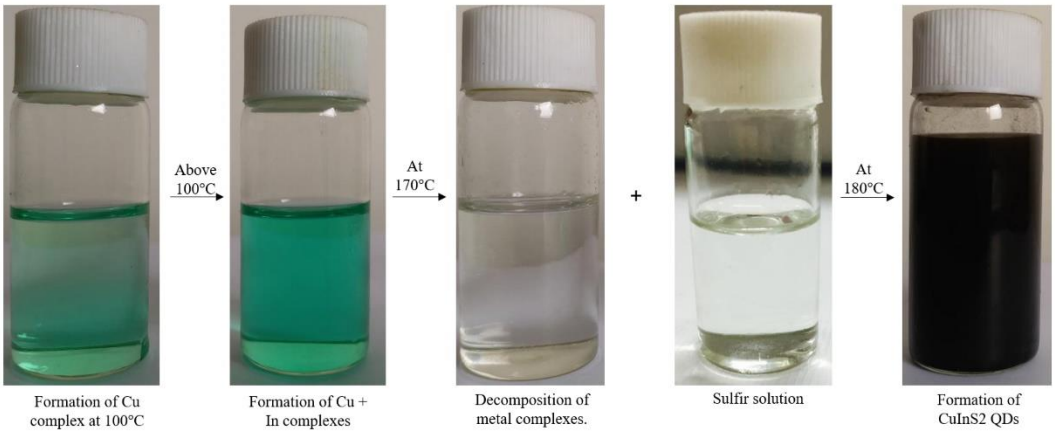

Fig. 2. Image of synthesis process of copper indium sulfide quantum dots in ethylene glycol via co-precipitation method.

$$Cu^{+} + In^{3+} + S^{2-} \rightarrow CuInS2 \quad (8)$$

In this experiment, ethylene glycol acted as a solvent as well as reductant, and in this reaction mechanism it reduced Cu(II) into Cu(I).

UV-Vis spectroscopy technique is used to find the maximum absorbance and the average particle size of the nanoparticles based on the "absorbance onset" at specific wavelength of the spectrum. Fig. 3 shows the UV Vis absorption spectra of as prepared $CuInS_2$ QDs. The spectra consist of three portions. First part is a slope indicating an absorption edge. Second part is a plateau region where absorption seems constant or show gradual change with increasing wavelength. Third part is the second absorption edge. The wavelengths of each nanoparticle that were obtained by the tangential fitting of the linear portion of the spectrum, called cut off wavelength, which gives the onset wavelength of light that is absorbed. The band gap of the $CuInS_2$ was calculated from the formula given in equation 5.

$$E_g = \frac{1240}{\lambda\ (nm)} \quad (5)$$

Where λ is the absorption edge and value of absorption edge was 530nm. So, the calculated E_g was 2.33 eV which was blue shifted in comparison with bulk $CuInS_2$ (E_g = 1.5eV). As reported in the literature, the nanoparticles smaller than excitation bohr diameter can be calculated from the absorption edge by using effective approximation method [22, 23]. The band gap can be calculated by Brus relation as shown in equation 6.

$$E_g^{nano} = E_g^{bulk} + \frac{\hbar^2\pi^2}{2r^2}\left(\frac{1}{m_e^*} + \frac{1}{m_h^*}\right) - \frac{1.786e^2}{\varepsilon r} \quad (6)$$

Where E_g^{nano} and E_g^{bulk} are the band gap energy of the $CuInS_2$ nanoparticles and the bulk materials respectively, r is the radius of QDs, ε is the dielectric constant which is 11 for $CuInS_2$, m_e^* and m_h^* are the effective mass of electron and holes [23]. In case of $CuInS_2$ nanoparticles the value of m_e^* and m_h^* are $0.16m_e$ and $1.3m_e$ respectively. Based on the above formula, the calculated radius of the $CuInS_2$ QDs was 4.2nm, so the estimated QDs size could be 8.4nm. The increase in crystallite size calculated through Scherrer equation might be due to increased agglomeration and fusion of particles as also evident through SEM images.

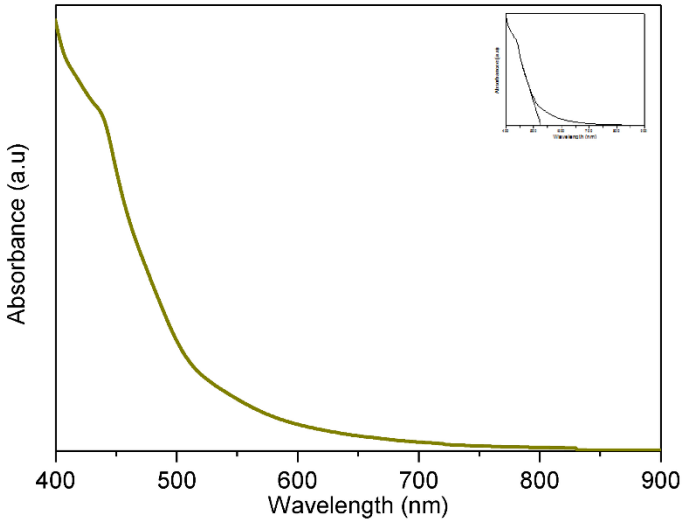

Fig. 3. UV- Vis absorption spectra of as prepared Copper indium sulfide quantum dots.

The surface morphologies of the annealed Copper indium sulphide ($CuInS_2$) films were characterized by optical microscopy. Fig. 4(a-c) shows the OM images of the $CuInS_2$ films deposited on FTO/TiO_2 at 90, 100 and 110V via electrophoretic deposition (EPD). The film deposited at 90V applied voltage shows the even and smooth surface. However, when the applied voltage increased up to 100V, micro cracks appear on the surface of the film as shown in Fig. 4(b). It is observed that the width of micro cracks increased by further rise in the voltage. Moreover, the large level of agglomeration and surface roughness also observed at higher applied voltages.

Fig. 4(d-f) shows the SEM images of Copper indium sulphide ($CuInS_2$) films. The top view of the samples shows that the surface morphology of the film is changed with increasing deposition voltages. At low applied voltage 90V deposited film is more uniform and non-porous. While by applying higher deposition voltages (100V) the film shows the interconnected and high agglomerated nanoparticles. Bluish circle in Fig. 4(e, f) shows the pores in the film, which may be caused due to instability of current densities. It can also see that the porosity of the film increased at higher deposition voltages. The rate of bubble bursting at higher applied voltage lead to abrupt change in the current densities, which may increase the porosity of the film.

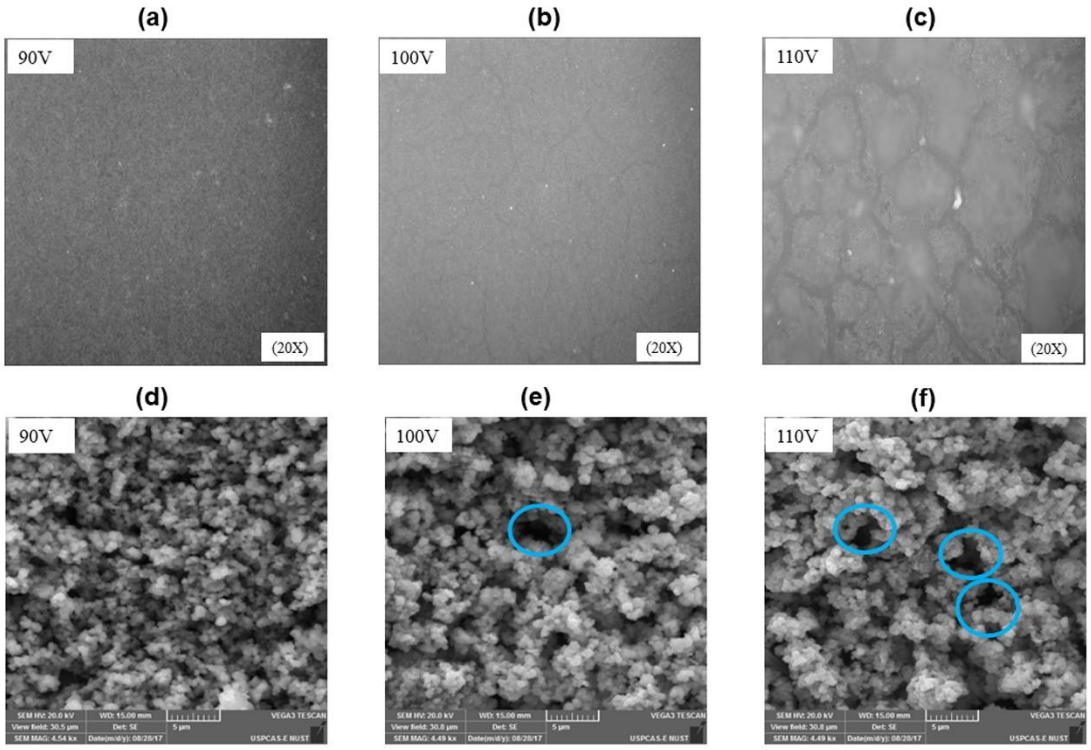

Fig. 4. OM and SEM images of CuInS2 films deposited at FTO/TiO2 substrate synthesized via Electrophoretic deposition at 90V (a and d), 100V (b and e), and 110V (c and f respectively).

It is essential to control the agglomeration and bubble bursting rate. The performance of deposited film can be drastically affected by these factors so voltage below the 100V is more effective. More uniform, non-porous and smooth film is achieved using 90V applied voltage.

Effect of deposition Voltage:

The effect of increasing applied voltage is shown in Fig. 4. The increase in deposition rate at higher voltage leads to non-uniformity of film. At higher voltage, the effect on current density also observed. Fig. 5 shows that at 90V the value of current density is constant (4 mA/cm^2) while by raised the value of voltage from 90 to 100V and then 110V current density varied from (6.5-4) mA/cm^2 and (9-7) mA/cm^2 respectively. At high current densities, the deposition rate is also high because the nanoparticles take less time to find a position on the substrate to deposit properly. This kind of deposition potentially gives the non-uniform and thick film.

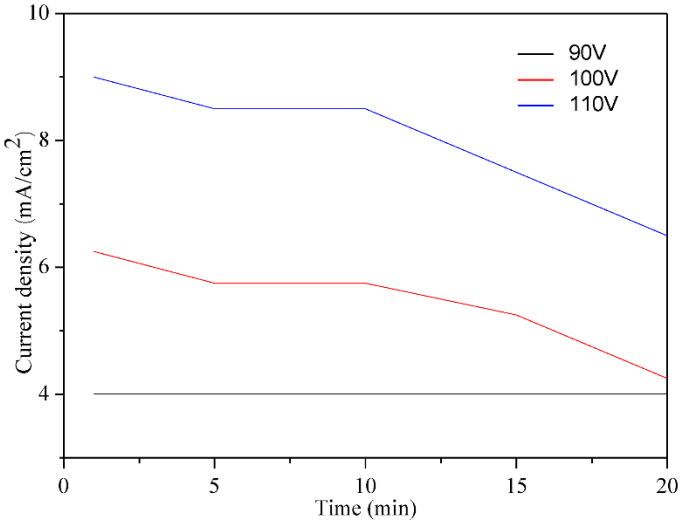

Fig. 5. Current density versus time curve at three different voltages (90, 100 and 110V).

The energy dispersive spectrometry analysis of the $CuInS_2$ film synthesized at 90V was performed to analyse the chemical composition. In EDS spectra of $CuInS_2$ obtained from the samples prepared from electrophoretic deposition shown in Fig. 5. Cu, In, S elements are detected from the film as shown in Fig. 6.

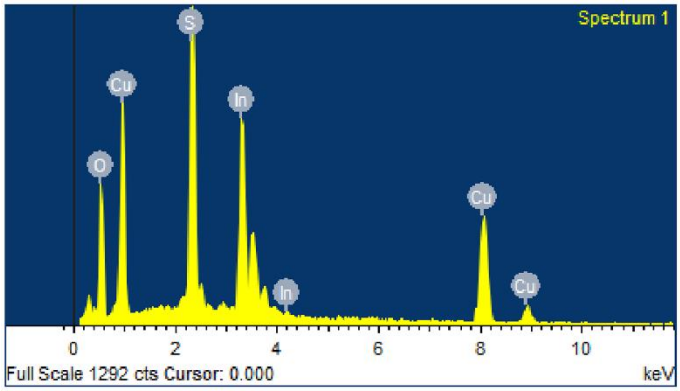

Fig. 6. EDS spectra of CuInS2 film deposited on TiO2/FTO/glass substrate via electrophoretic deposition.

The calculated molar ratio for Cu:In:S are 1.03:1:1.65, which is closely matched with the nominal stoichiometry of $CuInS_2$ materials (1:1:2). The purity of the sample detected by EDS spectra because the extra peak for oxygen (O) belongs to the FTO glass substrate.

Conclusion:

In summary, the ternary $CuInS_2$ QDs has been synthesized by modified co-precipitation method. The XRD patterns indicates the chalcopyrite structure of $CuInS_2$ QDs. Based on the UV-Vis spectral data the estimated band gap and particle size of the $CuInS_2$ are 2.33eV and 8.4nm respectively which confirmed the formation of QDs. After the synthesis, the synthesized particles are electrophoretically deposited on TiO_2/FTO/glass. The effect of the EPD at different voltages over the smoothness of the film was studied through OM and SEM. The images taken with SEM shows high agglomeration of the particles at higher applied voltages. The smooth film is obtained at low applied voltage (90V). So, the reported synthesis methodology and deposition technique is cost effective and safer to produce photovoltaic materials and films.

Acknowledgement:

We are grateful to the USAID and PGP Directorate of NUST Islamabad for their financial Assistance in this research work.

References

[1] Y. Zhang, W. Chen, J. Zhang, J. Liu, G. Chen, C. Pope, In vitro and in vivo toxicity of CdTe nanoparticles, Journal of nanoscience and nanotechnology, 7 (2007) 497-503.

[2] M. Redlinger, R. Eggert, M. Woodhouse, Evaluating the availability of gallium, indium, and tellurium from recycled photovoltaic modules, Solar Energy Materials and Solar Cells, 138 (2015) 58-71.

[3] J. Palm, V. Probst, F.H. Karg, Second generation CIS solar modules, Solar energy, 77 (2004) 757-765.

[4] H.Y. Ueng, H. Hwang, The defect structure of CuInS2. part I: Intrinsic defects, Journal of Physics and Chemistry of Solids, 50 (1989) 1297-1305.

[5] F. Shen, W. Que, Y. Liao, X. Yin, Photocatalytic activity of TiO2 nanoparticles sensitized by CuInS2 quantum dots, Industrial & Engineering Chemistry Research, 50 (2011) 9131-9137.

[6] K. Nose, Y. Soma, T. Omata, S. Otsuka-Yao-Matsuo, Synthesis of ternary CuInS2 nanocrystals; phase determination by complex ligand species, Chemistry of materials, 21 (2009) 2607-2613.

[7] A.H. Cheshmekhavar, A.R. Mahjoub, H. Fakhri, M. Dehghani, An all solution-based process for the fabrication of superstrate-type configuration CuInS 2 thin film solar cells, RSC Advances, 5 (2015) 97381-97390.

[8] M.G. Panthani, V. Akhavan, B. Goodfellow, J.P. Schmidtke, L. Dunn, A. Dodabalapur, P.F. Barbara, B.A. Korgel, Synthesis of CuInS2, CuInSe2, and Cu (In x Ga1-x) Se2 (CIGS) nanocrystal "inks" for printable photovoltaics, Journal of the American Chemical Society, 130 (2008) 16770-16777.

[9] S.E. Habas, H.A. Platt, M.F. Van Hest, D.S. Ginley, Low-cost inorganic solar cells: from ink to printed device, Chemical reviews, 110 (2010) 6571-6594.

[10] J.W. Cho, S.J. Park, W. Kim, B.K. Min, Fabrication of nanocrystal ink based superstrate-type CuInS2 thin film solar cells, Nanotechnology, 23 (2012) 265401.

[11] J.-H. Park, M. Afzaal, M. Kemmler, P. O'Brien, D.J. Otway, J. Raftery, J. Waters, The deposition of thin films of CuME 2 by CVD techniques (M= In, Ga and E= S, Se), Journal of Materials Chemistry, 13 (2003) 1942-1949.

[12] I. Oja, M. Nanu, A. Katerski, M. Krunks, A. Mere, J. Raudoja, A. Goossens, Crystal quality studies of CuInS 2 films prepared by spray pyrolysis, Thin Solid Films, 480 (2005) 82-86.

[13] K. Müller, Y. Burkov, D. Schmeißer, Spectromicroscopic characterisation of CuInS 2 surfaces, Thin Solid Films, 480 (2005) 291-294.

[14] M. Kanzari, B. Rezig, Effect of deposition temperature on the optical and structural properties of as-deposited CuInS2 films, Semiconductor science and technology, 15 (2000) 335.

[15] S. MAHMOUD, A.-H. EID, PACS numbers: 73.61. Jc, 78.66.–w, FIZIKA A, 6 (1997) 171-179.

[16] M. Gossla, T. Hahn, H. Metzner, J. Conrad, U. Geyer, Thin CuInS 2 films by three-source molecular beam deposition, Thin Solid Films, 268 (1995) 39-44.

[17] K.-i. Kondo, S. Nakamura, H. Sano, H. Hirasawa, K. Sato, Growth of CuInS2 films by rf ion plating and their characterization, Solar Energy Materials and Solar Cells, 49 (1997) 327-335.

[18] S.i. Kuranouchi, T. Nakazawa, Study of one-step electrodeposition condition for preparation of Culn (Se, S) 2 thin films, Solar Energy Materials and Solar Cells, 50 (1998) 31-36.

[19] S. Cabanas-Polo, A.R. Boccaccini, Electrophoretic deposition of nanoscale TiO 2: technology and applications, Journal of the European Ceramic Society, 36 (2016) 265-283.

[20] L. Besra, M. Liu, A review on fundamentals and applications of electrophoretic deposition (EPD), Progress in materials science, 52 (2007) 1-61.

[21] A. Singh, R. Manivannan, S.N. Victoria, Simple one-pot sonochemical synthesis of copper sulphide nanoparticles for solar cell applications, Arabian Journal of Chemistry, (2015).

[22] T. Trindade, P. O'Brien, N.L. Pickett, Nanocrystalline semiconductors: synthesis, properties, and perspectives, Chemistry of materials, 13 (2001) 3843-3858.

[23] S. Peng, Y. Liang, F. Cheng, J. Liang, Size-controlled chalcopyrite CuInS 2 nanocrystals: One-pot synthesis and optical characterization, Science China Chemistry, 55 (2012) 1236-1241.

Annexure I

The influence of different electrophoretic deposition (EPD) parameters on the thickness of the Titanium dioxide TiO_2 film.

Hina Pervaiz, Maham Akhlaq, Zuhair S Khan

Advanced Energy Materials & Systems Lab, US-Pakistan Center for Advanced Studies in Energy (USPCAS-E), National University of Science and Technology (NUST), H-12 Islamabad, Pakistan.

Abstract:

Electrophoretic deposition (EPD) is the one of most emerging technology due to its versatility, easy to use and low cost in the film synthesis techniques. In this study, the influence of different electrophoretic deposition (EPD) parameters on the titanium dioxide nanoparticles (NPs) is studied because TiO_2 NPs have gained great attention due to their wide potential applications in photo catalysts, solar cells, and optoelectronic devices. At first step, the titanium dioxide nanoparticles are synthesized by sol-gel technique. After that, the TiO2 suspension is prepared in ethanol by using ultra-sonicator bath. The effect of EPD on the thickness of the TiO2 film at different applied voltages, distance, deposition time, and suspension aging time are observed in this paper. After the synthesis, the titanium dioxide nanoparticles are characterized by X-ray diffraction to the identify the phase and crystallite size. The thickness of the deposited films is measured with CG204 coating thickness tester. Synthesized films are characterized by Optical Microscopy to study the top surface morphology.

Keywords: EPD, TiO2, Thickness

Introduction:

Electrophoretic deposition (EPD) is the one of most emerging technology due to its versatility, easy to use and low cost in the film processing techniques [20, 24]. It has been used for the processing of thin films, composite ceramics, and layered materials, high performance ceramic and composite coatings and for the deposition of nanoparticles to produced advanced nanostructured materials [19, 25]. Among the various semiconductors, Titanium dioxide is the most important candidate in thin film technology due to its unique

properties, e.g. non-toxicity, easy availability, and long-term chemical stability under several conditions [26, 27].

EPD is an electrochemical method generally carried out in two-electrode cell. It is attained by the movement of charged particles suspended in a liquid move towards the electrode surface under the influence of applied electric field [28]. Deposition on the surface of the electrode is achieved by particles coagulation [27, 29]. The mechanism of electrophoresis is based on two-step process. In the first step, the electric field is applied between the electrodes and the suspended charged particles move towards the oppositely charged electrode. While in the second step, the particle deposit on the electrode surface and form uniform, homogeneous and relatively compact film [30]. In EPD of the processing materials, the stability of suspension is an essential part, in which charged particles move freely under the influence of applied filed [19]. The size of the particle is also important in EPD generally it can be applied to any solid (fine powder) in the range of ~30μm.

In 1808, Russian scientist Ruess discovered the Electrophoretic deposition but in 1933 it was first time used in practical application [31]. After that, EPD was mainly used for the processing of traditional ceramics and vitreous enamel coating on metals. From the last few years, this technique is widely used to produce advanced materials both in academia and industrial sector [32]. The importance of EPD in material processing is significantly increasing follows from its high versatility for application with different materials and the combination of materials, its cost-effectiveness, simplicity and the requirement of only basic equipment. Furthermore, compared to other coating techniques, EPD is able to produce uniform and homogeneous coatings on the wide range of shapes.

In this paper, we investigate the main process parameters such as properties of the suspension, applied voltage, and distance between the electrodes and deposition time effect on the thickness of the TiO2 film. The table shows the variation in the Applied voltage, the distance between the electrodes and suspension aging time.

Experimental Procedure:

Materials:

Titanium tetra Isopropoxide ($C_{12}H_{28}O_4Ti$, Sigma Aldrich), Ethanol (C_2H_5OH, DBH-UK), Hydrochloric acid (HCl, Sigma Aldrich), Acetylacetone ($C_5H_8O_2$, Merck), and distilled

water were used as raw material for the synthesis and deposition of titanium dioxide nanoparticles.

Synthesis of TiO_2 Nanoparticles:

TiO2 nanoparticles were synthesized by sol-gel technique. Titanium tetra Isopropoxide (TIP), ethanol and distilled water were used to prepare the homogeneous sol. The below flowchart explains the whole process.

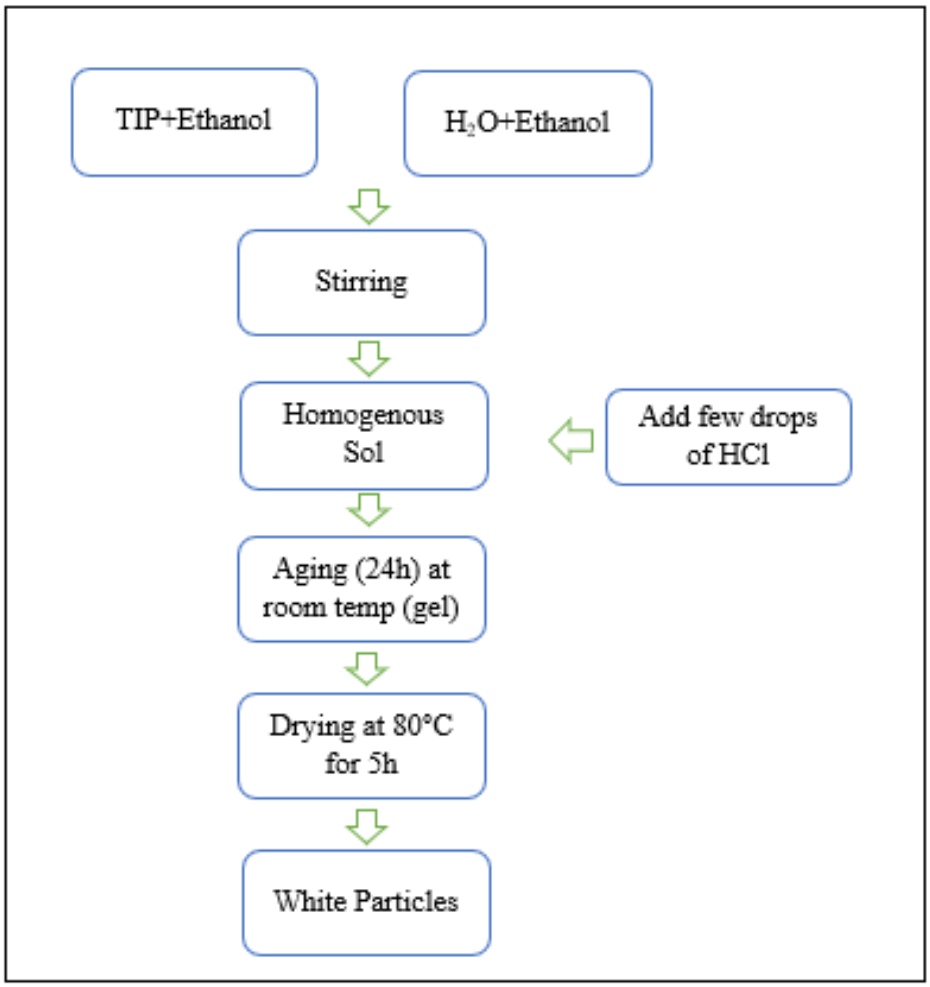

Figure. 7: Flowchart of Titanium dioxide (TiO2) nanoparticles synthesis via sol gel technique.

Electrophoretic Deposition:

As synthesized 0.2g TiO_2 nanoparticles were dispersed in 50ml ethanol and 1ml acetylacetone to prepare the suspension. To prepare the homogenous suspension the mixture was sonicated at room temperature for 1h using ultra-sonicator bath. The cathodic deposition of TiO_2 was carried out by Wealtec Elite 300 plus electrophoretic deposition setup. The setup contained two glass electrodes (25×75×1mm) covered with conductive Al

foil, one was used as a cathode and other was used as an anode. After the suspension preparation, the electrodes were immersed vertically in the suspension at a fixed distance shown schematically in figure 2. The deposition was carried out at constant voltage mode.

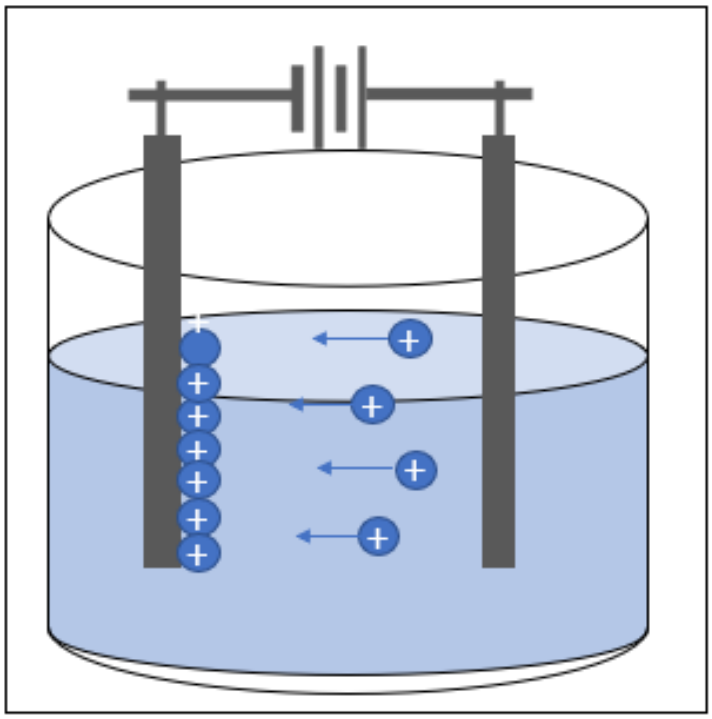

Figure. 8: Schematic of electrophoretic deposition (EPD).

The thickness of titanium dioxide nonoparticles film was optimized by various process parameters such as varied voltage between 50 to 130V and similarly by distance from 3mm to 1cm between the electrodes. Similarly, the effect of suspension aging time also observed in this paper.

Characterization:

The crystallinity of the TiO_2 powder was characterized by D8 Advance X-ray Diffractometer with monochromatic Cu Kα. The surface morphology of the films was studied by Advanced Metallurgical Microscope EQ-MM500T, ScopeTek. And the thickness of the film was measured with the help of EXTECH CG204 coating thickness tester.

Results and Discussions:

As the quality and thickness of the film can play important role on the performance of the advanced nanomaterials so to create stable and uniformly thick film is a great challenge in

EPD. A series of experiments were conducted under the same environmental condition and the effect of film thickness was observed. The four different sets of experiments were performed at constant voltage mode and data of the film thickness was recorded as shown in table .1.

Table.1: Applied voltage, distance variation and suspension aging effect on the thickness of the film at the same deposition time.

Group	Applied Voltage (V)	Distance b/w the electrodes (cm)	Deposition time (min)	Suspension aging time	Thickness (μm)
1	**30** **50** **70** **100** **130**	0.7	5	As prepared	3.25 4.10 4.98 10.48 14.11
2	70	**0.3** **0.5** **0.7** **1.0**	5	As prepared	7.81 4.86 4.98 3.58
3	70	0.7	**3** **5** **8** **10**	As prepared	2.90 4.98 7.32 9.63
4	30 50 70 100 130	0.7	5	**After 5 days**	0.65 0.88 2.01 2.43 3.48

The XRD analysis of TiO_2 nanoparticles was performed at scanning rate of 10^0/min and scan angle of 2θ=20-70^0 to collect the information of the crystal structure and phase composition. Figure 3 shows the XRD pattern of TiO_2 nanoparticles annealed at 450°C.

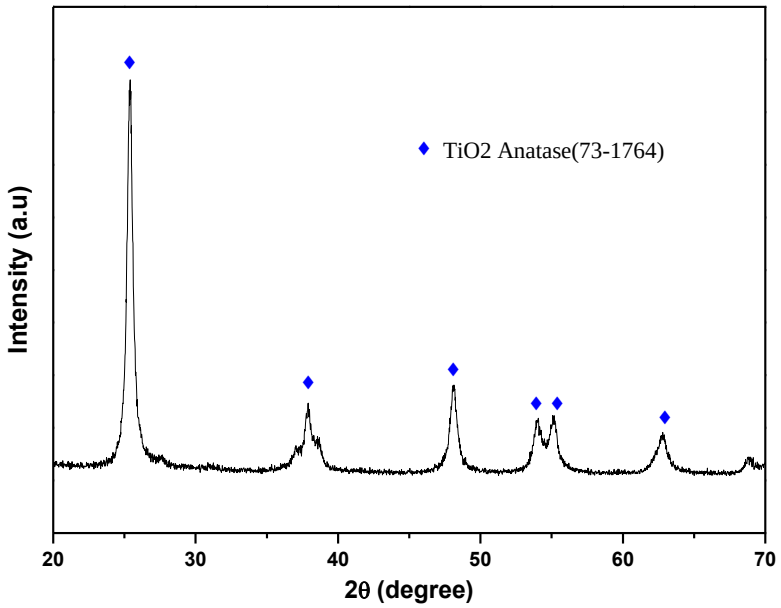

Figure.1: XRD pattern of TiO2 nanoparticles synthesized by sol gel technique and annealed at 450C.

The as prepared TiO_2 is well matched with the standard tetragonal crystal system of anatase pattern of TiO_2 (73-1764) [33]. The crystallite size of TiO2 was obtained from peak broadening of highest intensity peak using Scherrer's formula which is given below [34]:

$$D = \frac{k\lambda}{\beta cos\theta}$$

Where D is the average crystallite size in nm, k is the shape factor and its value is 0.9, λ is the wavelength of the radiation in nm, β is the FWHM value in radians and θ is the incident angle in radians. The average crystallite size of TiO2 was calculated to be 17.08nm.

Figure 4 shows the effects of applied voltage on the coating thickness. The films were fabricated at different voltages. The potential varied in the range of 30-130V and the time was fixed 5min per deposition. The present data reveals the direct relationship between the

applied voltage and coating thickness. The thickness of the films was measured with EXTECH CG204 coating thickness tester. The highest coating thickness (14.11 µm) was obtained at 130V because the increased applied voltage provides the greater dragging force therefore, this effect increases the deposition rate.

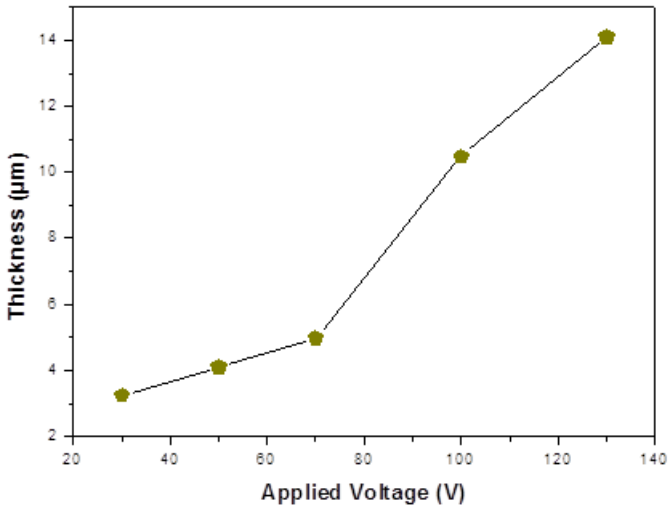

Figure.4: Effect of applied voltage on the thickness of TiO2 Film deposited by Electrophoretic deposition

Figure 5 shows that the thickness of the film decreases with the increasing distance between the electrodes. The decrease in the thickness was due to increase the collision between the nanoparticles at higher distance (between the electrode) which reduce the deposition rate due to deceleration of nanoparticles.

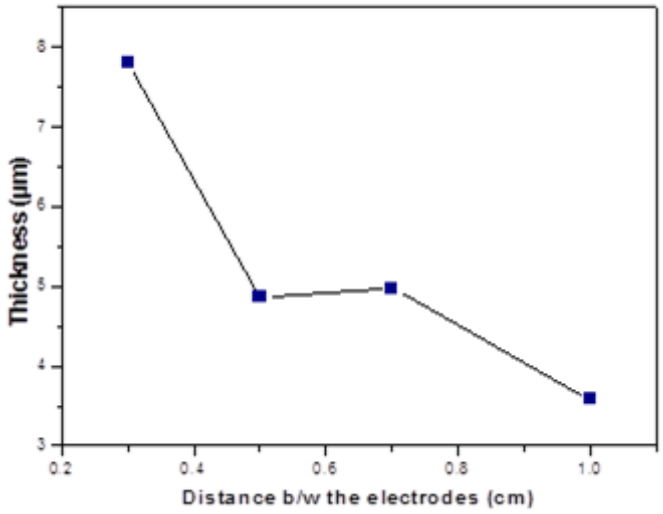

Figure.5: Effect of Distance (between cathode and anode) on the thickness of TiO_2 film.

Investigation towards the effect of deposition time to the deposition behaviour of TiO_2 nanoparticles using electrophoretic deposition (EPD) technique shows that coating thickness increases as increasing the deposition time.

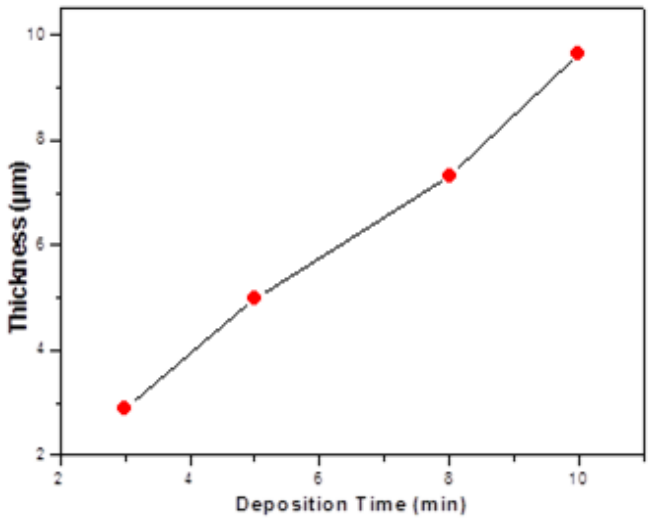

Figure.6: Effect of deposition time on the thickness of the TiO_2 film.

The film thickness as a function of suspension aging time are represented in Figure 7. After 5 days the huge change was observed. At higher voltage (130V) only 3.48µm thick film was obtained. This is 4 time less than the film deposited at 130V from as prepared suspension. So, suspension aging is the major factor that effect the film thickness because after five days the rate of current that pass between the electrodes decrease which effect the deposition rate.

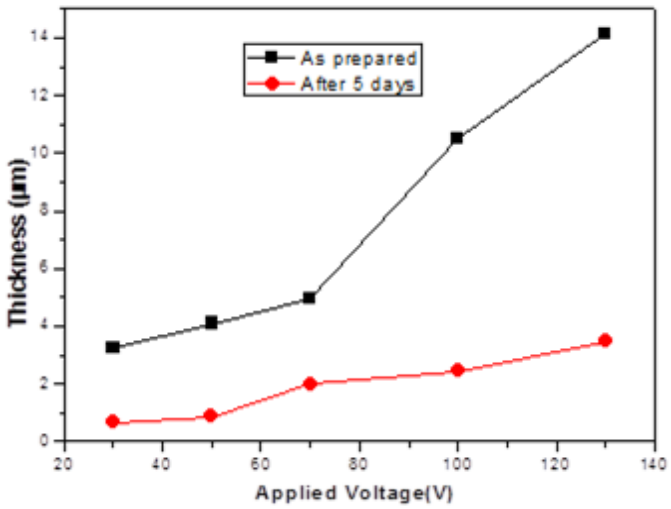

Figure.7: Effect of suspension aging time on the thickness of the film.

Optical Microscopy of un-annealed TiO_2 films were carried out by Advanced Metallurgical Microscope to investigate the top surface of the film. It was observed that increasing applied voltage and deposition time significantly increase the thickness of the film. The OM images reveal that the different deposition condition change the surface of the film. Figure 8(a) shows the uncoated Al substrate while figure 8(b & c) shows the TiO_2 coated surface at 70 and 100V respectively. The film synthesized at low voltage (70V) is more uniform and flat as compared to high (100V) applied voltage. At high voltage the thickness of the film increases due to faster deposition rate which reduce the uniformity of the film because the particles have less time to properly attached on the surface of the film. So, depending on the applied voltage and deposition time, smooth thin films of a few µm can be directly deposited on an electrically conductive substrate.

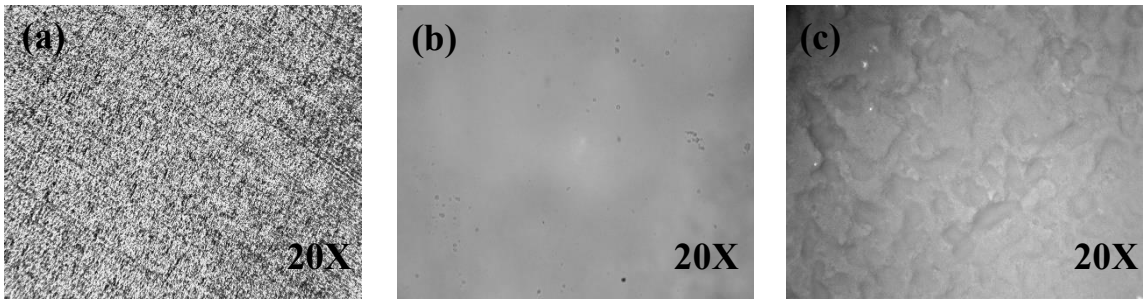

Figure.8: The OM images of (a) Al substrate without coating, (b) TiO_2 film deposited at 70V with 5 min deposition time on Al substrate, (c) TiO_2 film deposited at 100V with 5 min deposition time on Al substrate.

Conclusion:

Electrophoretic deposition is most effective, low cost and simplest technique to synthesize the TiO_2 films. Nanocrystallite films were deposited on electrically conductive Al substrate by this technique. The impact of applied voltage, deposition time, suspension aging and distance between the electrodes was observed on the thickness of the film. The film thickness was increased with increasing applied voltage and the deposition time. The effect of the distance also observed which show the inverse relation with the thickness of the film. The maximum thickness was achieved at 130V, but uniform and smooth film was attained at 70V for 5 min deposition period.

References:

[1] Y. Zhang, W. Chen, J. Zhang, J. Liu, G. Chen, C. Pope, In vitro and in vivo toxicity of CdTe nanoparticles, Journal of nanoscience and nanotechnology, 7 (2007) 497-503.

[2] M. Redlinger, R. Eggert, M. Woodhouse, Evaluating the availability of gallium, indium, and tellurium from recycled photovoltaic modules, Solar Energy Materials and Solar Cells, 138 (2015) 58-71.

[3] J. Palm, V. Probst, F.H. Karg, Second generation CIS solar modules, Solar energy, 77 (2004) 757-765.

[4] H.Y. Ueng, H. Hwang, The defect structure of CuInS2. part I: Intrinsic defects, Journal of Physics and Chemistry of Solids, 50 (1989) 1297-1305.

[5] F. Shen, W. Que, Y. Liao, X. Yin, Photocatalytic activity of TiO2 nanoparticles sensitized by CuInS2 quantum dots, Industrial & Engineering Chemistry Research, 50 (2011) 9131-9137.

[6] K. Nose, Y. Soma, T. Omata, S. Otsuka-Yao-Matsuo, Synthesis of ternary CuInS2 nanocrystals; phase determination by complex ligand species, Chemistry of materials, 21 (2009) 2607-2613.

[7] A.H. Cheshmekhavar, A.R. Mahjoub, H. Fakhri, M. Dehghani, An all solution-based process for the fabrication of superstrate-type configuration CuInS 2 thin film solar cells, RSC Advances, 5 (2015) 97381-97390.

[8] M.G. Panthani, V. Akhavan, B. Goodfellow, J.P. Schmidtke, L. Dunn, A. Dodabalapur, P.F. Barbara, B.A. Korgel, Synthesis of CuInS2, CuInSe2, and Cu (In x Ga1-x) Se2 (CIGS) nanocrystal "inks" for printable photovoltaics, Journal of the American Chemical Society, 130 (2008) 16770-16777.

[9] S.E. Habas, H.A. Platt, M.F. Van Hest, D.S. Ginley, Low-cost inorganic solar cells: from ink to printed device, Chemical reviews, 110 (2010) 6571-6594.

[10] J.W. Cho, S.J. Park, W. Kim, B.K. Min, Fabrication of nanocrystal ink based superstrate-type CuInS2 thin film solar cells, Nanotechnology, 23 (2012) 265401.

[11] J.-H. Park, M. Afzaal, M. Kemmler, P. O'Brien, D.J. Otway, J. Raftery, J. Waters, The deposition of thin films of CuME 2 by CVD techniques (M= In, Ga and E= S, Se), Journal of Materials Chemistry, 13 (2003) 1942-1949.

[12] I. Oja, M. Nanu, A. Katerski, M. Krunks, A. Mere, J. Raudoja, A. Goossens, Crystal quality studies of CuInS 2 films prepared by spray pyrolysis, Thin Solid Films, 480 (2005) 82-86.

[13] K. Müller, Y. Burkov, D. Schmeißer, Spectromicroscopic characterisation of CuInS 2 surfaces, Thin Solid Films, 480 (2005) 291-294.

[14] M. Kanzari, B. Rezig, Effect of deposition temperature on the optical and structural properties of as-deposited CuInS2 films, Semiconductor science and technology, 15 (2000) 335.

[15] S. MAHMOUD, A.-H. EID, PACS numbers: 73.61. Jc, 78.66.–w, FIZIKA A, 6 (1997) 171-179.

[16] M. Gossla, T. Hahn, H. Metzner, J. Conrad, U. Geyer, Thin CuInS 2 films by three-source molecular beam deposition, Thin Solid Films, 268 (1995) 39-44.

[17] K.-i. Kondo, S. Nakamura, H. Sano, H. Hirasawa, K. Sato, Growth of CuInS2 films by rf ion plating and their characterization, Solar Energy Materials and Solar Cells, 49 (1997) 327-335.

[18] S.i. Kuranouchi, T. Nakazawa, Study of one-step electrodeposition condition for preparation of Culn (Se, S) 2 thin films, Solar Energy Materials and Solar Cells, 50 (1998) 31-36.

[19] S. Cabanas-Polo, A.R. Boccaccini, Electrophoretic deposition of nanoscale TiO 2: technology and applications, Journal of the European Ceramic Society, 36 (2016) 265-283.

[20] L. Besra, M. Liu, A review on fundamentals and applications of electrophoretic deposition (EPD), Progress in materials science, 52 (2007) 1-61.

[21] A. Singh, R. Manivannan, S.N. Victoria, Simple one-pot sonochemical synthesis of copper sulphide nanoparticles for solar cell applications, Arabian Journal of Chemistry, (2015).

[22] T. Trindade, P. O'Brien, N.L. Pickett, Nanocrystalline semiconductors: synthesis, properties, and perspectives, Chemistry of materials, 13 (2001) 3843-3858.

[23] S. Peng, Y. Liang, F. Cheng, J. Liang, Size-controlled chalcopyrite CuInS 2 nanocrystals: One-pot synthesis and optical characterization, Science China Chemistry, 55 (2012) 1236-1241.

[24] H. Sa'adati, B. Raissi, R. Riahifar, M.S. Yaghmaee, How preparation of suspensions affects the electrophoretic deposition phenomenon, Journal of the European Ceramic Society, 36 (2016) 299-305.

[25] T. Dittrich, A. Belaidi, A. Ennaoui, Concepts of inorganic solid-state nanostructured solar cells, Solar Energy Materials and Solar Cells, 95 (2011) 1527-1536.

[26] C.S. Lim, J.H. Ryu, D.-H. Kim, S.-Y. Cho, W.-C. Oh, Reaction morphology and the effect of pH on the preparation of TiO 2 nanoparticles by a sol-gel method, Journal of Ceramic Processing Research, 11 (2010) 736-741.

[27] A.R. Boccaccini, I. Zhitomirsky, Application of electrophoretic and electrolytic deposition techniques in ceramics processing, Current Opinion in Solid State and Materials Science, 6 (2002) 251-260.

[28] W. Jarernboon, S. Pimanpang, S. Maensiri, E. Swatsitang, V. Amornkitbamrung, Optimization of titanium dioxide film prepared by electrophoretic deposition for dye-sensitized solar cell application, Thin Solid Films, 517 (2009) 4663-4667.

[29] S. Dor, S. Rühle, A. Ofir, M. Adler, L. Grinis, A. Zaban, The influence of suspension composition and deposition mode on the electrophoretic deposition of TiO 2 nanoparticle agglomerates, Colloids and Surfaces A: Physicochemical and Engineering Aspects, 342 (2009) 70-75.

[30] A.R. Boccaccini, J. Cho, J.A. Roether, B.J. Thomas, E.J. Minay, M.S. Shaffer, Electrophoretic deposition of carbon nanotubes, Carbon, 44 (2006) 3149-3160.

[31] I. Corni, M.P. Ryan, A.R. Boccaccini, Electrophoretic deposition: from traditional ceramics to nanotechnology, Journal of the European Ceramic Society, 28 (2008) 1353-1367.

[32] N.M.Y. Fitrh Rabani A. A., eposition Behaviour of Titanium Dioxide (Ti02) Nanoparticles During Electrophoretic Deposition (EPD) Technique-Effcts ofpH, IEEE Business Engineering and Industrial Applications Colloquium (BE lAC), (2013).

[33] M. Montazeri-Pour, N. Riahi-Noori, A. Mehdikhani, Synthesis of single-phase anatase TiO2 nanoparticles by hydrothermal treatment with application potential for photoanode electrodes of dye sensitized solar cells, J. Ceram. Process. Res, 14 (2013) 595-600.

[34] T. Theivasanthi, M. Alagar, Titanium dioxide (TiO2) Nanoparticles XRD Analyses: An Insight, arXiv preprint arXiv:1307.1091, (2013).